SIMULATING ENERGY, WATER AND CO_2 FLUXES AT REPRESENTATIVE DESERT ECOSYSTEMS OVER CENTRAL ASIA

Longhui Li

Examining Committee:

Prof.dr.ir. A. Veldkamp	University of Twente
Prof.dr.ing. W. Verhoef	University of Twente
Prof.dr. H-J Hendricks-Franssen	Forschungszentrum Juelich
Prof.dr. B.J.J.M. van den Hurk	KNMU/Free University Amsterdam
Prof.dr. Xin Li	CAREERI, Chine Academy of Sciences

ITC dissertation number 271
ITC, P.O. Box 217, 7500 AE Enschede, The Netherlands

ISBN 978-90-365-3883-1
DOI 10.3990/1.9789036538831

Cover designed by Longhui Li
Printed by ITC Printing Department

UNIVERSITY OF TWENTE.

FACULTY OF GEO-INFORMATION SCIENCE AND EARTH OBSERVATION

SIMULATING ENERGY, WATER AND CO_2 FLUXES AT REPRESENTATIVE DESERT ECOSYSTEMS OVER CENTRAL ASIA

DISSERTATION

To obtain
the degree of doctor at the University of Twente,
on the authority of the rector magnificus,
prof.dr. H. Brinksma,
on account of the decision of the graduation committee,
to be publicly defended
on Thursday 23 April 2015 at 15.45 hrs

by

Longhui Li
born on 16/08/1978
in Shangnan, Shaanxi, China

This thesis is approved by
Prof.dr. Zhongbo Su, promotor
Prof.dr. Qiang Yu, promotor
Dr. Christiaan van der Tol, co-promotor

Dedicated to my parents and family

Table of Content

Acknowledgements

I am sincerely grateful to supervisor Prof. Bob (Zhongbo) Su and Dr. Christiaan van der Tol for their elaborate guide in this thesis. Without their help, it would not have been possible for me to complete this work. Particularly, I deeply appreciate their patience as this thesis was delayed for a long time. I also thank Prof Qiang Yu who initially encouraged me to persue this PhD degree.

I thank ITC for financial support when I was studying in the Netherlands. I also thank the "Hundred Talent" Project of Chinese Academy of Sciences and Xinjiang Institute of Ecology and Geography, who provides a platform for me to conduct eddy covariance experiments in Kazakhstan and Xinjiang, China. I am indebted to Director Prof. Xi Chen and Prof Geping Luo for his generous supports.

I am grateful to Ms. Anke de Koning, Ms. Tina Butt-Castro, Ms. Loes Colenbrander for their warm support during the research.

I thank Xin Tian, Yijian, Ouyang, Xuelei, Lei Zhong, Guangyi, Qiuju, Changbo, Xia Li, Teng Fei, Meng Bian and many other Chinese friends for their hospitality and kind help in living at ITC.

Finally, I am deeply indebted to my parents and my families as I had very limited time to be with them when I was studying and workings overseas.

Chapter 1

General Introduction

1.1 Scientific Background

The Earth's climate is a solar powered system. Weather and climate on Earth are determined by the amount and distribution of incoming solar radiation (Trenberth et al., 2009). Energy from the Sun heats the Earth surface, warms the atmosphere, and powers the ocean currents. In weather forecast and climate change research, climate models are serving as principle tool to investigate the energy, water vapour and other mass movements and exchanges among the atmosphere, oceans, land surface, and ice. Climate models are quantitative approaches to simulate the interactions of the atmosphere, oceans, land surface, and ice, for a variety of purposes from the study of the dynamics of the climate system to projections of future climate. Climate models take account of incoming energy from the sun as short wave radiation, chiefly visible and short-wave (near) infrared, as well as outgoing energy and long wave (far) infrared radiation from the earth surface. Any imbalance of these energy components will results in a change in temperature. Another most use of the climate models in recent years has been to project temperature changes resulting from increases in atmospheric concentration of greenhouse gases (including CO_2). Climate models have been evolved from the relatively a simple one, which considers a simple radiant heat transfer model that treats the Earth as a single point and averages outgoing energy, to extremely complicated Earth System Model (ESM), which integrates the interactions of atmosphere, ocean, land, ice, and biosphere to estimate the state of regional and global climate and a wide variety of conditions (Heavens et al., 2013).

1.1.1 History of Land Surface Models (LSMs)

The land surface is a key component of Earth system, as it controls the partitioning of available energy at the surface between latent and sensible heat, and it regulates the partitioning of available water between land surface evapotranspiration and surface runoff as well. The land surface is also the location of the terrestrial ecosystem carbon sink (Pitman, 2003). Energy, water and carbon cycling in land surface are strongly coupled to the atmosphere, ocean, and ice, and finally alter and impact regional or global climate. Therefore, Land Surface Model (LSM), which is organised as a computational tool to describe the exchanges of mass and energy, interactions and feedbacks between land surface and atmosphere, have been widely used to estimate the energy and water fluxes (Bonan, 1996). LSM is one of indispensible components of ESM, which deals with the surface energy balance and the

surface water balance. The two cycling processes strongly influence momentum exchange and the carbon balance, and hence critically alter the future climate. The quantification of human-induced land-use/land-cover change (LUCC) effects on climate in ESM is also achieved via LSM, as LUCC significantly alter the Earth's surface, which is described in a LSM. Effects of LUCC on climate can be direct such as deforestation, reafforestation or agricultural intensification. The indirect effect, via CO_2 fertilization or CO_2-related climate change, is expected to cause global-scale changes in the terrestrial ecosystem (structure and function) (Pitman, 2003). Either direct or indirect effects induced by LUCC are able to significantly change the surface albedo, energy or water balances (Piao et al., 2007).

Since the release of the 1st LSM in 1969 (Manabe, 1969), development of LSM has experienced more than 40 years, and significant progresses have been achieved. In the first generation of LSM introduced by Manabe (1969), a simple energy balance equation was used, and the heat conduction into the soil (i.e., the ground heat flux) was ignored. Therefore, Manabe's LSM can't represent the seasonal or diurnal cycle of energy transfer. The first generation of LSM also adopted a commonly called the "Manabe bucket model" for hydrology, which means that a globally constant soil depth and water-holding capacity was used. Evapotranspiration was limited by soil water content below a threshold, and runoff produced from precipitation when soil moisture exceeded by a prescribed limit. In the first generation LSM, no explicit representation of vegetation was implemented, i.e. regulating effect of vegetation stomata on transpiration was not described. Instead, the total evapotranspiration (ET) was computed as the product of aerodynamic conductance and the difference between the surface humidity and atmospheric humidity. As the surface humidity is not easy to determine, ET was commonly calculated as the potential evaporation of the water body (ETp) multiplied by a beta factor to represent the limited effect of soil water availability and the beta factor is normally formulated as a linear function of soil water content. Limited by these over-simplifications, ET estimated by the first generation of LSM was generally too high (Sellers et al., 1997), and it is easy to understand that the first-generation LSMs did not provide a framework to simulate the CO_2 exchange between terrestrial land surface and to enable experiments to be performed to investigate the potential impacts of LUCC on climate (Pitman, 2003). Despite these simplifications, Manabe (1969) kicked off a crucial step in the representation of land surface processes in global climate models.

When an efficient approach for estimating ground surface temperature and soil moisture with inclusion of vegetation layer was introduced (Deardorff, 1978), it became possible to represent the heat and moisture transfer in LSMs. Sellers et al. included the soil temperature and moisture estimate approach and developed the Simple Biosphere Model (SiB) (Sellers et al., 1986; Sellers et al., 1996). Another key player who contributed to LSM development is R. E. Dickinson. Dickinson et al. (1986; 1993) developed the Biosphere Atmosphere Transfer Scheme (BATS) model, which was built mainly based on the philosophy of Deardorff (1978). The two LSMs, BATS (Dickinson, 1983; Dickinson et al., 1993; Dickinson et al., 1986) and SiB, were further developed into the Common Land Model (Dai et al., 2003). These kinds of LSMs were called "second generation" of LSM (Sellers et al., 1997). There are a very large number of the second-generation-type LSMs, but all essentially and fundamentally followed the framework of Deardorff, Dickinson and Sellers. In second-generation LSMs, the vegetation-soil system was represented as the surface, which interacts with the atmosphere (Sellers et al., 1997). The difference in albedo and in absorbing or reflecting solar radiation provided an opportunity to integrate satellite data into LSMs (Sellers et al., 1994). Second generation LSMs also explicitly described the effects of vegetation on energy, water balance and momentum transfer. The empirical formulation to describe CO_2 and water vapour exchange between vegetation and atmosphere (Jarvis, 1976), regulated by plant stomata, were incorporated into the second generation LSMs and the soil system was represented by more than two layers. Soil type specific Richards equation-based water transfer approach was used in second generation LSMs. Inclusion of vegetation stomatal conductance, and separation of soil and vegetation in the second generation LSMs allow us to explore the effects of LUCC on the change in climate. With improvements in these physical representations of the land-atmosphere interactions, the second generation LSMs was proven to perform better than the first generation LSMs, at least on shorter time scale (Beljaars et al., 1996; Viterbo et al., 1999).

The major advance of the second-generation LSMs is that they considered the effect of vegetation on energy, water vapour and momentum exchange by empirically simulating canopy conductance for transpiration. The major limitation is that the second-generation LSMs do not describe the photosynthesis process – the essential activity of plant. In the 1980s, several significant breakthrough achievements were made in the modeling of plant photosynthesis, transpiration, stomatal conductance, and their coupling

relationships. In the modeling of photosynthesis, a biochemical model photosynthetic CO_2 assimilation in leaves of C_3 species was proposed to predict the photosynthetic rate under multiple meteorological conditions (Farquhar et al., 1980). In 1987, Ball et al. developed a semi-empirical stomatal conductance model (Ball et al., 1987), which was theoretically enhanced for predicting the stomatal behaviour in response to environmental factors. The Ball's stomatal conductance model is commonly known as Ball-Berry model. The Ball-Berry model was further improved by Leuning (Leuning, 1990; Leuning 1995), which was found in better agreement with experiments compared to the Jarvis stomatal conductance model (Jarvis, 1976). Based on Farquhar's biochemical photosynthesis model and Ball-Berry type of stomatal conductance model, a coupled photosynthesis-stomatal conductance-transpiration model was built so that plant photosynthesis and transpiration regulated by stomata was modelled as a manner of tightly coupled system (Collatz et al., 1991). The coupled approach for simultaneously predicting photosynthesis, stomatal conductance and transpiration provides an elaborate tool to simulate energy, momentum, water vapour and CO_2 exchanges between vegetation and atmosphere. Once net carbon assimilation (photosynthesis) has been calculated, one can further model the carbon partitioning into different organs of plant, which allow dynamic vegetation growth. Therefore, the interactions or feedbacks between vegetation and climate can be considered in LSMs. Adding these processes and mechanisms into LSMs reflected a fundamental progress towards a realistic representation of interactions of climate and biosphere. Thus, one of the most important advances of the third-generation LSMs is identified as the use of approach which would be able to model carbon exchange between vegetation and atmosphere. Consequently, the third-generation LSMs make it feasible to investigate the effects of rising CO_2 on vegetation and climate. Actually, most second-generation LSMs have been updated to the third-generations by integrating the capacity of modeling carbon process and improving the representation of energy and water transfer processes. In parallel, a suite of ecological models, used for carbon and other biogeochemical cycles research, including Biome-BGC (Thornton et al., 2005), DGVM (Cox et al., 1999), have been developed.

Real land surface is far more complicated than any LSM can represent. Most LSMs are always on the way to improvement and development. An LSM with inclusion of DGVM and representation of full terrestrial carbon cycle process, i.e. carbon assimilation, plant and respiration, net carbon exchange, is also

called the four-generation model, but there is no essential progress compared with the third-generation LSMs and the term "forth-generation" LSM was not widely used in the community. Therefore, the latest generation LSMs were all termed the third generation. At present, widely used third generation LSMs consist of ORCHIDEE (ORganizing Carbon and Hydrology In Dynamic EcosystEms) (Krinner et al., 2005), JULES (Joint UK Land Environmental Simulator) (Best et al., 2011; Clark et al., 2011), CLM (Common Land Model) (Dai et al., 2003; Lawrence et al., 2011), SiB3 (Simple Biosphere Model) (Baker et al., 2008; Hanan et al., 2005), CABLE (CSIRO Atmosphere Biosphere Land Exchange) (Kowalczyk et al., 2006; Wang et al., 2010), and LPJ (Lund-Potsdam-Jena) (Bondeau et al., 2007; Stich et al., 2003). Most of these LSMs are ultimately coupled with General Circular Model (GCM) for Earth system research. However, prior to coupling with GCMs, all LSMs should be validated against measurements of energy, water vapour, and CO_2 fluxes. Such kind of validation is not only helpful to understand the performance of a specific LSM, but also helpful to improve LSMs. Evaluations of LSMs strongly rely on available measurements that are obtained under wide range of meteorological and soil conditions for different vegetation types. It is ideal to have long term, robust, high frequency (30 minutes) energy, water and CO_2 flux measurements to compare with the output of LSMs for testing model's performance.

1.1.2 Global FLUXNET

More than a century of theoretical development in meteorology and more recent advances in instrumentation established the basis of modern observational micrometeorology, including the appearance of eddy covariance (EC) measurement. EC was viewed as the most direct way of estimating the convective transport of energy, water vapour and trace gasses between the land surface and the atmosphere. The merge of EC technique is benefited from the fluid dynamics theory (Reynolds, 1895), universal length scales for transport in the atmospheric surface layer (Obukhov, 1946) and similarity theory (Monin & Obkuhov, 1954). The EC technique estimates the vertical flux density of atmospheric scalars such as energy, water vapour or CO_2 concentration between the land surface and the atmosphere by

$$F_s = \overline{\rho_a} \cdot \overline{w's'} \tag{1-1}$$

where F_s is the flux density of the scalar, ρ_a is air density (kg m^{-3}), w is vertical velocity (m s^{-1}) and s is the mixing ratio of the scalar in air. The overbar denotes time averaging and the prime denotes the instantaneous departure from the mean (e.g. $w' = w - \overline{w}$). In the case of the second term on the right of Eq. 1-1, the time averaging is of the instantaneous covariances of w' and s'.

With the important theoretical contributions in turbulent flux calculations (Moore, 1986; Webb et al., 1990), the EC method has experienced rapid development and has been widely used to monitor and measure the energy, water vapour and CO_2 exchange between the land surface and the atmosphere since 1990s. The pioneering monitoring and measurement based on EC technique starts from the middle of 1990s (Black et al., 1996; Grace et al., 1996; Valentini et al., 1996; Wofsy et al., 1993). These studies of EC measurements in North America and Europe provided first long term continuous data of energy, water vapour and CO_2 fluxes between terrestrial ecosystem and atmosphere. In the following decade, a large number of continuous long term EC sites was established globally, and the community of EC measuring teams shared their own EC data and established a global network of EC measurement – FLUXNET. The FLUXNET consists of several regional networks, including AmeriFlux (including Large-Scale Biosphere-Atmosphere Experiment, LBA, sites in Brazil), CarboEuroflux, ChinaFlux, AsiaFlux, OzFlux, CarboAfric and Fluxnet-Canada.

Up to date, more than 950 site-years of EC data have been archived in the international network of FLUXNET (Williams et al., 1999) (Figure 1-1), and the amount of EC data is still climbing year by year. With the increase in the size of EC data, one of the most important tasks of FLUXNET is facilitating large-scale synthesis research activities by producing quality control, gap filling and carbon flux partitioning procedures followed by some general algorithms (Moffat et al., 2007; Papale et al., 2006; Reichstein et al., 2005).

At present, EC sites within FLUXNET are operated in five continents and their latitudinal distribution ranges from 70 °N to 30 °S. Vegetation types cover cropland/natural vegetation mosaic, croplands, closed shrublands, deciduous broadleaf forest, deciduous needle-leaf forest, evergreen broadleaf forest, evergreen needle-leaf forest, grasslands, mixed forest, open shrublands, savannas, permanent wetlands, and woody savannas (Baldocchi et al., 2001). Despite the FLUXNET sites encompass wide ranges of ecosystem types,

tropical ecosystems and dry-land ecosystems are particularly poorly represented (Oliphant, 2012).

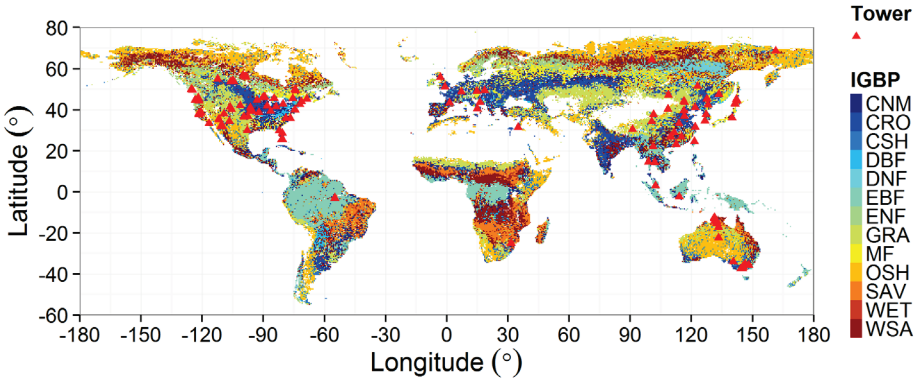

Figure 1-1. Geographical distribution of flux towers overlaid onto the 2001 MODIS IGBP land cover map at a 0.5º × 0.5º resolution. CNM: cropland/natural vegetation mosaic; CRO: croplands; CSH: closed shrublands; DBF: deciduous broadleaf forest; DNF: deciduous needle-leaf forest; EBF: evergreen broadleaf forest; ENF: evergreen needle-leaf forest; GRA: grasslands; MF: mixed forest; OSH: open shrublands; SAV: savannas; WET: permanent wetlands; WSA: woody savannas.

The global FLUXNET dataset is a rich source for land surface micrometeorology with widespread uses in local scale ecological and hydrological research. The dataset, with continuous long term and high frequency surface energy, momentum, water vapour and CO_2 fluxes, also provides irreplaceable significance and importance to calibrate, test, compare, and improve LSMs (Williams et al., 2009).

1.1.3 Improving LSMs Using EC data

LSMs represent our understanding of how terrestrial ecosystems (water and carbon fluxes) respond to the change in climate and soil conditions for a specific vegetation type. One of most crucial procedures before applying a LSM is to compare the model outputs against EC data. Traditional evaluation of LSMs is generally to compare the measured flux variables (energy components, CO_2 flux) vegetation metrics (leaf area index, biomass and so on), and other ancillary variables (soil moisture and soil temperature). A large number of evaluations of LSMs using EC data were conducted during the past three decades (Blyth et al., 2009; Li et al., 2011; Schwalm et al., 2012). Main purpose of such kind of evaluations is to determine how well the model agrees with the measurements. More frequently, the application of EC data to LSMs focused on the improvement of models by comparing model results with measurements and diagnosing the errors of the model (Li et al., 2011; Wang et al., 2011; Williams

et al., 2009). Improvements of LSMs can include refinement of parameters, adding or changing the representation of ecophysiological processes, and combinations of these aspects, or multiple comparisons among models (Baker et al. 2008; Schwalm et al., 2012; Stoy et al., 2013; Wang et al., 2007; Wang et al., 2012). Particularly, the representation of root water uptake function (RWUF) in LSMs and related root functioning have recently received much attentions (Smithwick et al., 2014), including different treatment of RWUFs (Li et al., 2013; Zheng & Wang 2007), comparison among various RWUFs (Canal et al., 2014; Jing et al., 2013), and incorporation of latest advances of root water uptake mechanisms (e.g. hydraulic redistribution) (Baker et al., 2008; Lee et al., 2005; Li et al., 2012).

1.2 Statement of Research Problem

1.2.1 Lack of EC data over Central Asia

Central Asia in this study is defined as the five Central Asian republics (CARs, Kazakhstan, Uzbekistan, Turkmenistan, Tajikistan, and Kyrgyzstan) plus Xinjiang province of China (XJ), with a total area of 5.67×10^6 km^2 (Figure 1-2). Total population in CA is around 78 million, with more than 129 ethnic groups. The Central Asia is covered by vast desert ecosystems, where mean annual precipitation is less than 300 mm. Grass and short to tall shrubs is the dominated vegetation in CA desert ecosystems.

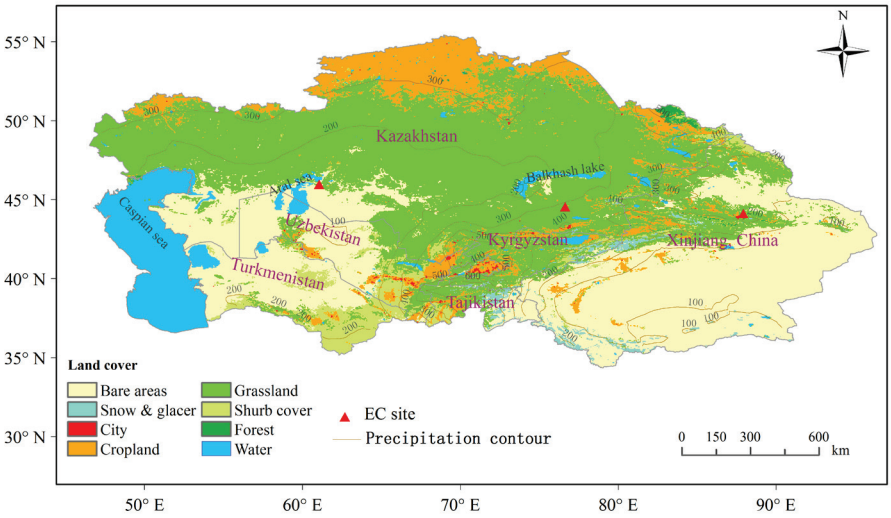

Figure 1-2. Geographical map of Central Asia, including 5 Central Asian republic and Xinjiang, China, and the land cover type obtained from 2001 MODIS IGBP land cover map at a 0.5º × 0.5º resolution. The contour showed mean annual precipitation, which is derived from the CRU T3.0.

1.2.2 Abiotic carbon process in alkaline soil desert ecosystems over Central Asia

The carbon cycle is central to Earth system; the increase in the concentration of atmospheric CO_2 is viewed as a major contributor to global warming (Mitchell et al., 2011). World-wide carbon balance estimates have been comprehensively conducted in most continents and nations, however, Central Asian is a relatively 'untouched' and of highly uncertain area, limited by climatic, ecological, and accurate satellite data.

In Central Asian dryland ecosystems, the primary production is small compared to other ecosystems; the carbon issue was commonly neglected. The previously limited number of studies on the carbon budget in Central Asia suffers from large uncertainties. A laboratory experiment reported that alkaline soil in Central Asia might absorb considerable amount of carbon via abiotic manner (Xie et al., 2009). Around the same time, Mojave Desert ecosystem showed large carbon sink capacity (Wohlfahrt et al., 2008). Such a strong strength of sink for CO_2 in these dryland ecosystem was hard to believe but may be explained by absorption of CO_2 from biotic crusts, alkaline soils or

photosynthesis of expanded shrubs (Stone, 2008), but these research were strongly questioned by some scientists (Schlesinger et al., 2009).

Dryland ecosystems cover about 35% of Earth's land area. Within this large area, the majorities of land are belonging to desert and semi-desert ecosystems, where alkaline soil dominates. According to the reported value of 62-622 gCO_2 m^{-2} a^{-1} being absorbed by the alkaline soils in Gubantonggut desert, much more evidence is needed to support and confirm the mechanism of CO_2 uptake in dryland ecosystems, which facilitates the accounting of regional carbon budget in Central Asia and significantly contributes to global carbon cycle research.

Therefore, the first scientific problem (Problem I) of this thesis is to investigate if abiotic carbon uptake dominated the carbon processes in alkaline soil desert ecosystems over Central Asia.

1.2.3 Applications of LSMs in simulating energy, water and CO2 fluxes over Central Asia

Accumulation of EC dataset in FLUXNET provided large potential to test the performance of LSMs, and facilitated research into poorly represented or missing ecosystem processes in models, leading to improvements of the model's performance (Baker et al. 2008; Baldocchi et al., 2001; Choi et al., 2010; Li et al., 2011; Li et al., 2012; Schwalm et al., 2008). In validating experiments against EC data, commonly used LSMs include SiB (Sellers et al., 1986), CLM (Dai et al., 2003), ORCHIDEE (Krinner et al., 2005), CABLE (Kowalczyk et al., 2006) and their modified versions (Baker et al., 2008; Bonan et al., 2011; Wang et al., 2011; Wang et al., 2010). These LSMs have been evaluated at different ecosystems including cropland, closed shrublands, deciduous broadleaf forest, evergreen broadleaf forest, evergreen needleleaf forest, grassland, mixed forest, open shrublands, savanna, wetlands, and woody savanna (Bonan et al., 2011; Li et al., 2011; Li et al., 2012; Wang et al; 2011; Wang et al., 2011; Wang et al., 2012; Williams et al., 2009). LSMs are also widely used for groundwater use, runoff or soil moisture in hydrological research (Zampieri et al., 2012; Zhang et al., 2013; Zhou et al., 2012). The evaluations showed that LSMs have good ability to simulate the energy, water vapour and CO_2 fluxes at the majority of the flux sites in global FLUXNET (Schwalm et al., 2010; Stoy et al., 2013). However, a large number of researches indicated that applications of LSMs in dryland ecosystems remained

quite challenging (Baker et al., 2008; Saleska et al., 2007). Compared to the above-ground processes (e.g. transpiration, photosynthesis, stomatal conductance, biomass partitioning), below-ground processes (root dynamics, root water uptake and so on) are poorly understood and notoriously difficult to model (Feddes et al., 2001), particularly in dryland ecosystems where water availability frequently is a limiting factors for plants. The root systems of plants show greatly plasticity in adapting to a dry environment and their significant effects on above-ground processes brings great difficulties into modelling energy, water vapour and CO_2 fluxes in dryland ecosystems (Feddes et al., 2001).

Therefore, the second scientific problem (Problem II) of this thesis is to apply a LSM for a Central Asian desert ecosystem, through improving the representation of root water uptake process in LSM for better simulating energy, water vapour and CO_2 fluxes from dryland ecosystems.

1.3 Statement of Objective

Based on the fact of the lack of EC measurement in Central Asian desert ecosystems and limited understanding of the application of LSMs in dryland ecosystems, the main objectives of this thesis are described below.

1.3.1 Conducting/compiling EC measurements in Central Asian desert ecosystems [OBJ1]

The first fundamental objective of this thesis (OBJ1) is to conduct EC measurements and obtain high quality data for investigating the energy, water vapour and CO_2 fluxes in representative desert ecosystems over Central Asia.

1.3.2 Investigating net ecosystem CO2 exchange over Central Asian desert ecosystems [OBJ2]

Based on obtained EC data at representative desert ecosystems, the second objective of this thesis (OBJ2) is to investigate the net ecosystem CO_2 flux over Central Asian desert ecosystems, for addressing the scientific Problem I, i.e. can abiotic carbon process significantly contribute the carbon process in alkaline soil desert ecosystems over Central Asia.

1.3.3 Determining the key ecological parameters of desert shrubs for the use in LSM [OBJ3]

The quantification of eco-physiological parameters is essential for any LSMs and all related parameter values must be known prior to the application of a specific LSM. The third objective of this thesis (OBJ3) is to determine the key ecological parameters of desert shrubs using field experiments. The determined parameter values will be ultimately used for LSM.

1.3.4 Developing an effective root water uptake function (RWUF) for CLM and comparing with other RWUFs [OBJ4]

As mentioned in section 1.2.3, one of known deficiencies of majority LSMs when applied to dryland ecosystems is the inappropriate representation in root water uptake process. Root water uptake process mainly involves the vertical distribution of root and the ability of root for absorbing water (i.e. root water uptake function, RWUF) from the soil profile, which essentially impacts stomatal conductance, transpiration and photosynthesis, and soil moisture (and soil respiration) as well. Therefore, the fourth objective of this thesis (OBJ4) is to modify the RWUF in LSM for improving the performance of LSM in simulating the energy, water vapour and CO_2 fluxes over Central Asian desert ecosystems. Meanwhile, multiple RWUFs comparison was conducted to determine which RUWF is suitable for LSM when applied in the study area.

1.3.5 Evaluation of CLM in simulating carbon fluxes over Central Asian desert ecosystems [OBJ5]

Water (transpiration) and carbon (photosynthesis) are intrinsically coupled as both are regulated by stomata of plant. The last objective of this thesis (OBJ5) is to evaluate the performance of CLM in simulating carbon fluxes over Central Asian desert ecosystems. Carbon fluxes consist of not only net ecosystem CO_2 exchange (NEE) but also its components gross primary production (GPP) and ecosystem respiration (RES). GPP and RES were obtained by partitioning NEE according to the algorithm developed by MPI-BGC (Max Planck Institute for Biogeochemistry) online tool (http://www.bgc-jena.mpg.de/~MDIwork/eddyproc/). OBJs 1-5 are jointly used for addressing the second scientific Problem II.

The overall objective of this thesis is to evaluate the performance of a LSM (CLM) in simulating the energy, water vapour and CO_2 fluxes measured from representative desert ecosystems over Central Asia, and to improve its predictive ability via representing or comparing the root water uptake process in

CLM. This research fills the gap of the application of LSM in this vast and extremely dry desert ecosystem at the moment.

1.4 Outline of the Thesis

With the five research objectives described in section 1.3 in mind, this thesis consists of seven chapters. Each chapter, except for the Chapter 1 (General Introduction) and the Chapter 7 (Concluding Remarks), has been prepared as an individual paper, already published or in preparation for submission to peer-reviewed journals. The outline of this thesis is described below.

Chapter 1: General Introduction
This chapter gives general introduction of the thesis, including scientific background, statement of research problem, statement of objective, and the outline and logic of the thesis.

Chapter 2: Growing Season Net Ecosystem CO_2 Exchange over Central Asian Desert Ecosystems
This chapter investigates the growing season net ecosystem CO_2 exchange to understand abiotic carbon contribution to the carbon process at two desert ecosystems with alkaline soils in Kazakhstan.

Chapter 3: Determining the key ecological parameters of desert shrubs for the use in LSM
This chapter determines the key ecological parameters of desert shrubs for the use in LSM. The parameters include the initial quantum efficiency (α) and the maximum carboxylation rate (V_{cmax}) and their seasonal variations. These parameters are crucially important as the input for any LSM.

Chapter 4: Representing the root water uptake process in the Common Land Model for better simulating the energy and water vapour fluxes in a Central Asian desert ecosystem.

This chapter modifies the original root water uptake function (RWUF) with a linear function of soil water potential to one with an exponential function for improving the performances of CLM for both latent and sensible heat fluxes in a Central Asian desert ecosystem.

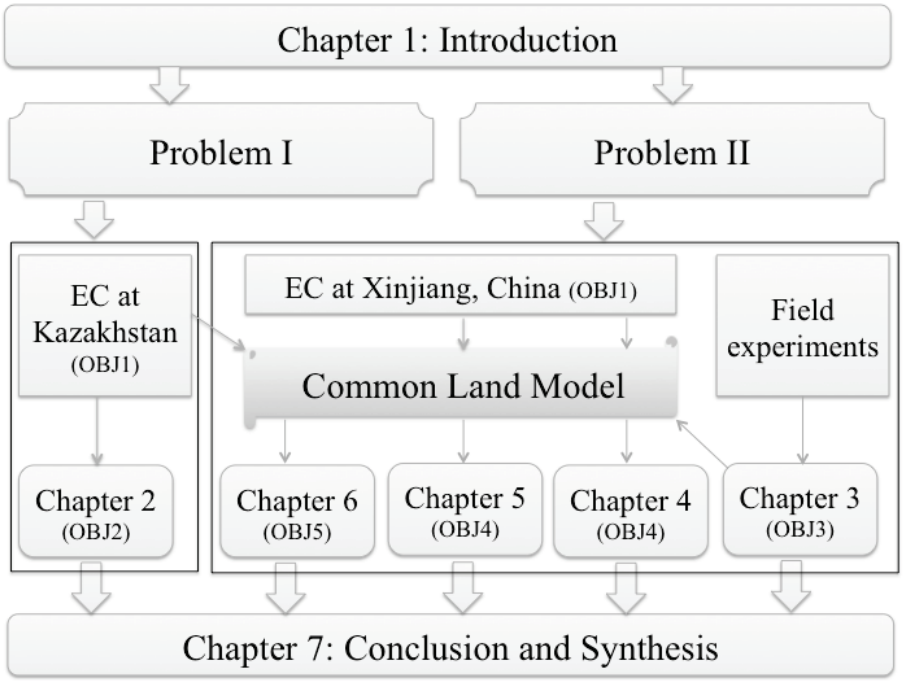

Figure 1-3. Diagram and logic of this thesis. Problem I and II are defined in section 1.2, and OBJ1-5 are defined in section 1.3.

Chapter 5: Comparison of RWUFs to simulate surface energy fluxes within a deep-rooted desert shrub ecosystem
This chapter compares the default RWUF with other three RWUFs and the effect of root distribution on the performance of CLM is also investigated.

Chapter 6: Evaluating the performance of CLM in simulating water and carbon fluxes at two Central Asian Desert Ecosystems
This chapter evaluates the performance of CLM in simulating water and carbon fluxes at two desert ecosystems in Kazakhstan.

Chapter 7: Concluding Remarks
This chapter gives conclusions and synthesis derived from the thesis. Discussion about the limitations of the current thesis and future research directions will be provided as well.

The structure and logic of this thesis are implicitly shown in Figure 1-3. The Figure 1-3 also shows the logic, the scientific problems, the objectives (OBJs 1-5) and their links with a specific chapter.

Chapter 2

Determination of Key Ecological Parameters of Desert Shrubs for the Use in the Land Surface Model*

* This chapter is based on:
Li LH*, Luo GP, Chen X, Cu GQ, Xu H, Li Y, Bai J (2011). Modelling evapotranspiration in a Central Asian desert ecosystem. Ecological Modelling 222(20–22): 3680-3691.

Abstract

In current terrestrial ecosystem modelling used by hydrological and biochemical cycle researchers, arid and semiarid biomes should receive much more attention because they cover a large proportion of total land area. Limited understanding of ecophysiological parameters of desert shrubs makes it very difficult to estimate evapotranspiration with ecosystem models over Central Asia. This research determined two important parameters, the initial quantum efficiency (α) and the maximum carboxylation rate (V_{cmax}), required in the current widely used modelling strategies for two desert shrubs (*Haloxylon ammodendron* and *Tamarix ramosissima*). The photosynthetic parameters were applied to a coupled model of stomatal conductance, photosynthesis and transpiration to simulate the diurnal dynamics of transpiration and seasonal patterns of evapotranspiration and soil evaporation. The stomatal conductance, photosynthesis, and transpiration models were adopted from Ball-Berry, Farquhar (for C_3), Collatz (for C_4), and Shuttleworth-Wallace as commonly parameterised in most current terrestrial ecosystem models. It was found that the Shuttleworth-Wallace model was able to explain 61% and 52% of the variances of the measured transpiration for *Tamarix ramosissima* and *Haloxylon ammodendron*, respectively. In addition, the model explained 78% and 57% of the variances of the observed total evapotranspiration and soil evaporation for a desert ecosystem where *Tamarix ramosissima* is sparsely distributed. This result suggests that the Shuttleworth-Wallace model implemented with a coupled photosynthesis-stomatal conductance-transpiration modelling strategy is a promising approach for estimating evapotranspiration in desert ecosystems over Central Asia. In contrast, a very simple format of evapotranspiration modelling approach, the Priestley-Taylor model, was only able to yield a fair estimation of evapotranspiration during some periods of the growing season even though the soil moisture effect is integrated into the Priestley-Taylor parameter. We recommend that the physically-based Shuttleworth-Wallace model be used for estimating evapotranspiration in related ecohydrological research in desert ecosystems over Central Asia.

2.1 Introduction

Arid and semiarid biomes make up about one third of Earth's land surface (Branson et al., 1972; Lal, 2004), and Central Asia accounts for a large proportion of global dryland area. The regulation of hydrological and biogeochemical processes by vegetation (although sparse) in arid regions has been an important research topic (Noy-Meir, 1973; Dunne et al., 1991; Whitford, 2002; Reynolds et al., 2004; Sellers et al., 1997; Baldocchi and Wilson, 2001; Savabi and Stockle, 2001). Recent studies demonstrate that the desert ecosystem has comparable capability in taking up CO_2 and modulating global atmospheric CO_2 levels (Wohlfahrt et al., 2008; Rotenberg and Yakir, 2010), suggesting that deserts play a more important role than previously expected in hydrological and biogeochemical cycles in the earth system. The hydrological significance of desert plants is of great importance to many environmental studies, including water management, climate change, ecological applications, and policymaking (Batra et al., 2006).

The Central Asia dryland area is characterized by extremely low precipitation and humidity and high summer temperature, climate conditions that lead to saline and alkaline soils. Because of rapid expansion of oasis cropland, the groundwater table depth is gradually increasing (Wang et al., 2008). Scarcity and large annual fluctuations in precipitation severely limit the survival of the desert plants. Because of their high tolerance of drought and salt, *Haloxylon ammodendron* and *Tamarix ramosissima* are widely distributed in Central Asia and are two of the dominant shrubs in the desert area. The geographical distributions of the two desert shrubs are highly dependent on meteorological conditions (Yan et al., 2008), groundwater table, and salinity of the soil (Cui et al., 2010).

Water resources in some parts of Central Asia are in great demand for use in agriculture, urban development, and ecosystem management. Because both *Haloxylon ammodendron* and *Tamarix ramosissima* are fully or partly sustained by groundwater (Horton and Clark, 2001; Xu et al., 2007), competing uses of the scarce water resources are coming more and more into conflict (Bastiaanssen and Harshdeep, 2005). The survival and sustainability of sparsely distributed desert shrubs in Central Asia may be threatened by environmental changes. Therefore, better understanding and accurate quantification of canopy evapotranspiration of dominant desert shrubs are of great importance to manage

limited water resources effectively, to sustain existing vegetation coverage, and to guarantee the stability of desert ecosystems in Central Asia.

Quantification of water consumption from phreatophyte desert shrubs can be experimentally made by porometer methods (Robinson, 1970; Romo and Haferkamp, 1989), sap flow methods (Sala et al., 1996; Cleverly et al., 1997a), lysimeters (van Hylckama, 1974; Gay and Fritschen, 1979), or eddy covariance techniques (Cleverly et al., 1997b; Wohlfahrt et al., 2008). Although these experimental methods could be used to monitor water consumption with a relatively high accuracy at a certain extent of spatial domains, they are of limited use for regional spatial extrapolation. This leads to the necessity of a modelling approach to estimate dryland ecosystem evapotranspiration because desert shrubs absorb considerable amounts of groundwater using their deep root systems (Xu et al., 2007). Furthermore, for current terrestrial ecosystem modelling, coupled terrestrial ecosystem and global climate modelling, and earth system modelling by hydrological and biogeochemical cycle researchers, desert ecosystems are always indispensable components because of their large areas. Past modelling attempts were able to predict evapotranspiration (ET) of desert plant communities from meteorological data, soil properties, and vegetation characteristics (Gay et al., 1976; Gay and Sammi, 1977; Zhang et al., 2008; Yang and Zhou, 2011). A large number of modelling approaches, such as Pemman-Monteith (Penman, 1948; Monteith, 1965; Allen et al., 1998), Priestley-Taylor (Priestley and Taylor, 1972), and other forms of so-called "climatic methods" (Katerji and Perrier, 1983; Li et al., 2009), can be used to estimate water vapor exchange between the plant canopy and the atmosphere. Among these models, the Priestley-Taylor (PT) model is a quite simple one; it is driven by air temperature and solar radiation only. The PT model has been successfully applied to a wide range of biomes and climatic conditions with variants of its original formula (Fisher et al., 2005; Sumner and Jacobs, 2005; Pereira et al., 2007; Agam et al., 2010). In contrast, the Shuttleworth-Wallace model (SW, Shuttleworth and Wallace, 1985), commonly called a "two source" (soil and plant) model, is considered to be one of the most complicated approaches for estimating evapotranspiration. The SW model comprehensively describes of five resistances (see Section 2.3.4) existing in energy and mass exchange and transport in the soil-vegetation-atmosphere system. Among the five resistances, stomatal conductance (the reciprocal of resistance) is one of most difficult to determine, and it greatly varies with meteorological and soil conditions (Ball et al., 1987; Leuning, 1995; Yu et al., 2002). Stomatal

conductance is tightly associated with transpiration and photosynthesis, and its calculation is commonly made by coupling the two physiological processes (Collatz et al., 1991; Yin and Struik, 2009). In modelling communities, combining of the SW evapotranspiration model (Shuttleworth and Wallace, 1985) and Farquhar's photosynthesis model (Farquhar et al., 1980) has been widely applied in diverse vegetations including crops (Baldocchi, 1994; Li et al., 2006), grasses (Hu et al., 2009), boreal ecosystems (Iritz et al., 1999), and temperate and tropical forests (Baldocchi, 1997; Fisher et al., 2005); however, there has been little application to desert shrubs. Furthermore, modelling of stomatal conductance for desert plants is particularly challenging because physiological processes of plants in dryland ecosystems are more likely to operate under extremely adverse conditions (Gao et al., 2005). Sound determination of initial quantum efficiency (α) and maximum carboxylation rate (Vcmax), as two of the key fundamental parameters in Farquhar's photosynthesis model (Farquhar et al., 1980), is crucial to the modelling of the coupled photosynthesis-stomatal conductance-transpiration complex (Dubois et al., 2007). These parameters for crops, grasses and trees have been intensively determined by measurement or model optimization (Medlyn et al., 2002; Wolf et al., 2006; Wang et al., 2006). Unfortunately, the two parameters of Farquhar's model are unknown for *Haloxylon ammodendron* and *Tamarix ramosissima* in Central Asia. In the presently reported research, both the Priestley-Taylor and the Shuttleworth-Wallace models were applied. They represented a very simple and a most complicated form of evapotranspiration model, respectively.

For better understanding of water consumption by desert shrubs and for establishing a reliable model to simulate the response of desert shrubs to climatic variables with accurate species-specific parameters, therefore, the objective of the present study was first to determine the values of α and Vcmax by investigating the response of desert shrubs to light measured by a portable photosynthesis system. Then a coupled photosynthesis-stomatal conductance-transpiration model was used to simulate leaf transpiration of two native desert shrubs validated by in situ measurements. Following this, the performance of the models in simulating soil evaporation and canopy evapotranspiration was tested against micro-lysimeter-measured soil evaporation and eddy-covariance-measured total evapotranspiration. Finally, the Shuttleworth-Wallace and the Priestley-Taylor models were inter-compared and a preferred model was identified for desert ecosystems in Central Asia.

2.2 Materials and Methods

2.2.1 Site characteristics and climate data

Field experiments were conducted near Fukang Station of Desert Ecology (FSDE, 44º17´N, 87º56´E, 475 m a.s.l.), Chinese Academy of Sciences. The vegetation is mostly *Tamarix ramosissima* with an average coverage of 30%. FSDE is located in the hinterland of the Eurasian Continent and presents a classical landscape in Central Asia. Central Asia is mostly characterized by hot summers and cold winters with low annual precipitation. The dominant vegetation covers are grassland (49% of total area), shrubland (9%), oasis cropland (10%), savanna (1%), and forests (1%).

The Sangonghe catchment is a representative region of Central Asia that includes most types of landscape. Along the vertical belt zone from high to low, alpine meadow, forests, oasis cropland, and desert shrubland are distributed. The two experimental sites, Beishawo (BSW, 44º22´N, 87º55´, 448 m a.s.l.) and Wujingnan (WJN, 44º22´N, 87º51´, 459 m a.s.l.), are located at the edge of the desert. The distance between the two sites is 8 km, and no significant topographic difference exists.

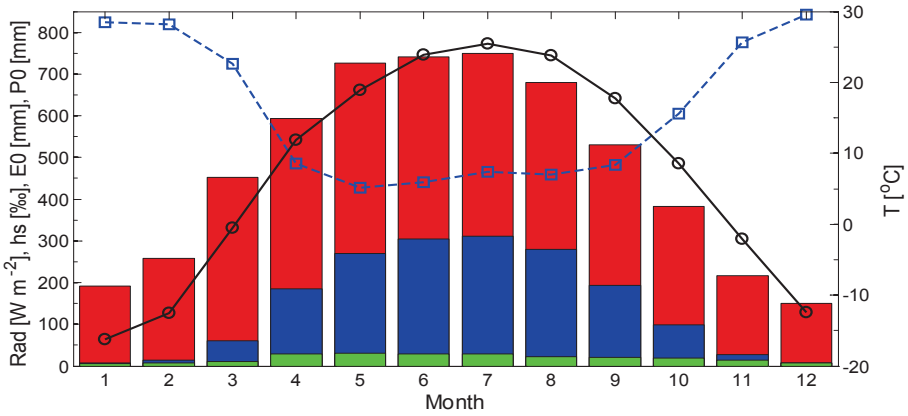

Figure 2-1. Climate conditions at Fukang meteorological station in Central Asia. Red, blue and green bars represent average monthly solar radiation (Rad), pan evaporation (E0), and precipitation (P0) during the period 1971-2008. Blue dashed line with squares indicates the average monthly relative humidity (hs), and the black solid line with circles stands for the average monthly air temperature (T) during the period 1971-2008.
Meteorological variables, including air temperature, relative humidity, wind speed, radiation, precipitation, and top layer (10 cm) soil water content, were monitored with a portable meteorological station (Campbell Scientific, Logan, UT, USA) installed midway between the two sites during the growing season (May to Sep.) in 2004 and 2006.

Historical climatic variables (solar radiation, air temperature, atmospheric relative humidity, and precipitation) measured at Fukang meteorological station at a distance of 16 km from the study sites are shown in Figure 2-1. Average growing season (April-September) solar radiation during the period 1971-2008 was 670 W m^{-2}, and average temperature was 20 °C. Relative humidity during the growing season was as low as 46%, and annual precipitation was 160 mm. However, total pan evaporation reached 1546 mm, about 10 times the amount of precipitation. Typical climate characteristics during the experimental period were severely low humidity and high temperature. Especially in the daytime, around noon, the humidity was as low as 10-25%, and the air temperature as high as 35-37 °C. Strong solar radiation (with noon peak greater than 800 W m^{-2}) (Figure 2-3) and high atmospheric evaporative demand (daily value around 10 mm) were typical. However, our measurements also covered several partly cloudy days with peak solar radiation less than 500 W m^{-2}, such as DOY 227, with accompanying lower maximum temperature (less than 30 °C) and higher minimum humidity (greater than 35%).

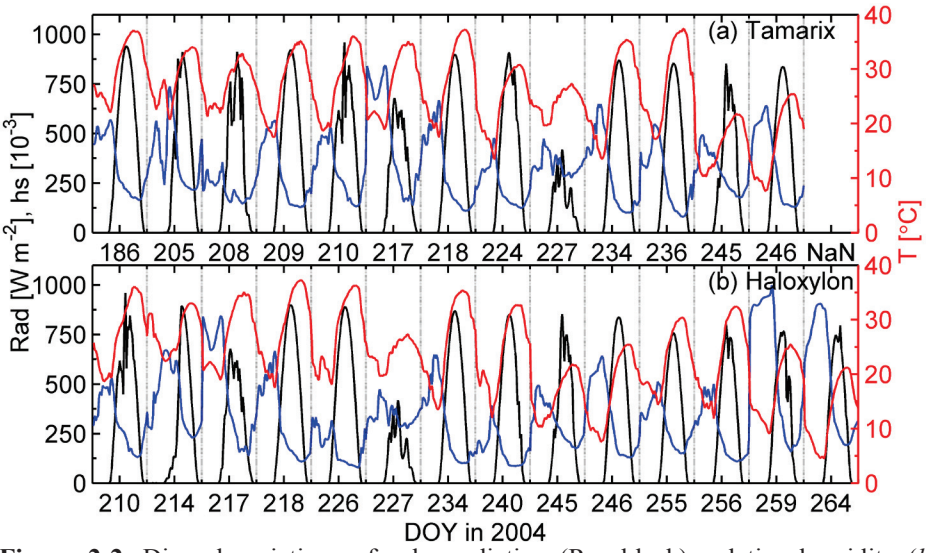

Figure 2-2. Diurnal variations of solar radiation (R_{ad}, black), relative humidity (h_s, blue), and air temperature (T, red) on experimental days for *Tamarix ramosissima* and *Haloxylon ammodendron* in 2004.

2.2.2 Response of photosynthesis to light

A photosynthetic light-response curve experiment was performed to derive initial quantum efficiency and maximum carboxylation rate for the coupled

photosynthesis-stomatal-transpiration model as described in Section 2.4.5 because the two parameters for the studied species are not available yet.

The responses of photosynthesis to light for *Haloxylon ammodendron* and *Tamarix amosissima* were measured with a Licor 6400 portable photosynthesis system (Li-Cor, Lincoln, NE, USA). Photosynthetic active radiation (PAR) in a 20×30 mm^2 leaf chamber was controlled with an LED light source (red + blue 6400-02B). The PAR gradient was set from 0 to 2200 μmol m^{-2} s^{-1}, with an interval of 100 μmol m^{-2} s^{-1}. Temperature and relative humidity in the chamber were controlled at 30 °C and 20-30%, respectively. Measurements were taken at local time 10 h to 16 h. All measurements were conducted at both sites, BSW and WJN, during the growing season in 2004 and 2006. The detailed procedure has been described previously (Xu and Li, 2006; Xu et al., 2007).

2.2.3 Leaf transpiration

As one of the adaptive and evolutional strategies to cope with extremely arid environments, the leaves of both *Haloxylon ammodendron* and *Tamarix ramosissima* have evolved into a branch type unlike a regular leaf shape. The leaves of both species are very fragile and pulplike, causing great difficulty in measuring their transpiration rates with common instruments, such as a heat-pulse flow meter, and large inaccuracies may arise from unavoidable damage.

In our experiment, an abscising procedure was used to measure the transpiration rate of the desert shrubs. One previous paper reported that the method of abscising leaf from the plant is valid for physiological observations as long as the measurement is made within a short period (Huang et al., 2009). The acceptable duration can vary from 3 to 20 minutes, depending on leaf temperature, which varied from 34 to 20 °C. In our experiment, we selected healthy and representative (in terms of plant height 1.75 m and crown width 1.50 m) plants, and a piece of fresh branch-shaped leaf was cut from the shrub cluster. The diameter (d) of the sampled leaf (branch) was measured with a reading vernier caliper (Mututoyo, Japan), and the length was measured with a scale with precision of 0.01 cm. The length of the selected branches was restricted to 10-15 cm. Such a branch generally weighed 10-15 g, accounting for a very small proportion of the total weight of the plant branches. Because the abscised branch was no longer attached to the xylem stream and the negative pressure in the xylem was increased for the subsequent cutting, only

five to ten samples (depending on the richness of branches) were made from an individual plant cluster.

The weight of the cut sample was measured immediately with an electronic balance (GS223, Shinko, Japan) with precision of 0.001 gram. The sample branch was allowed to transpire in air for 2 minutes and was weighed again. Choosing 2 minutes as the transpiring duration was based on the study of Huang et al. (2009) which reported that the valid duration for the abscising approach was effective within 3-20 minutes depending on temperature. The difference between the two readings (ΔW, g) was recorded. The area (S, m^2) of the sampled branch was calculated as a linear function of dry matter (DM), where the values of slope and intercept were determined by fitting measured DM and branch area based on different groups of branch diameter. The branch area was determined with a digital camera (Canon 300D, Cannon Inc., Tokyo, Japan) and CI-400 CIAS software (ComCID Co, Logan, UT, USA), as described in detail in the next paragraph. ΔW was divided by elapsed time (2 minutes), and the transpirational water consumption was calculated. To eliminate the effect of the differences in the diameter of sampled branches, weighted water consumption was scaled to a unit of leaf area (m^2), and actual transpirational rate (Transp, kg m^{-2} $hour^{-1}$) was calculated as:

$$\mathrm{Transp} = \frac{\Delta W * 0.001 * 30}{S} \tag{2-1}$$

where 0.001 and 30 are conversion factors from g to kg and from 2 minutes to 1 hour, respectively. The DM of sampled branches was measured by heating them in an oven for 8-10 hours. Each measurement was repeated 3 to 5 times, and measurements were made from 7h to 21h local time at half-hour intervals. Because of the extremely high air temperatures (around 35 °C) and land surface temperatures (55-60 °C) during midday in the desert, only a few measurements were made between 14h and 16h. Measurements were made over 13 and 14 days for *Haloxylon ammodendron* and *Tamarix ramosissima*, respectively, extending from day of year (DOY) 210 to 264 during the growing season at the BSW and WJN sites in 2004.

Each sampled branch was photographed with a 6M pixel digital camera (Canon 300D, Cannon Inc., Tokyo, Japan). The leaf surface area of each branch was calculated from the photographs using CI-400 CIAS software (ComCID Co, Logan, UT, USA). After collection of all leaves of one shrub, the leaf area

index (LAI) was determined based on a unit of ground area. There were at least three treatments for each shrub. This procedure for estimating leaf area of desert shrubs has been frequently used (Li et al., 2005; Xu et al., 2007; Zou et al., 2010).

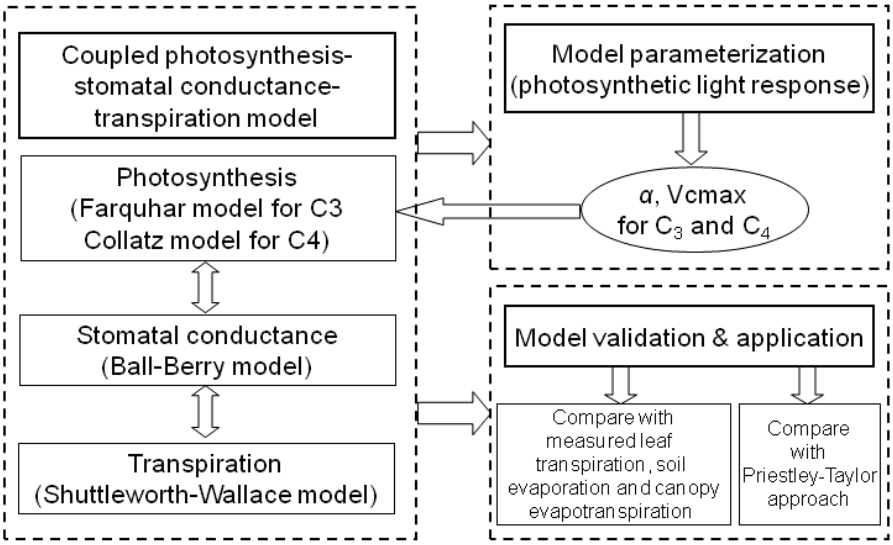

Figure 2-3. Flow diagram of the model structure, parameterisation, validation and application

2.2.4 Canopy evapotranspiration and soil evaporation

Evapotranspiration over the desert shrub canopy was measured with a fast-response infrared gas analyzer (LI7500, LI-COR Inc., Lincoln, NE, USA) and sonic anemometer (CSAT, Campbell Scientific Instruments, Logan, UT, USA) installed on an eddy covariance instrument at FSDE in 2004. The measured latent heat flux was corrected using the WPL method (Webb et al., 1980). Because of unfavorable weather conditions or instrument problems, there are 969 missing or bad values (accounting for 5.5% of annual observations) in the year. Gaps of measured latent heat flux were filled by the mean diurnal variation approach (Falge et al., 2001a; Falge et al., 2001b), one of the most frequently used methods for flux data gap filling in the CarboEurope project (Reichstein et al., 2005; Moffat et al., 2007). The energy balance closure was 82% (Xu et al., 2010).

Evaporation from bare soil was measured by daily weighing with 3 micro-lysimeters designed and built at FKDS. The depth of the micro-lysimeter was 15.2 cm and the inner diameter was 15.6 cm. The micro-lysimeters contain 2903.8 cm^3 of bare soil mounted flush with or slightly above the soil surface and were weighed daily at 09:00 h to determine water loss using electronic balances with 0.001 kg precision. In order to keep the soil moisture in the micro-lysimeters similar to that between the rows, the original soil in the instruments was changed every day. The measurements were continuously made at FKDS during the period between DOY 143 and 224 in 2004.

2.3 Model

The coupled photosynthesis-stomatal conductance-transpiration model follows the commonly used approach developed by Collatz et al. (1991; 1992). The coupled model consists of three submodels: photosynthesis, stomatal conductance and transpiration. The determination of values of parameters is very crucial to application of the model. For this study, two key parameters, α and V_{cmax}, were determined by fitting measured photosynthesis-light response data. Then the model was used to compare against measurements and against an alternative modelling approach. A simple flow diagram of the model structure, parameterisation, validation, and application is shown in Figure 2-1. Tables 2-1 and 2-2 give lists of parameters and variables used in the model.

Table 2-1. Model parameters.

Parameter	Value	Unit	Source
α	0.0235 (for Tamarix)	-	This study
	0.0164 (for Haloxylon)	-	This study
α_{PT}	1.26	-	Priestley and Taylor, 1972
θ	0.93 (for Tamarix)	-	Collatz et al., 1992
	0.83 (for Haloxylon)	-	Collatz et al., 1992
β	0.93	-	Collatz et al., 1992
V_{cmax} at 25 ºC	15 (for Tamarix)	µmol m^{-2} s-^{1}	This study
	10-25 (for Haloxylon)	µmol m^{-2} s^{-1}	This study
Kc at 25 ºC	270 (for Tamarix)	µbar	Bernacchi et al., 2002
	650 (for Haloxylon)	µbar	Bernacchi et al., 2002
Ko at 25 ºC	165000 (for Tamarix)	µbar	Bernacchi et al., 2002
	450000 (for Haloxylon)	µbar	Bernacchi et al., 2002
Q_{10}	2.0	-	Collatz et al., 1992
k	0.7	mol m^{-2} s^{-1}	Collatz et al., 1992
g0	0.01	mol m^{-2} s^{-1}	Sellers et al.,1996
	0.04	mol m^{-2} s^{-1}	Sellers et al.,1996
m	9 (for Tamarix)	-	Sellers et al.,1996
	4 (for Haloxylon)	-	Sellers et al.,1996
Oi	21	kPa	Collatz et al., 1992
b1	3.5	-	Lin and Sun, 1983
b2	3.85	-	This study
b3	33.5	s m^{-1}	Lin and Sun, 1983
ka	0.41	-	-
σ_b	0.5	-	Brisson et al., 1998
a_{PT}	0.35	-	This study
b_{PT}	0.14	-	This study

Table 2-2. List of model variables.

Symbol	Description	Unit
η_c	intermediate variable	-
η_s	intermediate variable	-
Δ	slope of saturation vapour pressure curve	kPa ºC^{-1}
ρ	air density	g m^{-3}
γ	latent heat of water vaporization	kPa ºC^{-1}
A	gross photosynthesis	µmol m^{-2} s^{-1}
Ac	Rubisco activity	µmol m^{-2} s^{-1}
Aj	RuBP regeneration	µmol m^{-2} s^{-1}
An	net photosynthesis	µmol m^{-2} s^{-1}
An_mod	modelled An	µmol m^{-2} s^{-1}
An_obs	observed An	µmol m^{-2} s^{-1}
Ca	atmospheric CO_2 concentration	Pa
Ci	CO_2 concentration at the carboxylation site	Pa
Cp	specific heat of moist air	MJ kg^{-1} ºC^{-1}
d0	the zero plane displacement of canopy	m
dp	the "preferred" zero plane displacement	m
D	vapour pressure deficit	kPa
ET	evapotranspiration	mmH_2O m^{-2}
fsoil	influence of soil water limitation on stomatal conductance	-
G	soil heat flux	W m^{-2}
gs	stomatal conductance to CO2	µmol m^{-2} s^{-1}
gw	stomatal conductance to water	µmol m^{-2} s^{-1}
hc	vegetation height	m
hs	relative humidity	-
k	PEP case rate constant for CO2	-
kT	intermediate variable	-
Kc	Michelis-Menten constant for enzyme catalytic activity for CO2	Pa
Kh	the eddy diffusion coefficient at the top of canopy	-
Ko	Michelis-Menten constant for enzyme catalytic activity for O_2	kPa
LAI	leaf area index	m^2 m^{-2}
M	the flux determined by the rubsico and light limited capacities	µmol m^{-2} s^{-1}
n	eddy diffusivity decay constant	-
P	atmospheric pressure	Pa
PAR	photosynthetic active radiation	µmol m^{-2} s^{-1}
PMc	intermediate variable	mmH_2O m^{-2}
PMs	intermediate variable	mmH_2O m^{-2}
Ra	intermediate variable	kPa ºC^{-1} s m^{-1}
raa	aerodynamic resistance from canopy to reference height	s m-1
rac	boundary layer resistance	s m-1
Rad	solar radiation	W m^{-2}

Symbol	Description	Unit
ras	aerodynamic resistance from soil to canopy	s m^{-1}
rb	intermediate variable	-
Rc	intermediate variable	kPa $ºC^{-1}$ s m^{-1}
rc	stomatal resistance	s m-1
Rd	nonphotorespiratory respiration	μmol m^{-2} s^{-1}
Rn	net radiation above canopy	W m^{-2}
Rns	net radiation to soil surface	W m^{-2}
Rs	intermediate variable	kPa $ºC^{-1}$ s m^{-1}
rsc	canopy stomatal resistance	s m^{-1}
rss	soil resistance	s m^{-1}
RT	intermediate variable	μmol m^{-2} s^{-1}
swc	soil water content in the top layer	m^3 m^{-3}
swcs	saturated soil water content	m^3 m^{-3}
T	air temperature	ºC
u	wind speed	m s^{-1}
u*	friction velocity	m s^{-1}
Vc	rate of carboxylation	μmol m^{-2} s^{-1}
Vcmax	maximum rate of RuBP carboxylation	μmol m^{-2} s^{-1}
Vj	potential rate of RuBP regeneration capacity	μmol m^{-2} s^{-1}
Vjmax	maximum potential rate of Vj	μmol m^{-2} s^{-1}
VT	intermediate variable	μmol m^{-2} s^{-1}
w	leaf width	m
z0	the "preferred" roughness length	m
z0g	The roughness length of ground	m
za	reference height	m
Γ	CO_2 compensation point	Pa

2.3.1 Photosynthesis model

The net photosynthesis (An) of C_3 plants was calculated according to Farquhar et al. (1980):

$$A_n = V_c\left(1 - \Gamma / C_i\right) - R_d \tag{2-2}$$

where V_c is the rate of carboxylation, Γ is the CO_2 compensation point at which there is no nonphotorespiratory respiration, R_d is the rate of nonphotorespiratory respiration, and C_i is the CO_2 concentration at the carboxylation site.

The rate of carboxylation is expressed as the two limiting factors or Rubisco activity (A_c) and RuBP regeneration (A_j):

$$V_c = \min(A_c, A_j) \tag{2-3}$$

$$A_c = \frac{V_{cmax} C_i}{C_i + K_c\left(1 + O_i / K_o\right)} \tag{2-4}$$

where V_{cmax} is the maximum rate of RuBP carboxylation, K_c and K_o are Michelis-Menten constants for enzyme catalytic activity for CO_2 and O_2, respectively, and O_i is the intercellular concentration of oxygen.
The RuBP-regeneration-limited rate is defined by:

$$A_j = \frac{V_j(C_i - \Gamma)}{4C_i + 8\Gamma} \tag{2-5}$$

where V_j is the potential rate of RuBP regeneration capacity, which depends on the incident photosynthetic active radiation (PAR). V_j can be described using a nonrectangular hyperbola:

$$V_j = \frac{1}{2\theta}\left[\alpha PAR + V_{jmax} - \sqrt{(\alpha PAR + V_{jmax})^2 - 4\theta\alpha PAR V_{jmax}}\right] \tag{2-6}$$

where α is the initial quantum efficiency, Vjmax is the maximum potential rate of RuBP regeneration at quantum-saturation, and θ is the curvature of the quantum response.

In Farquhar's model, the kinetic properties of Rubisco (involving V_{cmax}, K_c and K_o) are all considered to be temperature dependent with an Arrhenius function normalized with respect to their values at 25 °C (Long, 1991; Yin and Struik 2009). A modified Arrhenius function was used to describe the response of Vcmax to temperature (Long, 1991; Medlyn et al., 2002). All involved parameter values were according to the review of Yin and Struik (2009).

It is well known that *Tamarix ramosissima* is a C_3 plant, while foliar stable carbon isotope analysis has demonstrated that *Haloxylon ammodendron* has significant features of the photosynthetic pathway of C4 species (Chen et al., 2008). An equivalent simplified model of photosynthesis for C_4 plants proposed by Collatz et al. (1992) was used to simulate the assimilation of *Haloxylon ammodendron*. Gross photosynthesis (A) is described as a function of PAR, air temperature (T), and Ci in the form of a pair of nested quadratic equations. The smaller roots of the nested quadratic equations are the appropriate solutions. Then the net photosynthetic rate is defined as the difference between A and the temperature-dependent nonphotosynthetic respiration RT. Calculation of RT is referred to Collatz et al. (1992).

2.3.2 Stomatal conductance model

Ball et al. (1987) (Ball-Berry model hereafter) concluded that stomatal conductance to water vapor (g_w) is linearly proportional to a term consisting of A_n, relative humidity (h_s), and atmospheric CO_2 pressure (C_a):

$$g_{\square} = m\frac{A_{\square}h_{\square}f_{soil}}{C_a} + g_0 \tag{2-7}$$

where m and g_0 are the slope and intercept of a linear regression, f_{soil} is the influence of soil water limitation on stomatal conductance, and is calculated from Li et al. (2006). Eq. 2-7 proved to be able to account for much of the variation in the response of stomatal conductance to temperature, light, humidity, and CO_2 for both C_3 and C_4 plants (Collatz et al., 1991). Although Leuning (1995), Yu et al. (2001), and Tuzet et al. (2003) proposed some variants of the Ball-Berry model to predict more realistic response of stomatal to environmental factors, many more parameters are required. Therefore, the Ball-Berry model is still widely used in modelling communities and in some complex terrestrial ecological models, such as ORCHIDEE (Krinner et al., 2005) and CABLE (Kowalczyk et al., 2006).

The parameter m is generally called Ball-Berry parameter. The values of m are commonly considered to be constant for specific biomes; however, numerous studies have shown that m varies with environmental factors, especially with water supply (Lai et al., 2000; Tanaka et al., 2002). The parameter g_0 is also called the residual stomatal conductance, and its value represents the stomatal conductance when photosynthesis is equal to photorespiration.

2.3.3 The coupling of photosynthesis and stomatal conductance

Another equation is introduced to relate photosynthesis and stomatal conductance to the gradient of CO_2 between the atmosphere and the carboxylation site of the leaf:

$$C_i = C_a - 1.6A_n / g_w \tag{2-8}$$

where the value of 1.6 is the ratio of water vapour diffusivity to CO_2 diffusivity. The system consisting of Eqs. 2-2 – 2-8 is commonly solved using a numerical iterative method (Collatz et al., 1991). For faster computational speed, an analytical approach can be devised by combining all equations in the system

into a form of standard cubic equation with respect to An The general analytical approach for solving a cubic equation followed that of Baldocchi (1994) and Yin and Struik (2009). The solution for An can be substituted into Eq. 2-7 to calculate g_w, and C_i from Eq. 2-8.

2.3.4 Evapotranspiration model

Because of the low vegetation coverage in the studied area of dryland, a "double source" (soil and plant) evapotranspiration model (SW) is considered for calculating the transpiration from plants and evaporation from the soil surface (Shuttleworth and Wallace 1985). The SW model integrates five resistances of the soil-plant-atmosphere continuum and formulates the total evapotranspiration (ET) from a "mixed" vegetation-soil surface. Among the five resistances that are used to implement the SW model, canopy stomatal conductance (r_{sc}) is the most direct one governing photosynthesis and transpiration. The value of r_{sc} is determined in a manner similar to that used by Shuttleworth and Wallace (1985) by upscaling leaf level stomatal resistance to canopy level:

$$r_{sc} = \frac{r_c}{2\mathrm{LAI}} \tag{2-9}$$

where r_c is the stomatal resistance of the photosynthetic leaf (calculated as the reciprocal of stomatal conductance g_w, derived from the coupling approach), and 2 is a species-specific factor to represent the mean effective LAI. The calculations of the remaining four of five resistances required to implement the SW model are adopted from Zhou et al. (2006), Shuttleworth and Wallace (1985), Brisson et al. (1998), Lin and Sun (1983), and Hess (1998).

2.3.5 Determination of photosynthetic parameters

A nonlinear search algorithm in Matlab's Optimization Toolbox (MathWorks Inc., 1999) was used to determine several of the main parameters in the model system. Given a series of Licor 6400 measured An, it is not impossible to estimate many parameters; however, in reality, it is a difficult computation task. In the present study, α was determined by fitting observed net photosynthetic rate (An_obs) to PAR less than 300 μmol m^{-2} s^{-1} as suggested by Yin and Struik (2009). Only Vcmax was selected as an estimable variable with the nonlinear search algorithm, and all others were assumed to be constant and were derived from the literature (see Table 2-1). The algorithm made utilized iteration until convergence based on:

$$\min\sum(An\_mod-An\_obs)^2 \quad (2\text{-}10)$$

where An_mod is model-predicted An with the Eqs. 2-2 – 2-8 system. Two other important parameters, Ball-Berry parameter *m* and residual stomatal conductance g_0 were determined from previous research for C_3 and C_4 plants (Collatz et al., 1992; Sellers et al., 1996).

2.3.6 Priestley-Taylor model

The Priestley-Taylor (PT) model (Priestley and Taylor, 1972) is a very simple approach to calculate surface evapotranspiration. The model is defined as:

$$ET=\alpha_{PT}\Delta(R_n - G)/(\Delta+\gamma) \quad (2\text{-}11)$$

where γ is the psychometric constant. The parameters Δ and γ are functions of air temperature, and α_{PT} is termed a Priestley–Taylor parameter.
The Priestley–Taylor parameter has a standard value of 1.26 for wet surfaces (Priestley and Taylor, 1972; Stannard, 1993). However, in practice, varies widely with different vegetation types, soil moisture conditions, and strength of advection (Nichols et al., 2004). Flint and Childs (1991) reported a wide range of values, from 0.7 to 1.6. Numerous studies have shown that the value of 1.26 is suitable for potential conditions only and is invalid under advective or water-stressed conditions (Pereira and Nova, 1992; Li and Yu, 2007). To apply the PT model for estimating actual evapotranspiration, has to be refined as a linear function of soil moisture (Flint and Childs, 1991; Fisher et al., 2005),

$$\alpha_{PT} = a_{PT}swc + b_{PT} \quad (2\text{-}12)$$

where swc is soil water content of the top layer of soil, a_{PT} and b_{PT} are empirical coefficients, which are determined by same procedure as V_{cmax} with Eq. 2-10.

2.4 Results

2.4.1 Response of transpiration to meteorological variables

Transpiration rates of both species are dependent on solar radiation (Rad), relative humidity (h_s), air temperature (*T*), and wind speed (*u*) (Figure 2-4). On the whole, Rad explained 60% and 43% of the measured transpiration for *Tamarix ramosissima* and *Haloxylon ammodendron*, respectively, and hs and T explained 23% and 25% of the variance of the measured transpiration for

Tamarix ramosissima (Figure 2-4 and Table 2-3). For *Haloxylon ammodendron*, 43% and 34% of the variances of measured transpiration could be explained by h_s and T. The correlation coefficients between the transpiration and u for both shrubs are relatively small but still statistically significant ($p<0.01$). Generally, the responses of transpiration rate for both species to Rad levels are comparable because the slopes of linear regressions between transpiration and Rad are the same (0.0002). The variations of transpiration under different Rad are similar. In contrast, under conditions of low h_s and high T, the variations of transpiration rates of the two species are apparently larger than those under low T and high h_s, indicating that other meteorological factors, for example Rad, may dominate the rate of transpiration for both shrubs. The slope values of the linear regression between transpiration and h_s are -0.27 and -0.12, and those between transpiration and T are 0.0065 and 0.0052 for Tamarix ramosissima and Haloxylon ammodendron, respectively (Figure 2-4 and Table 2-3). The inter-species differences indicate that the responses of transpiration to h_s and T are different for the two desert shrubs.

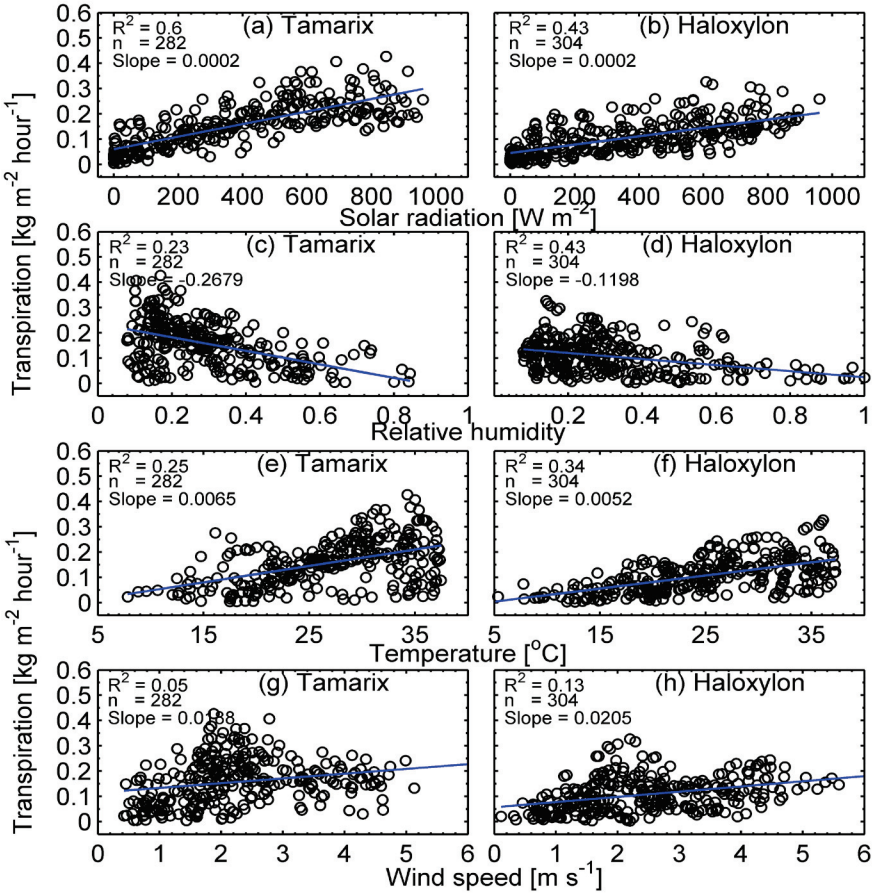

Figure 2-4. Responses of measured transpiration to solar radiation (Rad), relative humidity (h_s), and air temperature (T) on experimental days for *Tamarix ramosissima* (a, c, e) and *Haloxyon ammodendron* (b, d, f) in 2004.

Table 2-3. Statistics of linear correlationship between transpiration and meteorological variables. R_{ad}, T, h_s, and u are solar radiation, air temperature, relative humidity, and wind speed, respectively. R^2 and Slope represent the square of the correlation coefficient and the slope of the linear regression equation between transpiration and meteorological variable. n is the number of data.

	Tamarix				*Haloxylon*			
	R_{ad}	T	h_s	u	R_{ad}	T	h_s	u
n	282	282	282	282	304	304	304	3404
R^2	0.60	0.23	0.25	0.05	0.43	0.43	0.34	0.13
Slope	0.0002	-0.2679	0.0065	0.0188	0.0002	-0.1198	0.0052	0.0205

The measured maximum transpiration rate of *Tamarix ramosissima* is slightly larger than that of *Haloxylon ammodendron*, with average values of 0.46 and

0.37 kg m^{-2} $hour^{-1}$, respectively. This indicates that *Tamarix ramosissima* potentially transpires more water in similar survival habitats in the study area. The differences between the two species in the correlations between transpiration and meteorological variables, indicated by R^2, demonstrate that Rad is the primary forcing factor dominating leaf transpiration at the hourly scale for *Tamarix ramosissima* at the study site. However, *Tamarix ramosissima* has a weaker correlation with h_s and T than that does *Haloxylon ammodendron*.

2.4.2 Initial quantum efficiency and maximum carboxylation rate

The initial quantum efficiency of *Tamarix ramosissima* is larger than that of *Haloxylon ammodendron*, 0.0235 versus 0.0164 (Figure 2-5). This implies that *Tamarix ramosissima* may rapidly increase its photosynthesis when PAR increases from weak to strong in the morning, and *Haloxylon ammodendron* may increase it more gradually with PAR. Under weak solar radiation, *Tamarix ramosissima* has stronger photosynthesis than *Haloxylon ammodendron*.

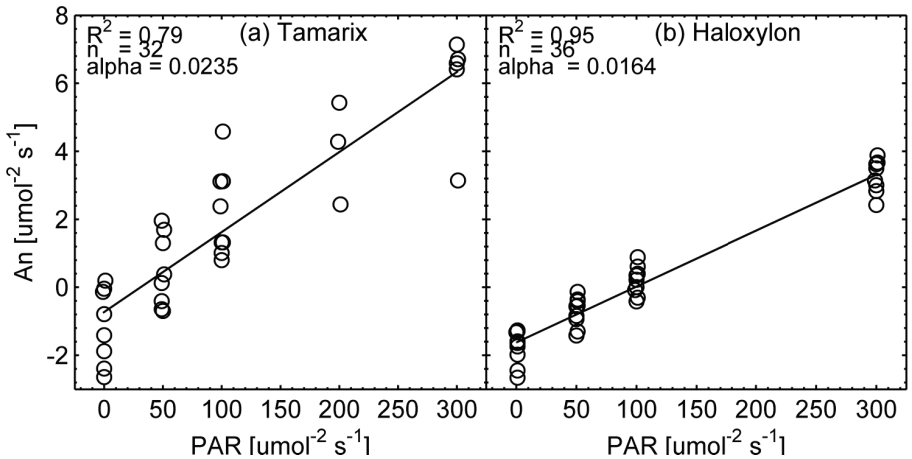

Figure 2-5. Determination of initial quantum efficiencies (alpha) for *Tamarix ramosissima* (a) and *Haloxylon ammodendron* (b) based on the measured net photosynthesis rate (An_obs) and photosynthetic active radiation (PAR) in the range of 0-300 μmol m^{-2} s^{-1} in Central Asia.

Based on least square error algebra, V_{cmax} was inversely fitted by the measured net photosynthesis (Figure 2-6). During the active growing period, V_{cmax} of *Tamarix ramosissima* presented obviously dynamic variations. From DOY 150 to 220, V_{cmax} gradually increased from a low value of 10 μmol m^{-2} s^{-1} to a high value of 25 μmol m^{-2} s^{-1} in our experiments. After DOY 220, V_{cmax} dropped to

around 10 μmol m-2 s-1. In contrast, *Haloxylon ammodendron* maintained a relatively constant maximum carboxylation rate, 15 μmol m^{-2} s^{-1}, during the investigated period. Therefore, the value of V_{cmax} for *Haloxylon ammodendron* was set at a constant 15 μmol m^{-2} s^{-1}. The daily value of V_{cmax} for *Tamarix ramosissima* was derived by interpolating the two segments (before and after DOY 220) of the linear regression and was used for the coupled photosynthesis-stomatal conductance-transpiration modelling.

Overall, *Tamarix ramosissima* has obviously higher initial quantum efficiency and maximum carboxylation ability, hence higher stomatal conductance and transpiration rate, than *Haloxylon ammodendron*. This supports the results derived in Section 2.3.2 (comparing Figures 2-5 and 2-6 with Figure 2-4).

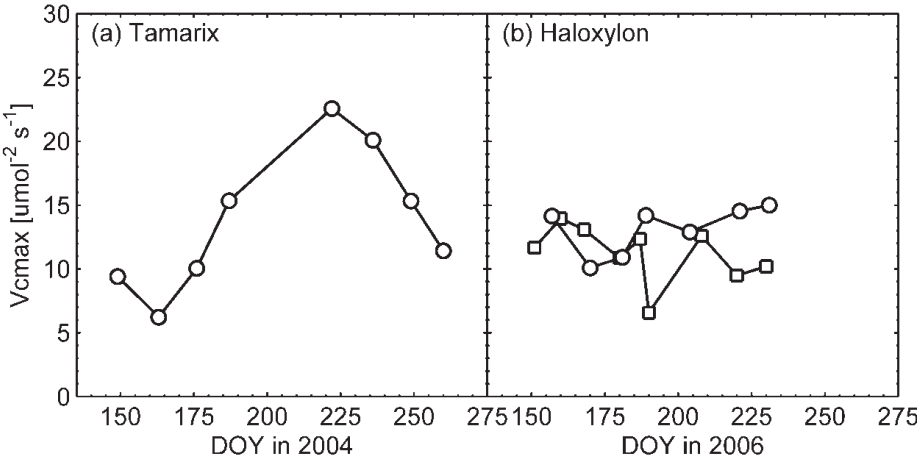

Figure 2-6. Seasonal course of the fitted maximum carboxylation rates (V_{cmax}) of *Tamarix ramosissima* (a) and *Haloxylon ammodendron* (b) at two sites, Wujingnan (circle) and Beishawo (square), in Central Asia.

2.4.3 Diurnal patterns of the measured and simulated transpirations

The time series of half-hourly measured and simulated transpirations show close agreement (Figure 2-7). The SW model reproduces well the transpirational rate of both species in response to meteorological variables. Measured transpiration of *Tamarix ramosissima* on a very sunny day, for example DOY 218, was obviously greater than that on a partially cloudy day (DOY 245) because of the difference in solar radiation. The simulated peak transpirations under both meteorological conditions are very comparable.

The difference in the measured transpirations between the two species was well resolved by the model. Modelled transpiration for *Tamarix ramosissima* was generally larger than that for *Haloxylon ammodendron*, as shown by the measurements. The R^2 values between measurement and simulation are 0.61 and 0.52, with RMSE of 0.06 and 0.07 kg m^{-2} $hour^{-1}$ for T*amarix ramosissima* and *Haloxylon ammodendron*, respectively (Table 4). The slopes of the linear regression between the measured and simulated transpiration values for *Tamarix ramosissima* and *Haloxylon ammodendron* are very close to the 1:1 line, 0.90 and 0.97, respectively. However, the modelled peak transpirations in daytime deviate far from the measurements, such as on DOY 208 and 234. The model deficiency on these occasions may result from the calculation of stomatal conductance using a coupled approach. Under the condition of very high solar radiation, photoinhibition effects on stomatal opening could limit the transpiration (Yu et al., 2002). Under very low humidity, the feedback mechanism between stomatal conductance and humidity could vary in a way that is yet not clear to us (Collatz et al., 1992).

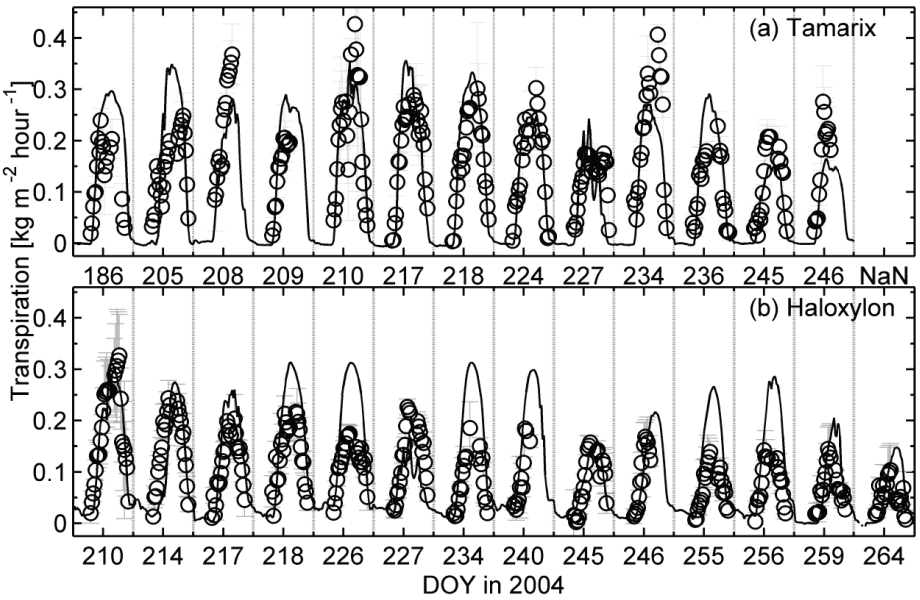

Figure 2-7. Comparisons between half-hourly measured and simulated transpiration rates for *Tamarix ramosissima* and *Haloxylon ammodendron*. DOY represents day of year in 2004. Blue lines indicate the simulation and circles the measurements. Error bar attached to the circle stands for one standard deviation computed by 3 to 5 repetitive measurements.

2.4.4 Comparisons between the measured and simulated daily canopy evapotranspiration and soil evaporation

We used the same parameters as those used in section 2.4.4 and applied them to the Shuttleworth-Wallace model for the entire year of 2004. The simulated daily evapotranspiration produced by the model agrees well with the evapotranspiration observed by eddy covariance (Figure 2-8a). The square of the correlation coefficient (R^2) between the observations and the simulations is 0.78, the RMSE is 0.25 mm day^{-1}, and the slope is 0.88 (Table 2-3). The SW model perfectly captured the seasonal dynamics of the evapotranspiration over a sparse desert shrub canopy. The SW model accurately described the response of evapotranspiration to the variation of solar radiation (Figure 2-8b), as shown by the measurements.

Soil evaporation simulated by the SW model showed good agreement with the values observed by micro-lysimeter (R^2=0.57, RMSE=0.14 mm day^{-1}). In particular, the simulated soil evaporation exactly described the response of soil evaporation to soil moisture increase by precipitation. During the period DOY 143-163, no precipitation event occurred (Figure 2-8b), and both observed and simulated soil evaporation continuously decreased as the top layer of soil became drier. On days 201 and 202, significant precipitation occurred, and soil evaporation increased, a change that was reproduced well by the SW model.

Table 2-4. Statistics of the comparisons between the simulated and the observed leaf transpiration, evaporation and soil evaporation. R^2, Slope and RMSE represented the square of correlation coefficient, the slope of linear regression equation and root mean square error between the simulated and the observed values, respectively. NA indicated that the model is not applicable for estimating the variables explicitly.

Variables	Shuttleworth-Wallace			Priestley-Taylor		
	R^2	Slope	RMSE	R^2	Slope	RMSE
Leaf transpiration for C_3 plant	0.61	0.90	0.06 mm h^{-1}	NA	NA	NA
Leaf transpiration for C_4 plant	0.52	0.97	0.07 mm h^{-1}	NA	NA	NA
Soil evaporation	0.57	0.89	0.14 mm d^{-1}	NA	NA	NA
Evapotranspiration	0.78	0.88	0.25 mm d^{-1}	0.65	0.67	0.3 mm d^{-1}

2.4.5 Comparison between Shuttleworth-Wallace and Priestley-Taylor models

Compared to the SW model, the PT model severely overestimated evapotranspiration during the entire year when the standard value of (1.26) was used. Evapotranspiration results from the PT model were 5.1 times the eddy covariance observations on average (data not shown). With same procedure to derive Vcmax, the parameters aPT and bPT were determined by implying Eq. 2-10 to Eq. 2-11, and the derived values for a_{PT} and b_{PT} are 0.35 and 0.14, respectively. The average value for across the year of 2004 was 0.16, which is lower than any reported value from previous studies.

A modified PT model could reasonably reproduce the evapotranspiration during some short segments (DOY 100-190 and DOY 220-270) of a year (Figure 2-8a). Before DOY 100 and after DOY 270, the PT model overestimated evapotranspiration. During DOY 190-220, the PT model obviously underestimated evapotranspiration. As shown in Figure 2-8b, both solar radiation and air temperature have obvious seasonal dynamics, and the PT-simulated evapotranspiration showed obvious seasonality as well; however, the PT-simulated evapotranspiration did not match the measurements very well. This indicates that the PT model performed much worse than the SW model. This is because the PT model considered only the effects of available energy, air temperature, and soil moisture, whereas our experiments showed that transpiration (the dominant component of evapotranspiration) by the desert shrubs depended strongly on relative humidity and wind speed (Figure 2-4) as well. More important, stomatal conductance in the modified PT model was implicitly considered as a linear function of soil moisture, which seemed not sufficient for desert shrubs. The SW model integrated all factors; therefore, it yielded good estimates for evapotranspiration.

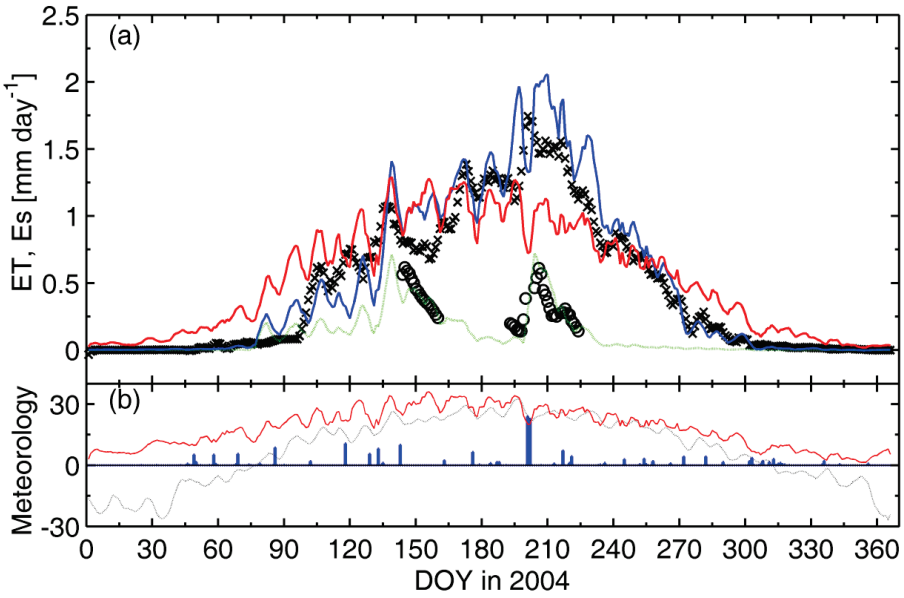

Figure 2-8. Comparisons between simulated and observed soil evaporation and evapotranspiration (a) and main meteorological variables (solar radiation, air temperature, and precipitation) (b) in 2004. All variables are smoothed over consecutive 5 days. Red, blue, and green solid lines in panel a represent the evapotranspiration (ET) from the modified Priestley-Taylor model, the Shuttleworth-Wallace model, and the soil evaporation (Es) from the Shuttleworth-Wallace model. The symbols "×" and "o" indicate observed evaporation and soil evaporation, respectively. The vertical bars in panel b represent precipitation (mm), and the dotted and solid lines indicate air temperature (°C) and solar radiation (×10 W m^{-2}).

2.5 Discussion and Conclusion

The primary goal of this study was to find a modeling approach for evapotranspiration that can be effectively applied in desert ecosystems where shrubs are sparsely distributed. The main motivation came not only from this feature of sparse coverage but also from many aspects of special ecophysiological responses and morphological adjustments to the extremely arid environment. For this purpose, a coupled model of stomatal conductance, photosynthesis, and transpiration was constructed. Two of the required parameters were well determined from experiments, and the rest were derived from the literature. The experimental results showed that *Tamarix ramosissima* has a higher assimilation capacity in terms of initial quantum efficiency and maximum carboxylation rate than *Haloxylon ammodendron*. They also showed that *Tamarix ramosissima* had varied maximum carboxylation rate during the growing period but that *Haloxylon ammodendron* had a relatively constant

photosynthetic potential. In Central Asian desert ecosystems, climate is characterized by high solar radiation, temperature, and atmospheric evaporative demand and by scarce precipitation and low humidity. It is found that solar radiation is the dominant forcing factor governing transpiration for both shrubs at the hourly time scale. Solar radiation is able to explain 60% and 43% of the variance of the measured transpiration for *Tamarix ramosissima* and Haloxylon *ammodendron*, respectively. However, *Tamarix ramosissima* is shown to be less sensitive to temperature and humidity than *Haloxylon ammodendron*. Moreover, plant transpiration by *Tamarix ramosissima* is slightly larger than by *Haloxylon ammodendron* and *Tamarix ramosissima* has a weaker correlation with hs and T than that does *Haloxylon ammodendron* (Figure 2-4). These results indirectly reflect the fact that *Tamarix ramosissima*, to a great extent, is more dependent on groundwater depth than *Haloxylon ammodendron* because *Tamarix ramosissima* has a significantly deeper root distribution than *Haloxylon ammodendron* (Xu et al., 2007; Xu and Li, 2008). The weaker dependency of transpiration of *Tamarix ramosissima* on hs and Ta also supports the report by Xu et al. (2007) about different water use strategies: the deep-root shrub *Tamarix ramosissima* is sustained mainly by groundwater, while the medium-depth-root shrub *Haloxylon ammodendron* is sustained partly by groundwater and partly by precipitation.

The SW model captured well the diurnal pattern of leaf transpiration and seasonal dynamics of soil evaporation and total evapotranspiration. It explained 61% and 52% of the variance of the measured transpiration for *Tamarix ramosissima* and *Haloxylon ammodendron*, respectively. The apparent discrepancy of diurnal simulations of leaf transpiration between the model and measurement could result from several factors. One of the principle reasons lies in the experimental method. The abscission measurement, using a simple weighing method, involved cutting of the leaf from the stem and determination of the water loss by weighing within a few minutes to determine the transpiration rate. Although previous study has demonstrated the validity of the abscission approach (Huang et al., 2009) under certain conditions, some errors or uncertainties may be easily induced, including exceptional short responses of the twigs to drought stress, secondary responses due to wounding, and under-representation of midday measurements. The second reason for the mismatch between the simulation and measurement may lie in the calculation of the stomatal conductance, the so-called Ball-Berry stomatal conductance. The stomatal conductance parameter (m in Eq. 7) has been shown to vary with

growth stage and environmental factors in other vegetation, such as grasses (Wolf et al., 2006), trees (Kenzo et al., 2006), and crops (Mo et al., 2008). In the present research, it was assumed to be constant, and this assumption may have led to some errors. Finally, deep soil moisture or groundwater table depth can affect the rate of transpiration (Gries et al., 2003; Cui et al., 2010), but this was not taken into account in the present modelling because of the unavailability of soil moisture data from different layers of the soil profile. In spite of these limitations, however, the SW model performed very well for daily soil evaporation and total evapotranspiration and thus can be viewed as a promising approach for estimating evapotranspiration over desert ecosystems in Central Asia.

Compared to the complex SW model, the PT model, is a very simple one for estimating canopy evapotranspiration and could not reasonably predict the evapotranspiration over desert shrub canopy. The original PT model with is suitable only for estimating potential evapotranspiration, i.e., under a condition of no water stress. Essentially, the original PT model is based on the assumption that the effect of turbulence on evapotranspiration is small compared to the effect of radiation, so the aerodynamic and canopy resistances are considered to be zero (Li and Yu, 2007). However, the desert ecosystem in Central Asia is commonly in a condition of high water stress, low atmospheric relative humidity, and low soil moisture. A modified PT model with inclusion of soil moisture effect on the PT parameter () was still not able to give good estimates of evapotranspiration for desert shrub. This suggested that a linear relationship between and soil moisture was not sufficient for desert shrubs. All of these factors could explain the deficiency in the application of the PT model to desert shrubs over Central Asia.

Although numerous studies have been conducted on desert shrubs in arid or semiarid regions over the world (Gay and Fritschen, 1979; Cleverly et al., 1997a, b; Wohlfahrt et al., 2008; Hayes et al., 2009), there are still many unknowns for ecologists, especially for modelling communities. Lack of good quantification over desert ecosystems undoubtedly causes large uncertainties in hydrological and carbon-cycling research because arid and semiarid biomes make up over 30% of the Earth's land surface. In the face of climate change, with water resources becoming increasingly scarce and competing use by other sectors increasing, investigation of water consumption by desert phreatophytic vegetation becomes crucial to maintaining the stability and sustainability of

dryland ecosystems, especially in regions close to oasis ecosystems where large amounts of groundwater are extracted for agricultural irrigation. The increase in groundwater table depth may exert substantial effects to constrain the expansion and survival of the deep-root shrub *Tamarix ramosissima* because precipitation may not be too beneficial to its water supply (Xu et al., 2007).

This paper contributes to the body of literature reporting physiological characteristics and application of the Shuttleworth-Wallace model to hydrological and carbon-cycle modelling of Central Asian desert shrubs. The results are applicable to similar biomes in other arid or semiarid regions such as northern Australia, western America, and northwestern Mexico, where introduced saltcedar has become a dominant or subdominant species that may produce profound effects on species constitution and hydrological cycling in these dryland ecosystems (Smith et al., 1998, Stromberg and Chew, 2002, Hayes et al., 2009).

Chapter 3

Growing Season Net Ecosystem CO_2 Exchange over Central Asian Desert Ecosystems*

* This chapter is based on:
Li LH*, Chen X, van der Tol C, Luo GP, Su ZB (2014) Growing season net ecosystem CO_2 exchange of two desert ecosystems with alkaline soils in Kazakhstan. Ecology & Evolution 4(1): 14-26.

Abstract

Central Asia is covered by vast desert ecosystems, and the majority of these ecosystems have alkaline soils. Their contribution to global net ecosystem CO_2 exchange (NEE) is of significance simply because of their immense spatial extent. Some of latest research reported considerable abiotic CO_2 absorption by alkaline soil, but the rate of CO_2 absorption has been questioned by peer communities. To investigate the issue of carbon cycle in Central Asian desert ecosystems with alkaline soils, we have measured the NEE using eddy covariance (EC) method at two alkaline sites during growing season in Kazakhstan. The diurnal course of mean monthly NEE followed a clear sinusoidal pattern during growing season at both sites. Both sites showed significant net carbon uptake during daytime on sunny days with high photosynthetically active radiation (PAR) but net carbon loss at nighttime and on cloudy and rainy days. NEE has strong dependency on PAR and the response of NEE to precipitation resulted in an initial and significant carbon release to the atmosphere, similar to other ecosystems. These findings indicate that biotic processes dominated the carbon processes and the contribution of abiotic carbon process to net ecosystem CO_2 exchange may be trivial in alkaline soil desert ecosystems over Central Asia.

3.1 Introduction

Worldwide paucity of measurements of net ecosystem CO_2 exchange (NEE) in desert and semiarid ecosystems limits our understanding on their contributions to global atmospheric carbon cycle (Falge et al., 2002). In the last few years, more and more measurements of NEE have been implemented in some desert and semiarid ecosystems, including Majove Desert in US (Wohlfahrt et al., 2008), Baja California desert shrub ecosystem in in Mexico (Belle et al., 2012; Hastings et al., 2005), Burkina Faso shrub savanna in West Africa (Bruemmer et al., 2008), temperate desert steppe (Shao et al., 2013; Yang et al., 2011) and desert shrub ecosystems (Gao et al., 2012; Liu et al., 2012a; Liu et al., 2012b) in China. The data from these sites indicate that the carbon sequestration capacity by desert and semiarid ecosystems varies over a wide range. Some papers reported considerably high net carbon uptake by desert ecosystems (Jasoni et al., 2005; Wohlfahrt et al., 2008), and pointed out that desert ecosystem CO_2 exchange may be more important than previously thought.

Alkaline soils are widely distributed in desert ecosystems, especially around oasis croplands and in areas along dryland rivers where evaporation is quite high but rainfall is low. At the southern periphery of the Gubantonggut Desert in western China, where oasis agriculture is practiced, alkaline soils were reported to have large ability to sock CO_2 from atmosphere in an inorganic form, as concluded from a night time downward pointed net flux (Xie et al., 2009). Serrano-Ortiz et al. (2010) reviewed abiotic CO_2 processes in the terrestrial carbon cycle and confirmed that inorganic CO_2 absorption in alkaline soils can indeed be significant. These findings, combined with other recent papers reporting a high carbon sequestration by desert ecosystems, raise the question whether the long-sought “missing carbon sink” for global carbon cycle can be located in the desert and in semiarid ecosystems (Stone, 2008). However, Schlesinger et al. (2009), by comparing with previous measurements, argued that desert net ecosystem production and carbon pool have been largely overestimated, and that the carbon absorption rates by alkaline soils as reported by Xie et al. (2009) are physically impossible.

Eddy covariance (EC) techniques have commonly been used to measure the NEE between the terrestrial ecosystem and the atmosphere during the past few decades. Although more than 950 site years of eddy covariance (EC) data has been collected in the international network of FLUXNET (Williams et al., 2009) and the size of EC data is still climbing year by year, data from Central

Asian are still unavailable, resulting in great uncertainties in the carbon sequestration capacity of Central Asian desert ecosystems. Central Asian desert ecosystems account for a large proportion of global dryland area. Due to the high evaporation-precipitation ratio, most of the soils are alkaline with high pH. This offers a good opportunity to investigate the Central Asian desert ecosystem production and employ their contribution to the global land-atmosphere CO_2 exchange.

The first objective of this paper is to quantify the growing season NEE of two desert ecosystems with alkaline soils in Kazakhstan using EC techniques. The second objective is to test the hypothesis that desert ecosystem with alkaline soils act as a carbon sink at night during growing season. For this purpose we analyze half-hourly mean NEE data at daytime and nighttime. Finally, this paper investigates the responses of NEE to meteorological variables and soil moisture and temperature, in order to interpret the magnitude of maximum uptake ability of CO_2 absorption by alkaline soil.

3.2 Materials and Methods

3.2.1 Site descriptions

We selected two sites in Kazakhstan. One site is close to Aral Sea and the other is close to Balhash Lake (Figure 3-1). Both sites are representative of Central Asian desert ecosystems, and both are dominated by alkaline soils, as one can be visually recognize from satellite images (Figure 3-1).

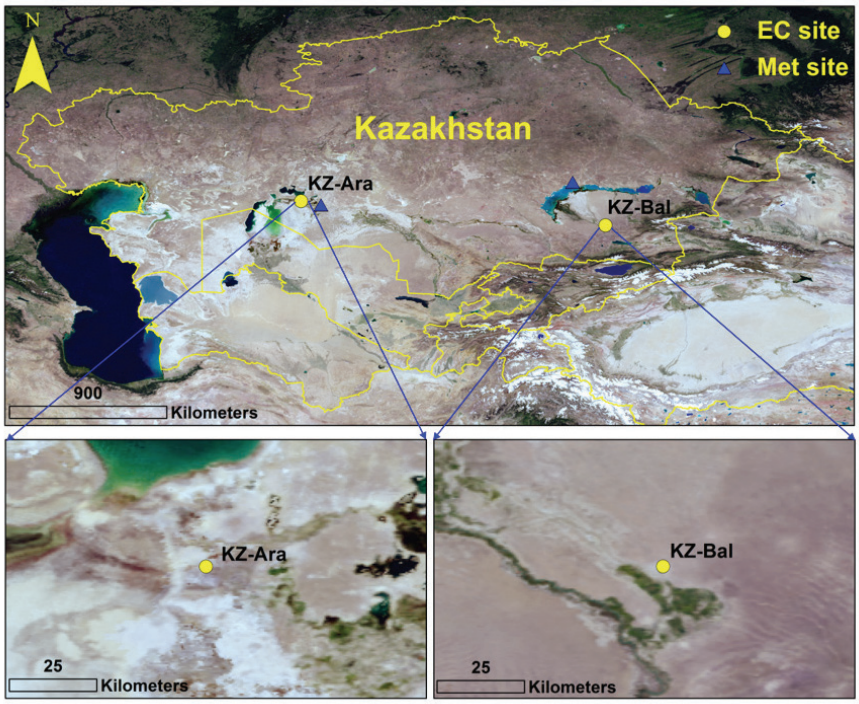

Figure 3-1. Study area and location of the two eddy covariance (EC) sites in Kazakhstan. Alkaline soil was visually recognized by white pixels in desert regions from satellite image.

The Aral Sea site (KZ-Ara, 61.08°E, 45.96°N) is located northeast of the Aral Sea. During the past half century, the surface area of Aral Sea has significantly decreased by 75% (Bai et al., 2011). The KZ-Ara site is actually located at the edge of Aralkum Desert, a man-made desert formed by the desiccated seafloor of the Aral Sea. Presently the KZ-Ara site is located at 23 km from Small Aral Sea coast. Within radius of 5 km of the KZ-Ara site, no residential building or croplands are present. Both vegetation and soil are in various stages of development and temporally and spatially varied. The dominant plant species around the KZ-Ara site are meadow weed-grass, reed and tugaic vegetation (*Elaeagnus oxycarpa*, *Salix species*) in combination with xerophytic dwarf semishrub, halophytic shrub and psammophytic grasses (*Calamagrostis epigeios*, *Pseudosophora alopecuroides*, *Phragmites australis*, *Artemisia terraealbae*, *Halostachys belangeriana*, *Tamarix spp*., *Agropyron fragile*). The fraction of vegetation coverage varied from 0 to 90%, with average value about 30-40% (Breckle et al., 2012). Dominant soil type has been solonchak (medium loamy or loamy) since 1990, and the electric conductivity of soil suspension

ranged from 1.33 to 7.38. Soil pH value varied between 8.15 and 8.36 (Breckle et al., 2012). Historical climatic records from the nearest meteorological station Kazalinsk (62.16°E, 45.77°N) with long term observations showed that annual precipitation is 140.5 mm and mean annual air temperature is 8.3 °C (ftp://sidads.colorado.edu/pub/DATASETS/NOAA/G02174/).

The Balhash Lake site (KZ-Bal, 76.63°E, 44.57°N) is located between the Balhash Lake (200 km away) and the Kapshagay Reservoir (100 km away). The nearest town is Bakbakty, a town along the Ili River, 17 km north of the site. The KZ-Bal site is located at the transect between oasis croplands and original desert habitats. Around 3-5 km west of the site, irrigated crops, well-grown reed and grasses are distributed. In the south of the site, a small village is resided. Both east and north regions of the KZ-Bal site are original desert ecosystems where desert semi-shrubs, shrubs (*Haloxylon aphyllum*, *Haloxylon persicum)* and grasses (with relatively large proportion in vegetation component) are distributed. The soil in the KZ-Bal site is takyr-like saline solonchak (Starodubtsev & Truskavetskiy, 2011). Historical climatic records from the nearest meteorological station Balhash (75.08°E, 46.80°N) with long term observations showed similar amount of annual precipitation (140.2 mm) but lower mean annual air temperature (5.7 °C) compared to the KZ-Ara site (ftp://sidads.colorado.edu/ pub/DATASETS/NOAA/G02174/).

3.2.2 Eddy covariance and ancillary measurements

In order to investigate the net ecosystem CO_2 exchange of Central Asian desert ecosystems, two eddy covariance systems have been established to monitor the fluxes of CO_2, H_2O, energy and momentum at KZ-Ara and KZ-Bal in Kazakhstan in April 2012. To measure mean and fluctuating values of vertical, streamwise and lateral wind speed and temperature, a fast response (10 Hz) three-dimensional sonic anemometer thermometer (Wind Master Pro, Gill Instruments, Lymington, UK) was utilized. A fast response (10 Hz) open path gas analyzer (LI-7500, LICOR) was used to measure the mole densities of CO_2 and H_2O. Both instruments are mounted at 2.0 m above ground. The dominant wind direction at both sites was on average northeast (Figure 3-1) and thus the head of the sonic anemometer at both sites pointed towards northeast.

Raw data of the three wind components, the speed of sound, and CO_2 and H2O mole densities were acquired and stored at 10Hz by a data logger (CR5000, Campbell Sci. Inc., USA). The data are stored in the format of GHG. Each

GHG file is an archive containing the raw high-speed data (.data) and information on the study site (.metadata), both in readable text format.

Ancillary meteorological and soil measurements of relevance included photosynthetically active radiation (PAR) flux density (Li-190SA, LI-COR), air temperature and humidity (HMP45C, Campbell), downward and upward shortwave and longwave radiation (CNR-1, Kipp & Zonen, Delft, the Netherlands) at 2.0 m above ground, precipitation (TE525MM, Texas Electronics, Dallas, TX, USA). Soil temperature (TCAV, Campbell), soil moisture content (CS616, Campbell Sci.), and soil heat flux (HFP01, Hukseflux, Delft, the Netherlands) were measured at 0.20, 0.40, 0.60, 0.80 m depth below the ground. These data were recorded by the data logger at 10Hz and saved as half-hourly averages.

Up to date, available data covered the period between 30 April and 18 August 2012 at the KZ-Ara site and between 23 May and 6 Sep 2012 at the KZ-Ara site. These data will be used for analysis in this study.

3.2.3 Data processing and gap-filling

Data processing and gap-filling was carried out in three steps. Firstly, GHG files were imported into EddyPro software (version 4.0.0) to calculate out 30 min blocks of flux data. Tilt correction, turbulent fluctuation blocking, time lag compensation, spike detection and removal, and other statistical tests and spectral corrections were applied with the standard functionality of the 'Express Model' option in the software. EddyPro also outputs quality flags for all flux variables (sensible and latent heat, momentum and CO_2 fluxes) according to (Mauder & Foken, 2006). During the study period, the average gaps in CO_2 flux data were 15.7% (836 in 5328) and 30.1% (1544 in 5136) at the KZ-Ara and KZ-Bal sites, respectively.

Secondly, gap filling was applied in order to derive continuous time series of flux data, required for calculating the daily accumulated CO_2 flux and the completeness of the data. A Self Organising Linear Output map (SOLO) Artificial Neural Network (ANN) (Hsu et al., 2002) was employed to fill the gaps in the data flagged with -9999 and 2 resulting from EddyPro software. SOLO "learns" the relationship between 11 input variables (meteorological and soil related) and the interested output flux (CO2, latent or sensible heat) by using a training data set without any "bad" value. The input data are firstly

classified into 5 nodes based on Self Organising Feature Map, so that each node represents an individual region of the input space. At each node, a linear regression is implemented between input variables and the interested output flux variable. Finally, the flux time series with gaps is estimated based on a piecewise linear approximation of the training data set (Hsu et al., 2002).

In EddyPro, spikes were detected as 3 consecutive outliers, dropping outside a plausibility range defined within a certain time window moving through the time series (Vickers & Mahrt, 1997). Detected spikes are replaced by linear interpolation of neighboring values. After this outlier remover, visual inspection showed a small number of spikes remained. Although the number of these data is small, mean and accumulated flux values will be strongly affected. To eliminate this flaw in the data set, the final step of data processing is to implement a Hampel filter for detecting outliers. Outliers detected by Hampel filter with 3 times of variance were replaced with the mean values at the same time in 2 weeks.

3.3 Results

3.3.1 Climatical and meteorological conditions

Fig. 2 shows historically mean monthly precipitation and mean monthly temperature at the KZ-Ara and KZ-Bal sites. Historical annual precipitation at both sites was 140 mm, but mean monthly precipitation exhibited large variability. The KZ-Ara site received lower rainfall in summer season than the KZ-Bal site. At KZ-Bal site, low precipitation occurred in Aug-Oct. During the current study period, monthly precipitation were higher than historically mean value at the KZ-Ara site but monthly precipitation in 4 out of 5 months were obviously less than historically mean values at the KZ-Bal site (Figure 3-2a and 3-2b).

Mean monthly temperature at both sites followed a clear sinusoidal pattern in a year. The maximum temperature was 26°C and 24 °C in July and the minimum temperature was -10 °C and -15 °C in Jan at the KZ-Ara and KZ-Bal, respectively. Mean monthly temperature in 5 months (Jan – Mar, Nov – Dec) in a year was below 0 °C and mean temperature exceeding 10 °C were from May to Sep (Figure 3-2c and 3-2d). Thus we defined the period from May to Sep as growing season. In the current study period, variation of mean monthly

temperature basically followed the historical pattern except that mean temperature in Jul was lower than long term mean value at both sites.

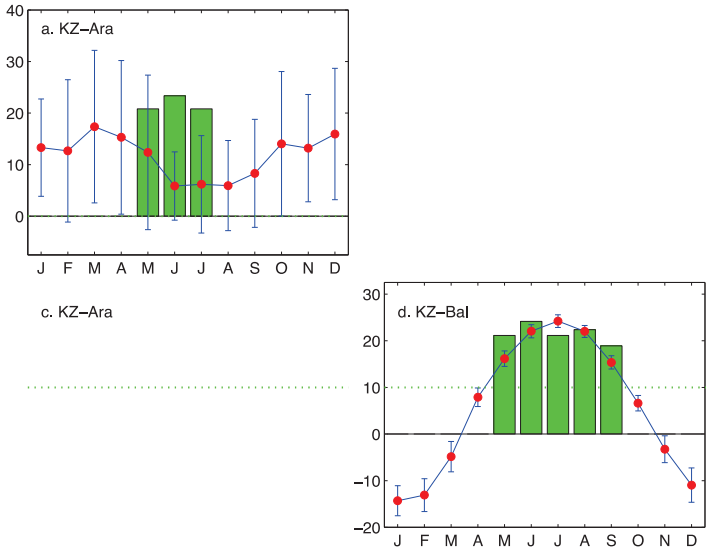

Figure 3-2. Historical (filled circle with line) and current study period mean monthly (green bars with blue outline) precipitation (a, KZ-Ara; b, KZ-Bal) and mean monthly temperature (c, KZ-Ara; d, KZ-Bal).

3.3.2 Effects of friction velocity on nighttime NEE

EC measured nighttime NEE in low turbulence conditions may be subject to systematic bias and the dependence of nighttime NEE on friction velocity (u*) could vary site by site (Anthoni et al., 2004). Relating nighttime NEE and u* helps to identify the uncertainty caused by low turbulence. At the KZ-Ara site, nighttime NEE (i.e., ecosystem respiration) was independent of u* in a broad range between 0 and 0.9 m s^{-1} as shown by a relatively horizontally linear regression between normalized nighttime NEE and u* (Figure 3-3a). A wind rose diagram showed that the dominant wind flow direction is northeast (Figure 3-3b) where vast desert region was (Figure 3-1). At the KZ-Bal site, the nighttime respiration was influenced by u*, especially under very low turbulence conditions (u*<0.15 m s^{-1}) (Figure 3-3c). The dependence of nighttime NEE on u* may be partly explained by the heterogeneous landscapes around the site (see Site descriptions) and wind direction distribution (Figure 3-3d). At the KZ-Bal site, considerable wind flows were from the west (Figure 3-3d) where oasis croplands were distributed (Figure 3-1) and hence EC measurement may be impacted. In contrast, dominant wind directions were

northeast and north, where only desert shrub communities were present (Figure 3-1) at the KZ-Ara site. However, the NEE data under low u* conditions was flagged as "bad" values and replaced by SOLO estimations. Further, the difference between the maximum and minimum normalized nighttime NEE was only 38% of the average nighttime NEE, thus the impact of the development of turbulence (u*) on nighttime respiration is apparently small. (Figure 3-3c).

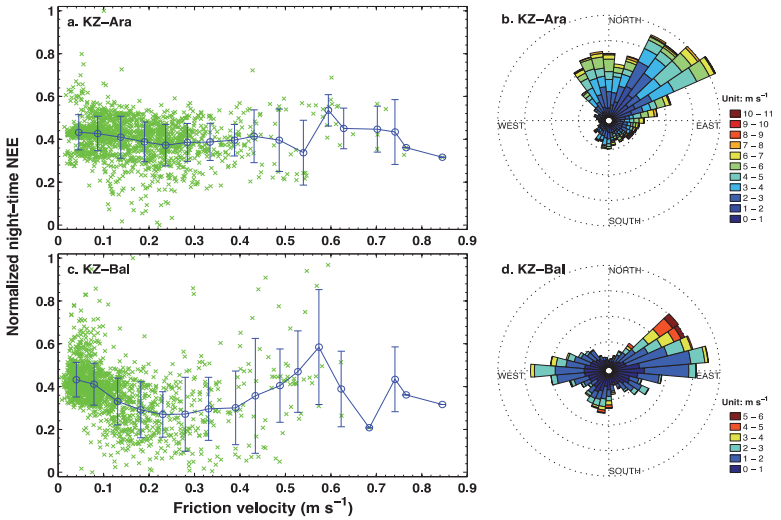

Figure 3-3. Dependence of normalized nighttime NEE (defined as the ratio of NEE-min(NEE) to max(NEE)-min(NEE)) on friction velocity (left panel), and the wind rose diagram (right panel) at the KZ-Ara and KZ-Bal sites in Kazakhstan. Symbol with 'x' represents half-hourly data during the study period, and open circle indicates bin-averages of 0.05 m s^{-1} width. Error bars refer to ±1 standard deviation.

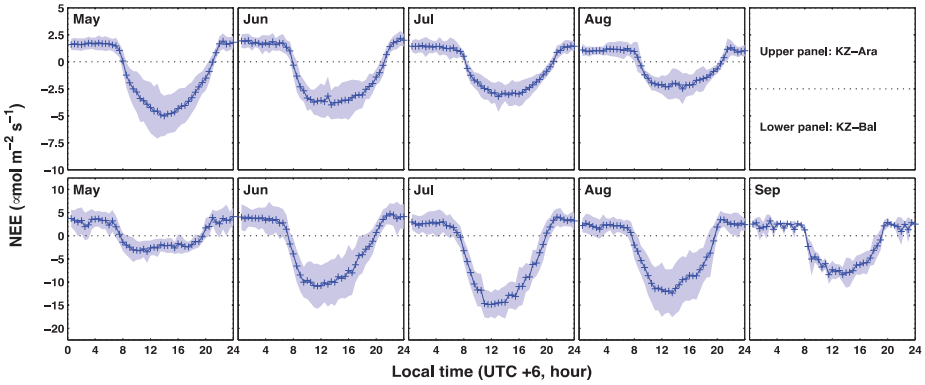

Figure 3-4. Diurnal courses of mean NEE during study months from May to Sep at the KZ-Ara (upper panel) and KZ-Bal (lower panel) sites. Shaded areas represent ±1 standard deviation.

3.3.3 Diurnal variations of NEE

The mean diurnal NEE in each month followed a clear sinusoidal dynamic during the growing season (Figure 3-4). Mean diurnal variations of NEE at each month showed a net carbon uptake (negative NEE) at daytime and a net carbon release (positive NEE) at nighttime at both sites. The peak NEE occurred at 12:00 local time for all months at both sites (corresponding to a local solar time of 10:00 for KZ-ARA and 11:00 for KZ-BAL). Diurnal maximum rates of carbon uptake varied per month, and the highest amplitudes during the study period were observed in May and July, while mean uptake rates reached up to -5.0 and -15.0 μmol m^{-2} s^{-1} at the KZ-Ara and KZ-Bal sites, respectively. The significant difference in maximum carbon uptake rates between the two sites and the difference in the month of peak carbon uptake rates were possibly related to the vegetation compositions and climatic conditions. At the KZ-Ara site, the vegetation around the site was all desert plants, shrubs or grasses and no human disturbance applied. The temperature at the KZ-Ara site is higher than that at the KZ-Bal site, which may cause earlier phenology for plants' primary production. At the KZ-Bal site, the observed NEE may be impacted by surrounding oasis crops and reed and grasses grown alongside the acequia.

Both sites show a typical pattern of net carbon uptake at daytime and net carbon release at nighttime (Figure 3-5). At the KZ-Ara site, the daytime mean monthly NEE ranged from -2.5 μmol m^{-2} s^{-1} in May to -1.1 μmol m^{-2} s^{-1} in Aug. The daytime mean NEE decreased from May to Aug. In contrast, mean monthly nighttime NEE ranged from 1.65 μmol m^{-2} s^{-1} in May and Jun to 1.0 μmol m^{-2} s^{-1} in Aug (Figure 3-5a). At the KZ-Bal site, daytime carbon uptake rates during May-Sep months ranged from -0.7 μmol m^{-2} s^{-1} in May to -7.2 μmol m^{-2} s^{-1} in July. The differences among months were obvious, and the peak carbon uptake rate was in July. The mean nighttime ecosystem respiration ranged between 2.15 μmol m^{-2} s^{-1} in Sep and 3.88 μmol m^{-2} s^{-1} in June (Figure 3-5b). At both sites, the maximum mean nighttime ecosystem respiration occurred in June, different from the months of maximum mean daytime NEE.

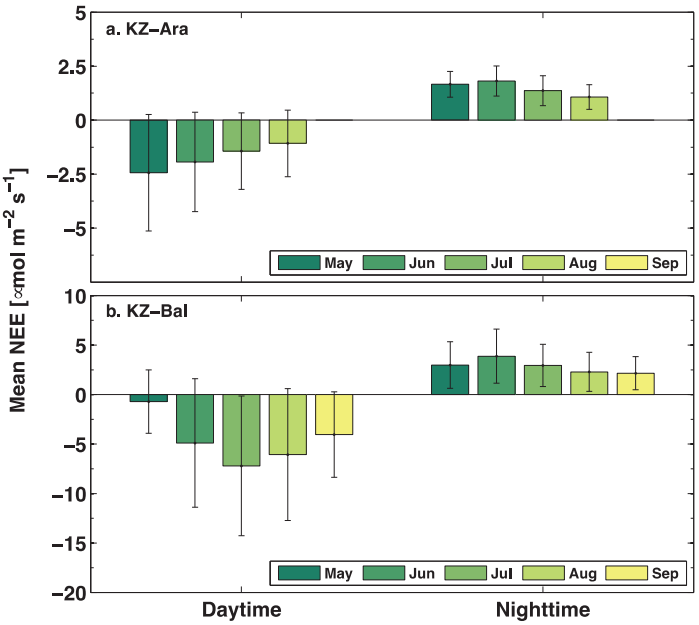

Figure 3-5. Mean monthly NEE at daytime and nighttime at the KZ-Ara (a) and KZ-Bal (b) sites. Error bars represent ±1 standard deviation.

3.3.4 Dependency of daytime NEE on PAR

The dependence of daytime NEE on PAR was assessed by fitting a first-order exponential decay model in the form of NEE (µmol m^{-2} s^{-1}) = Aexp(-PAR/B) + C (Figure 3-6) for every month. All parameters and the square of the correlation coefficient are listed in Table 1. The parameter C in the fitting equation represented the CO_2 uptake saturation threshold: its absolute value represents the maximum uptake that occurs if photosynthesis is light saturated. The sum A+C (where C has a negative and A a positive value) represents night time respiration. Monthly variations of parameter C indicate seasonal changes in maximum CO_2 uptake. A comparatively good match between the measured data and the resulted model output was derived for the months with the highest net CO_2 exchange (parameter C in the fitting equation), i.e., May (C=-5.53 µmol m^{-2} s^{-1}, R^2=0.66) at the KZ-Ara site and Jul (C=-16.36 µmol m^{-2} s^{-1}, R^2=0.82) at the KZ-Bal site (Table 3-1 and Figure 3-7a). Similarly to the absolute value of parameter C, the value of A+C is a factor three higher at the KZ-Bal site than at the KZ-Ara site (Table 3-1 and Figure 3-7d). The seasonal cycle exhibited by C is not present in A+C: nighttime respiration appears to be much more constant than daytime maximum (absolute) NEE (Figure 3-7d).

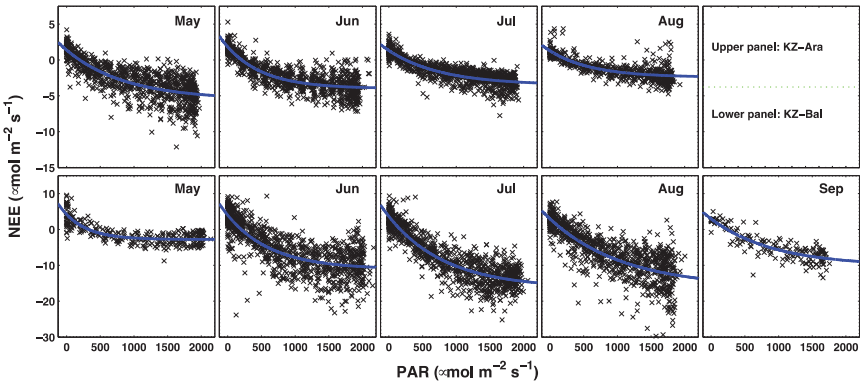

Figure 3-6. Dependency of half-hourly mean NEE on photosynthetically active radiation (PAR) during the study period (May - Sep) at the KZ-Ara (upper panel) and KZ-Bal (lower panel) sites. The blue curve was fitted with a first-order exponential decay model in the form of NEE (μmol m^{-2} s-1) = Aexp(-PAR/B) + C. All model parameters were listed in Table 1.

Table 3-1. Parameters of the exponential decay model in Figure 3-7. The model was expressed as NEE (μmol m^{-2} s^{-1}) = Aexp(-PAR/B)+C, where PAR is photosynthetically active radiation (μmol m^{-2} s^{-1}), and A, B, and C are fitting parameters. R^2 is square of correlation coefficient between the measured and modeled NEE. C represents the maximum uptake, while A+C represents night time respiration.

	KZ-Ara				**KZ-Bal**				
	May	Jun	Jul	Aug	May	Jun	Jul	Aug	Sep
A	6.91	5.81	4.81	3.68	7.01	15.05	20.01	19.1	13.13
B	874	551	777	625	358	656	845	1095	931
C	-5.53	-3.99	-3.48	-2.41	-2.81	-11.09	-16.36	-16.2	-10.18
A+C	1.38	1.82	1.33	1.27	4.2	3.96	3.65	2.9	2.95
R^2	0.66	0.74	0.76	0.62	0.68	0.63	0.82	0.66	0.79

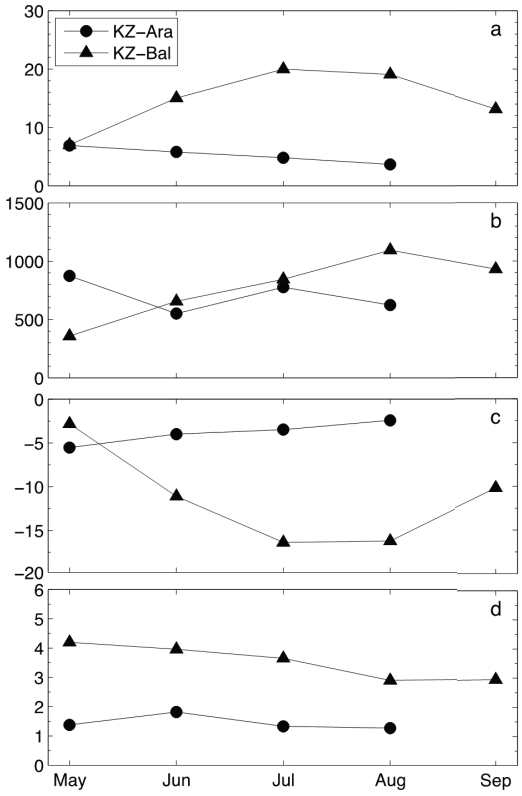

Figure 3-7. Monthly variations of parameter values in the fitted first-order exponential decay model (NEE = Aexp(-PAR/B) + C) between daytime NEE and PAR at the KZ-Ara (black circule) and KZ-Bal (blue triangle) sites. All model parameters were listed in Table 1.

3.3.5 Responses of nighttime NEE to soil temperature and soil moisture

The sensitivity of nighttime respiration was to temperature further inspected. Nighttime respiration is usually described as an exponential function (Q_{10} model) of near surface air or soil temperature (Reichstein et al., 2005; Xu and Baldocchi, 2004). In most cases, Q_{10} model has been used separately at relatively short time periods, to avoid the confounding effects of phenology and soil moisture. At the KZ-Ara site, mean nighttime ecosystem respiration does not significantly respond to soil temperature but behave relatively constant at 1.5 μmol m^{-2} s^{-1} in a wide range of soil temperature from 15 to 35 °C (Figure 3-8a). The variation of nighttime respiration tends to be large at high soil temperature, while mean nighttime respiration slightly increases with the increase in soil moisture (Figure 3-8b). At the KZ-Bal site, the response of

respiration to soil temperature exhibits an increasing trend but the dependency between them is not statistically significant (Figure 3-8c), while nighttime respiration does not significantly respond to the change in soil moisture (Figure 3-8d).

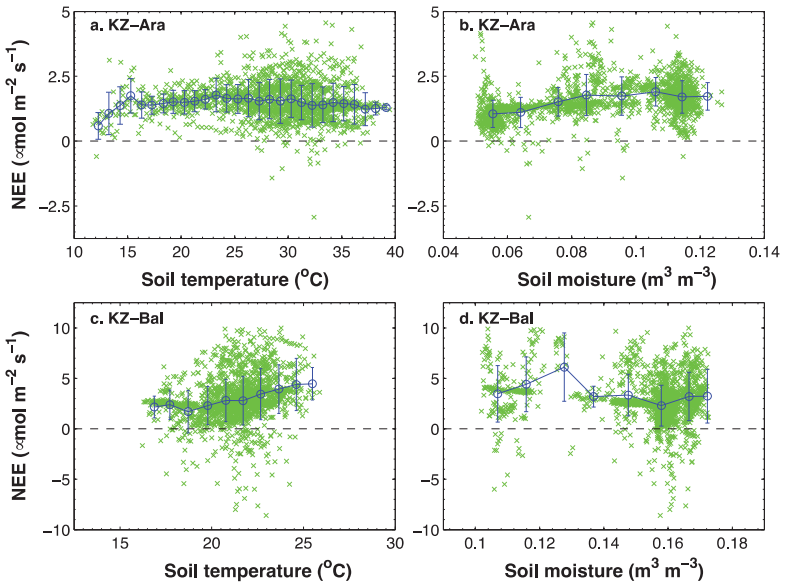

Figure 3-8. Response of half-hourly mean nighttime NEE to soil temperature and soil moisture during the study period (May - Sep) at the KZ-Ara (a and b) and KZ-Bal (c and d) sites. The blue open circle with line indicates bin-averages of 1.0 °C and 0.01 m^3 m^{-3} widths for soil temperature and moisture, respectively. Error bars refer to ±1 standard deviation.

Several attempts to fit Q_{10} models (Reichstein et al., 2005; Xu and Baldocchi, 2004) showed that neither of these models was able to represent the response of nighttime NEE to variations of soil temperature for the two sites, even after categorized soil moisture into classes (results not shown). There is a relatively wide range of soil temperature at the KZ-Ara site, and independency of respiration on soil temperature may be explained by the small carbon pool in soil profile (Breckle et al., 2012). However, the response of nighttime respiration to soil temperature is clear as the potential of nighttime ecosystem respiration in grassland is larger at the KZ-Bal site. These results indicate the determinant of ecosystem respiration in different Central Asian ecosystems could be either soil carbon pool or environmental factors.

3.3.6 Daily NEE dynamics during growing season

Fig. 9 display the dynamics of daily accumulated NEE as well as daily precipitation and mean daily PAR. Overall, carbon uptake rates of the Aralkum desert at the KZ-Ara site were lower than those at the KZ-Bal site. At both sites, daily NEE showed high variability during growing season, indicating that they are highly sensitive to the changes in environmental factors such as PAR and precipitation. The maximum daily NEE can reach up to -3 gC m^{-2} day^{-1} at the KZ-Ara site (Figure 3-9a), and daily NEE can exceed -8 gC m^{-2} day^{-1} at the KZ-Bal site (Figure 3-9b). Correspondingly, the magnitude of carbon loss on and after cloudy or rainy days at the KZ-Bal site was higher than that at the KZ-Ara site. Daily NEE at both sites can exhibit negative values, i.e. net carbon uptake, on sunny days with high PAR (> 600 µmol m^{-2} s^{-1}). On cloudy or rainy days, daily NEE at both sites tended to be positive, i.e. net carbon release to the atmosphere. For instance, consecutive rainfall on the days 23-24 June caused noticeable carbon loss at the KZ-Ara site. Similarly, 5 consecutive days of rainfall from 30 May to 3 Jun led to consecutively significant and considerable carbon release (0.5 to 3.5 gC m^{-2} day^{-1}) into the atmosphere at the KZ-Bal site. On other cloudy days, for example, the day on 27 May at the KZ-Ara site with low PAR of 250 µmol m^{-2} s^{-1} showed a net carbon loss.

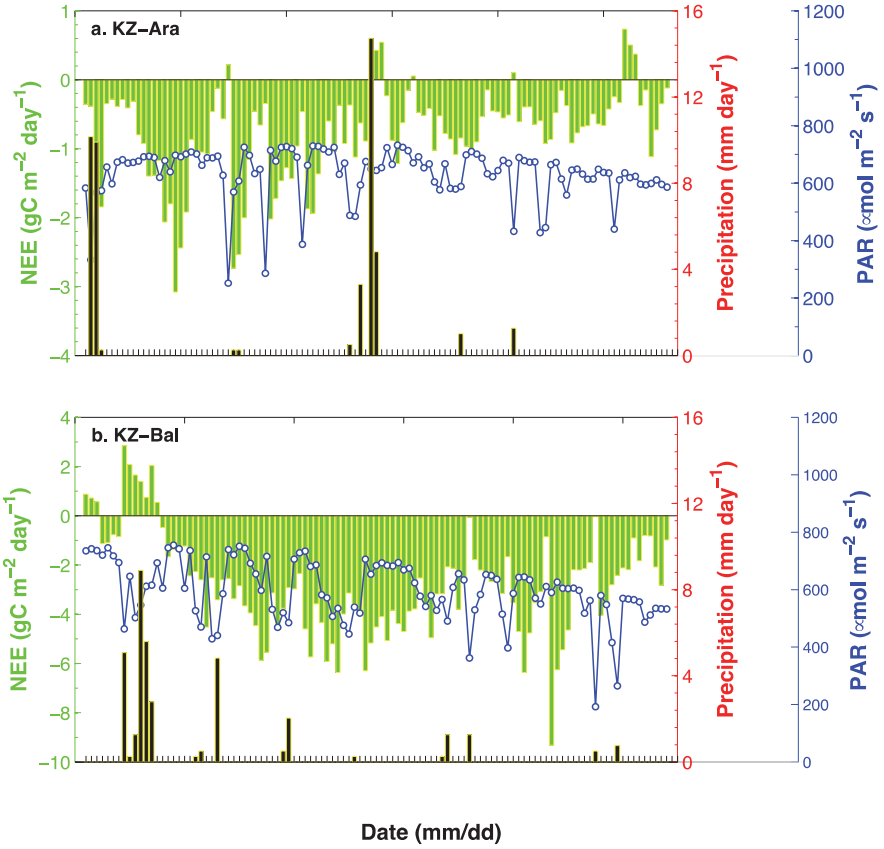

Figure 3-9. The daily NEE (green bar) accumulated by half-hourly values and daily precipitation (black bar with green outline) as well as mean daily PAR (blue line with open circle) during growing season at the KZ-Ara (a) and KZ-Bal (b) sites.

3.4 Discussion

During the past decade, the net ecosystem CO_2 exchange from desert areas has received much attention. Underlying reasons may come from the vast extent of arid and semiarid ecosystems in terrestrial ecosystems (Dregne, 1983), and the high variability of net ecosystem CO_2 exchange which is strongly dependent on climatic conditions, especially precipitation (Bell et al., 2012). Moreover, Wohlfahrt et al. (2008) reported that desert ecosystem in Mojave Desert of USA can act as a strong carbon sink whose capacity could be compared with many forests. Almost at the same time, a similar finding was reported in Gubantonggut Desert in China, where the strong carbon sink was attributed to CO_2 absorption by alkaline soil at night-time (Stone, 2008; Xie et al., 2009). Although lots of research can support the existence of carbonate dissolution (i.e.

abiotic process) in alkaline soils (Serrano-Ortiz et al., 2010), the rate of carbon uptake reported by Xie et al. (2009) were questioned by Schlesinger et al. (2009).

The growing season net ecosystem CO_2 exchange data that we have measured are the first data for desert ecosystem with alkaline soils in Kazakhstan which may offer, to certain extent, improved understanding on the carbon sequestration capacity of desert ecosystems in Central Asia. Although Liu et al. (2012a) have reported the annual net carbon balance based on daily integrated NEE data in the Gubantonggut Desert of China, a similar desert ecosystem as the two sites in Kazakhstan used in the current research, the rates of daytime, nighttime and diurnal variations of net ecosystem CO_2 exchange were unknown. We addressed these questions and found that the diurnal course of the growing season net ecosystem CO_2 exchange in the two desert ecosystems with highly alkaline soils followed clear sinusoidal pattern, which are quite similar as in crop, forest, grass ecosystems (Baldocchi & Meyers, 1998; Falge et al., 2002) and the desert ecosystems in other areas where soil may not be alkaline (Bell et al., 2012). Net carbon release at nighttime and on cloudy and rainy days and net carbon uptake on daytime on sunny days are in consistent with ecosystems where biological factors dominated the variation of NEE. Then what is the effect of alkaline soil on net ecosystem CO_2 exchange and what is the magnitude and aptitude of the contribution from abiotic processes in the desert ecosystems? Eddy covariance alone might be insufficient to answer this question. However, comparing the variations of NEE in the two sites with high alkaline soils in this research with that in other desert ecosystems and identifying the rates of NEE at daytime, nighttime and its diurnal course could provide some insights on the mentioned questions.

Summarizing the previous reports on the net ecosystem CO_2 exchange in desert ecosystems globally, the annual NEE has a very broad ranges of -127 to 258 gC m^{-2} $year^{-1}$, although annual site-received precipitations were comparable (140-186 mm) (Table 2). Our measurements show a net ecosystem production in the growing season (May - Sep) of -86.6 and -297.8 gC m^{-2} at the KZ-Ara and KZ-Bal sites, respectively. Obviously, the estimates at the two sites did not take account of NEE out of the study periods which were mostly possible net carbon loss inferred from the monthly variations of NEE (Figures 3-4 - 3-5 and 3-9). In addition, large carbon sink strength in the KZ-Bal site (-297.8 gC m^{-2}) during the growing season was strongly related to the fact that the site was actually

impacted by human interference (surrounding irrigated croplands and well-grown vegetation supplied by adequate soil water from adjacent acequia, see Figure 3-1). The NEE in desert ecosystem are highly sensitive to environmental factors, especially precipitation (Bell et al., 2012; Liu et al., 2012). The significant difference between the measured growing season NEE at the two sites also indicated that the EC measured NEE can be strongly influenced by the specific location of the EC system established and the surrounding conditions (especially soil moisture and hence the vegetation condition), as addressed by Schlesinger et al. (2009).

Global terrestrial ecosystem showed a quasi-Gaussian probability distribution with the mean NEE of -183 gC m^{-2} $year^{-1}$ and the standard deviation of -270 gC m^{-2} $year^{-1}$ based on 506 site-years of data (Baldocchi, 2008). Using 18 site-years of measured NEE from desert ecosystems (Table 3-2), a superimposed Gaussian probability distribution showed the mean value with -20 and the standard deviation with 190 gC m^{-2} $year^{-1}$. Desert ecosystems located in the right side of the global NEE distribution (Figure 3-10), which indicated that the strength of NEE in desert ecosystems was lower than the global mean value. The NEE of desert ecosystems had a wide range from -250 to 250 gC m^{-2} $year^{-1}$, and significantly influenced by annual precipitation (Bell et al., 2012) and human interference (for example surrounding acequia at the KZ-Bal site). The reported low annual NEE (<-100 gC m^{-2} $year^{-1}$) were questionable (Schlesinger et al., 2009). The compiled 18 site-years of EC-measured annual NEE may exceed the -100 gC m^{-2} $year^{-1}$ boundary (Figure 3-10). However, desert ecosystems tend to be neutral or week sink of carbon in the long term.

Both sites of desert ecosystems with alkaline soils in Kazakhstan acted as obvious net carbon release at nighttime and on cloudy and rainy days, but net carbon uptake at daytime on sunny days (Figures 3-4 – 3-5 and 3-9). Comprehensively considering the strong dependency of daytime NEE on PAR, the responses of nighttime ecosystem respiration to soil temperature and moisture, and monthly variations of mean NEE and their responses to precipitation (Figures 3-6 – 3-9), we can conclude that biological processes of carbon cycle still dominated the net ecosystem CO_2 exchange at the two desert ecosystems in Kazakhstan where soil was featured as alkaline and high soil pH value. Latest reports based on continuously measured soil respiration in alkaline soil exhibited significant net carbon loss at both daytime and night-time (Ma et al., 2012). These recent findings were in contrast with the report (Xie et al.,

2009) and hypothesis of Stone (2008), but consistent with the viewpoint of Schlesinger et al. (2009). Even recognizing the existence of CO_2 absorption by alkaline soil (Serrano-Ortiz et al., 2010), the magnitude and aptitude of CO_2 uptake by alkaline soils may not be noticeable and its contribution to net ecosystem CO_2 exchange should be fairly limited.

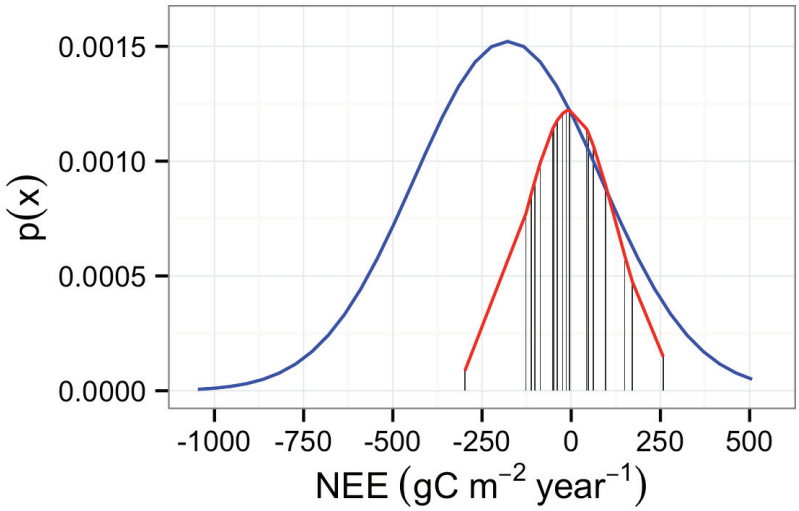

Figure 3-10. Gaussian probability distribution (p(x)) of published measurement of annual net ecosystem CO_2 exchange (NEE) for global terrestrial ecosystems (blue line) and desert ecosystems (red line). For global dataset, the mean is -183 and the standard deviation is 270 gC m^{-2} $year^{-1}$ from 506 site-years of data (source: Baldocchi, 2008). For desert ecosystems, data are retrieved from literature. In the superimposed Gussian distribution for desert ecosystems, the mean NEE is -20 and the standard deviation is 190 gC m^{-2} $year^{-1}$.

3.5 Conclusions

The present study provides the first insight on the diurnal, daytime, nighttime and daily rates of net ecosystem CO_2 exchange based on the measurements of EC in two sites of desert ecosystems with alkaline soils in Central Asia. The results found that the diurnal courses of NEE in each month followed clear sinusoidal patterns during growing season. Negative values of mean NEE were found at daytime on sunny days, indicating a net carbon uptake. In contrast, positive values of mean NEE were observed on cloudy or rainy days, and at nighttime, which implied a net carbon source. Further, strong dependency of NEE on PAR and the response of NEE to precipitation indicated that desert ecosystems with alkaline soils were still dominated by biotic factors, similar to

other ecosystems, and abiotic CO_2 absorption by alkaline soils may be trivial in terms of magnitude and aptitude.

Table 3-2. Comparison of annual net ecosystem CO_2 exchange (NEE) using eddy covariance (EC) technique or equivalent experiments among different desert ecosystems in the world. Tair and Prcp represent mean annual air temperature and precipitation.

Site	Longitude	Latitude	Soil	Dominant vegetation	Tair (°C)	Prcp (mm)	Annual NEE (gC m^{-2} $year^{-1}$)	Period	Source
Aralkum Desert, Kazakhstan	61.08°E	45.96°N	Alkaline	Shrub	8.3	140	> -86.6	May-Aug, 2012	This study
Balkhash Lake, Kazakhstan	76.63°E	44.57°N	Alkaline	Grass	5.7	140	> -297.8	May-Sep, 2012	This study
Gubantonggut Desert, China	87.93°E	44.28°N	Alkaline	Shrub	6.6	150	-49 - -5	2006-2007	Liu et al., 2012a
Gubantonggut Desert, China	87.93°E	44.28°N	Alkaline	Shrub	6.6	150	-622 - -62	2005-2006	Xie et al., 2009
Mojave Desert, USA	115.92°W	36.82°N	Loamy	Shrub	15.8	150	-110 - -102	2005-2006	Wohlfahrt et al., 2008
Mojave Desert, USA	115.92°W	36.82°N	Loamy	Shrub	15.8	150	-127	2003-2004	Jasoni et al., 2005
Baja California, Mexico	110.44°W	24.13°N	Yermosols	Shrub	23.8	174	-52 - -39	2002-2003	Hastings et al., 2005
Baja California, Mexico	110.44°W	24.13°N	Yermosols	Shrub	23.8	174	-52 - 258	2002-2008	Bell et al., 2012
Inner Mongolia, China	113.57°E	44.08°N	Loamy sand	Desert steppe	3.2	184	-7.2	2008	Yang et al., 2011
Mongolia Plateau	118.89°E	41.79°N	Loamy sand	Desert steppe	6.7	180	43 - 48	2010-2011	Shao et al., 2013
Tenger Desert, China	105.03°E	37.52°N	Sandy	Revegetation	10.6	186	-23.4 - -13.9	2009-2010	Gao et al., 2012

Chapter 4

Representing the Root Water Uptake Process in the Common Land Model for Better Simulating the Energy and Water Vapour Fluxes in a Central Asian Desert Ecosystem*

* This chapter is based on:
Li LH*, Van der Tol C, Chen X, Jing CQ, Su ZB, Luo GP, Tian X (2013) Representing the root water uptake process in the Common Land Model for better simulating the energy and water vapour fluxes in a Central Asian desert ecosystem. Journal of Hydrology 502: 145-155.

Abstract

The ability of roots to take up water depends on both root distribution and root water uptake efficiency. The former can be experimentally measured, while the latter is extremely difficult to determine. Yet a correct representation of root water uptake process in land surface models (LSMs) is essential for a correct simulation of the response of vegetation to drought environment. This study evaluates the performance of the Common Land Model (CLM) to reproduce energy and water vapour fluxes measured with an eddy covariance system in a Central Asian desert ecosystem. The default CLM appears to be able to reproduce observed net radiation, soil subsurface temperature, and wet period latent (Qle) and sensible heat (Qh) fluxes, but significantly underestimates Qle and overestimates Qh during dry period. Underestimation of Qle is attributed to the inappropriate representation of root water uptake process in the CLM model. Modifying the original root water uptake function (RWUF) with a linear function of soil water potential to one with an exponential function significantly improves the performances for both Qle and Qh. The net radiation and ground heat flux simulations did not change noticeably with the new RWUF. It is concluded that an exponential RWUF is a valuable improvement of the CLM model and likely for other similar LSMs that use a linear RWUF- for Central Asian desert ecosystems.

4.1 Introduction

Quantitative assessment of energy and water fluxes is essential to understand the complex interactions between land surface and the atmosphere (Kustas et al., 1996). Land surface models (LSMs) describing plant physiological behaviour in relation to soil and atmospheric processes have been widely used to estimate the energy and water fluxes (Bonan, 1996). Roughly 50 LSMs have been published during the last few decades, and this number is increasing every year. This indicates the general recognition of the importance of land processes in modern climatic, ecological and hydrological research (Dai et al., 2003). LSMs typically serve as a critical component (usually the lower boundary) of global carbon cycle models or generic circulation models (GCM) for assessing and predicting the likely impacts of climate change and anthropogenic forcing on terrestrial ecosystems and their feedbacks.

More than 950 site years eddy covariance (EC) data have been archived in the international network of FLUXNET (Williams et al., 2009). The amount of EC data is still climbing year by year. The increase in EC data obtained from various terrestrial land surfaces facilitates research into poorly represented or missing ecosystem processes in models, leading to improvements of the model's performance (Baker et al., 2008; Baldocchi et al., 2001; Choi et al., 2010; Li et al., 2011; Schwalm et al., 2010; Stockli et al., 2008; Williams et al., 2009). Commonly used LSMs include SiB (Sellers et al., 1986), Common Land Model (CLM) (Dai et al., 2003), ORCHIDEE (Krinner et al., 2005), CABLE (Kowalczyk et al., 2006) and their updated versions (Bonan et al., 2011; Sellers et al., 1996; Wang et al., 2010). These LSMs have been evaluated at different ecosystems including cropland, closed shrublands, deciduous broadleaf forest, evergreen broadleaf forest, evergreen needleleaf forest, grassland, mixed forest, open shrublands, savanna, wetlands, and woody savannah (Wang et al., 2012; Williams et al., 2009). LSMs are also widely used for groundwater use, runoff or soil moisture in hydrological research (Ridler et al., 2012; Zampieri et al., 2012; Zhou et al., 2012). The evaluations showed that LSMs have good ability to simulate the energy, water vapour and CO_2 fluxes at the majority of the flux sites in global FLUXNET (Schwalm et al., 2010). Some of LSMs are even able to well capture the effects of occasional large scale or seasonal drought on ecosystem functions (carbon and water fluxes) (Ciais et al., 2005; Li et al., 2012).

Although the majority of the key processes controlling the energy and mass exchange between the terrestrial ecosystems and the atmosphere have been described in sufficient detail in the current LSMs to reproduce the fluxes, applications of LSMs in some ecosystems were found to be not successful. The ability to simulate energy and gas exchange in drought conditions remains especially limited. For example, IBIS and TEM (Saleska et al., 2003), SiB3 (Baker et al., 2008) and CABLE (Li et al., 2012) all required modification before they could reproduce the observed latent heat flux and net ecosystem exchange in Amazon forest where rainfall varied seasonally and obvious wet and dry seasons appeared. Some ecophysiological or ecohydrological processes such as modified root water uptake function (RWUF) and hydraulic redistribution must be reformulated or incorporated into the model to improve the model's performance (Baker et al., 2012; Li et al., 2012). The essence is that the plants may have adopted to the seasonality of rainfall by means of morphological adjustment in developing rich and deep root systems for utilizing deep soil water during dry season (Davidson et al., 2011), and this is notoriously difficult to model.

The roots of plants could impact transpiration by means of two aspects. One is the root depth and its vertical distribution in the soil profile. Another is the efficiency of absorbing soil water. The former could be reasonably obtained with experiment. The latter, however, is hard to describe. In majority of LSMs, root water uptake efficiency is formulated with empirical functions of root fraction and soil water content (Feddes et al., 2011; Lai & Katul, 2000; Li et al., 2006; Zheng & Wang, 2007). One of known deficiencies of some LSMs (for example CABLE) is the underestimation of latent heat flux due to inappropriate description of root water uptake process (Baker et al., 2008; Li et al., 2012).

The availability of soil water is a limiting factor for plant transpiration in Central Asia (CA) desert shrubs. Limited by climate with extremely low precipitation and humidity and high summer temperature, the dominantly distributed species *Tamarix ramosissima* in CA have evolved to have rich and deep root systems and high root/shoot ratio (Xu & Li, 2008), in adaptation to extreme aridity and heat conditions. Ecophysiological characteristics of the CA desert shrub do not significantly respond to rainfall (Xu et al., 2007), suggesting that morphological adjustment associated with the ecophysiological regulation of photosynthesis and transpiration with rich-developed root systems is important. Morphological changes (for example root/shoot ratio) tend to be the

primary reaction which mitigates the effects of droughts in drought environment (Susiluoto & Beringer, 2007).

These effects of drought on root water uptake are not described well in current LSMs. It is unknown how well LSMs predict the fluxes in the CA desert ecosystem, since this has, to our knowledge, not been studied. The first objective of this research is to conduct a critical evaluation of CLM against EC data of a representative desert shrub ecosystem in CA area. The second objective of this research is to represent the RWUF in the CLM model for improving the model's performance in simulating the energy and water vapour fluxes in a Central Asian desert ecosystem.

4.2 Material and Methods

4.2.1 Site description

A set of EC instruments has been established by the Chinese Academy of Sciences to monitor the energy, water and CO_2 fluxes at Fukang Station of Desert Ecology (FSDE, 44º17´N, 87º56´E, 475 m a.s.l., Figure 4-1) The site is representative of desert ecosystem in Central Asia. The station is located at the southern periphery of the Gubantonggut Desert. Soil is a saline-alkali gault of moderate salinity, with 71% sand and 21% clay. The research area is mostly characterized by hot summers and cold winters with low annual precipitation. Historical mean annual precipitation is 163 mm and mean annual air temperature is 6.6ºC. The dominant vegetation is the desert shrub *Tamarix ramosissima*, characterized by deep root systems, with a small proportion of herbaceous species including Salsola nitraria and Suaeda acuminate. Average height of *Tamarix* is approximately 1.75 m. Within the area of 5000 m around the site, some proportion of dryland irrigated cropland is distributed.

The EC system consisted of a three-dimensional ultrasonic anemometer thermometer (STA-5055, KAIJO Corporation, Tokyo, Japan) and an open path infrared gas (CO2/H2O) analyzer (LI-7500, LI-COR, USA). The instrument was installed at a height of 3 m above the ground, and measurements were made with a frequency of 10 Hz and integrated as half-hour averages in the CR23X data-logger (Campbell Scientific, USA). The ground heat flux was measured with a heat flux plate installed at 5 cm below the soil surface. Recorded half-hour fluxes has been corrected using the WPL method (Webb et al., 1980). The ground heat flux at 5 cm below the soil surface was corrected to the surface

based on the soil temperature gradient approach proposed by van de Tol (van der Tol, 2012). The EC system also measured meteorological variables, including downward long wave radiation, downward short wave radiation, wind speed, pressure, air temperature, specific humidity, which were used to force the CLM model. Data from 2007 to 2009 were used in the current research.

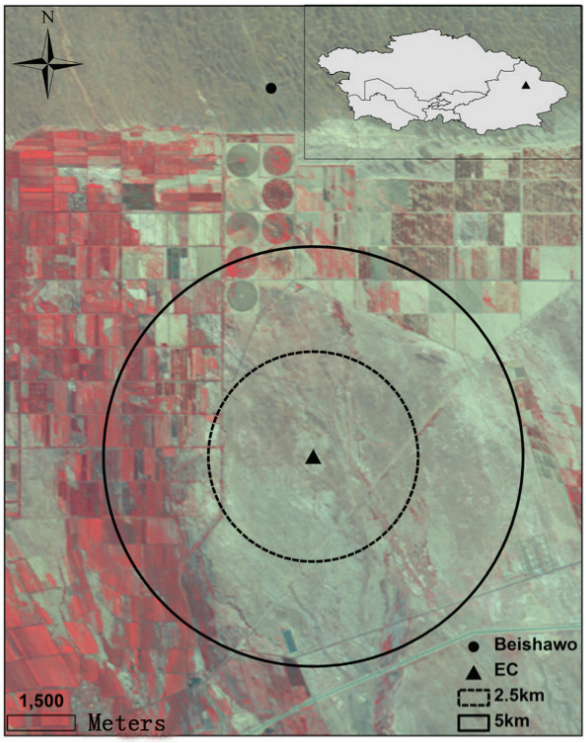

Figure 4-1. Location of the eddy covariance (EC) site in Fukang, Xinjiang (44º17´N, 87º56´E, 475 m a.s.l.) and map of the surrounding desert shrubs and irrigated croplands. The inner and outer rings show 2.5 and 5 km distance from the EC instruments.

The high salinity of soil, strong dust, and power outage caused occasional malfunctioning of the EC equipment. To obtain fully calendar yearly meteorological data required by the model, missing variables except long wave radiation at FSDE site were replaced with the corresponding variables measured at another site Beishawo (BSW, 44º22´N, 87º55´, 448 m a.s.l.) where climate was highly similar to FSDE. The distance between the two sites was around 5 km, and no significant topographic difference existed. Missed long wave radiation data was calculated based on the formula proposed by Idso (1981).

4.2.2 Common Land Model (CLM)

By combining the best features of the Land Surface Model (Bonan, 1996), BATS (Dickinson et al., 1993) and IAP94 (Dai & Zeng, 1997), CLM was originally developed for weather forecast and climate studies (Dai et al., 2003). CLM has been widely used to simulate the energy, water vapour and CO_2 fluxes from the land surface (Choi et al., 2010; Zheng and Wang, 2007), and it has been coupled to GCMs for climate research (Steiner et al., 2005; Zeng et al., 2002). Although the CLM model has been updated by the modelling community (Maxwell & Miller, 2005; Oleson et al., 2008; Rihani et al., 2010; Zampieri et al., 2012), its core sub-modules remained unchanged.

The basic version of CLM (Dai et al., 2003) with a two-big leaf model for canopy temperature, photosynthesis, and stomatal conductance scheme (Dai et al., 2004) has been used in this research. In CLM, the total surface evapotranspiration consists of evaporation from wet stems and leaves, transpiration through the plant T, and initial evaporation from the ground (i.e., bare soil or snow surfaces). The calculations for stem and leaf evaporation and transpiration are similar to those used in BATS, while Philip's (Philip, 1975) formulation is used for the computation of soil evaporation. A detailed description of CLM can be found in, for example (Dai et al., 2003), but in many other papers as well. Only some parts related to soil water movement and root water uptake process were described here.

Water movement in soil was calculated by Darcy's law:

$$\frac{\partial \theta}{\partial t} = -\frac{\partial}{\partial z}\left(K - D\frac{\partial \theta}{\partial z}\right) - E_{\mathrm{x}} \tag{4-1}$$

where θ is soil water content ($m^3\ m^{-3}$), K is hydraulic conductivity ($m\ s^{-1}$), D is soil moisture diffusivity ($m^2\ s^{-1}$), z is soil depth (m), and t is time (s).

The sink term Ex ($m\ s^{-1}$) is calculated as root water extraction from soil layer (also including soil evaporation for the first top soil layer). Total transpiration (T) is allocated to each soil layer (i) by a fraction η_i:

$$E_x = T\eta_i \tag{4-2}$$

It is noteworthy that both T and η_i are impacted by soil water availability. The fraction η_i is estimated as

$$\eta_i = \frac{f_{\mathrm{root,i}} f_{\mathrm{sw,i}}}{\sum_{i=1}^{n} f_{\mathrm{root,i}} f_{\mathrm{sw,i}}} \tag{4-3}$$

where n is the total number of soil layers, $f_{\mathrm{root,i}}$ and $f_{\mathrm{sw,i}}$ are the root fraction and soil water availability in the ith soil layer, respectively. The fraction $f_{\mathrm{sw,i}}$ is assumed a linear proportion of soil water matric potential (, mm):

$$f_{\mathrm{sw,i}} = \frac{\varphi_{\max} - \varphi_i}{\varphi_{\max} + \varphi_{\mathrm{sat}}} \tag{4-4}$$

where $\varphi_{\max}$ is the potential at the wilting point (set to -1.5×10^5 mm), and φ_{sat} the soil water matric potential at saturation. The value of φ_{sat} depends on soil texture, and $f_{\mathrm{sw,i}}$ is thus a linear scale from 1 when at saturation, to 0 at wilting point.

There is evidence (Zheng & Wang, 2007) that the fact that $f_{\mathrm{sw,i}}$ is a linear function of causes an underestimate of evapotranspiration under when water stressed conditions. Lai and Katul (2000) found that the efficiency of root water uptake changed with water availability: the efficiency was the highest in the wettest part of the root profile, and deep roots can take over the role of shallow roots if the top soil dries out. More realistic and nonlinear response curves between root water uptake efficiency and soil water availability were proposed (Lai & Katul, 2000; Li et al., 2006; Zheng & Wang, 2007) and some of them were found very useful for some other LSMs (Li et al., 2006; Li et al., 2012) but few have been incorporated into the CLM and applied to a desert environment. One of the most significant features of a desert environment is the low soil moisture content during the growing season. Previous research have found that deep roots have water transport conduits with much greater diameters and therefore, higher hydraulic conductivity compared with shallow roots or stems (Jackson et al., 2000; McElrone et al., 2004). Based on the understanding on the mechanisms and modelling of root water uptake, we propose a simple RWUF, describing $f_{\mathrm{sw,i}}$ as an exponential function of soil water matrix with a power m:

$$f_{\mathrm{sw,i}} = \left(\frac{\varphi_{\max} - \varphi_i}{\varphi_{\max} + \varphi_{\mathrm{sat}}}\right)^m \tag{4-5}$$

The value of m has been empirically determined. When the value of m is equal to 1, our proposed $f_{sw,i}$ (Eq. 4-5) is exactly same as the original one (Eq. 4-4). In all other cases, , the parameter m represents the nonlinearity of water uptake in relation to soil water potential. We found empirically that m<1, and hence, the new RWUF always computes larger values for fsw than the default RWUF (Eq. 4-4). The soil water uptake with the new RWUF is thus than with the default RWUF, especially under low soil water conditions (low soil water matric potential). This agrees with the assumption that desert plants maintain their physiological activities under low matrix potentials (Xu et al., 2007). The introduced parameter m is entirely empirical, and it does not represent a physical process directly.

We first applied the default RWUF (Eq. 4-4) to evaluate the performance of CLM against EC data, and next evaluated the effect of the modified RWUF (Eq. 4-5) on the model's performance, as shown in a flow diagram (Figure 4-2). All model parameters and variables are listed in Table 4-1.

Table 4-1. List of model parameter and variables appeared in this paper.

Symbol	Description	Value	Unit
$\bar{O}$	Mean of observation		--
$\bar{P}$	Mean of prediction		--
φ_{max}	Soil water potential at wilting point	-1.5×10^5	mm
φ_{sat}	Saturated soil water potential		mm
φ_i	Soil water potential		mm
b0	Intercept of linear regression		--
bs	Slope of linear regression		--
D	Soil moisture diffusivity		$m^2\ s^{-1}$
EBR	Energy balance closure		--
Er	Root water uptake		$m\ s^{-1}$
Ex	Water extraction		$m\ s^{-1}$
froot	Root fraction		--
fsw	Soil water availability		--
G	Ground heat flux		$W\ m^{-2}$
K	Hydraulic conductivity		$m\ s^{-1}$
m	Parameter in modified root water uptake function	0.01	--
n	Data number		--
O	Observation		--
P	Prediction		--
PFT	Irrigated crop	25	%
PFT	Desert shrub	75	%
Qh	Sensible heat flux		$W\ m^{-2}$
Qle	Latent heat flux		$W\ m^{-2}$
R	Correlation coefficient		--
RMSE	Root mean square error		--
Rnet	Net radiation		$W\ m^{-2}$
t	Time		--
T	Transpiration		$m\ s^{-1}$
Ts	Soil temperature		^oC
z	Soil depth		m
ηi	Soil water availability		--
θ	Soil water content		$m^3\ m^{-3}$

4.2.3 Sensitivity analysis

The sensitivity of the model to parameter m has been assessed with four simulations: v1, representing the original RWUF (Eq. 4-4) with m=1, and v2-v4

(Eq. 4-5) with m empirically calibrated (v2), and with the empirically calibrated value for m multiplied by 5 (v3) or and by 0.5 (v4).

Among model simulations v1-v4, the total soil depth was unchanged and kept at 3.5 m. To investigate if increasing the soil total depth impacts the model's performance, another simulation (v5) in which the total soil depth was increased to 7.0 m was carried out. Table 4-2 lists the specific configurations of all simulations.

4.2.4 Statistical analysis

Energy balance ratio (EBR) (Gu et al., 1999; Mahrt, 1998) was calculated by

$$\mathrm{EBR} = \frac{\sum_{i=1}^{n}(Q_{\mathrm{le}}+Q_h)}{\sum_{i=1}^{n}(R_{\mathrm{net}}-G)} \tag{4-6}$$

where n is the number of half hours of data. The use of EBR was able to give an overall evaluation of energy balance closure by averaging over random errors in the half-hour measurements at a flux tower site.

We used linear correlation coefficient R and root mean square error (RMSE) between the observed and simulated variables to evaluate the agreement between the simulations and the observations.

R is calculated as:

$$R = \frac{\sum_{i=1}^{\mathrm{n}}(O_i-\bar{O})(P_i-\bar{P})}{\sqrt{\sum_{i=1}^{n}(O_i-\bar{O})^2\sum_{i=1}^{n}(P_i-\bar{P})^2}} \tag{4-7}$$

where $\bar{O}$ and $\bar{P}$ are the mean values of the observed and modelled fluxes, O and P are the observed and modelled fluxes at time step i. The regression coefficients, the slope (b_s) and the intercept (b_0) were also used to justify the model's performance.

RMSE is calculated as:

$$\mathrm{RMSE} = \sqrt{\frac{\sum_{\mathrm{i}=1}^{\mathrm{n}}(P_{\mathrm{i}}-O_{\mathrm{i}})^2}{\mathrm{n}-1}} \tag{4-8}$$

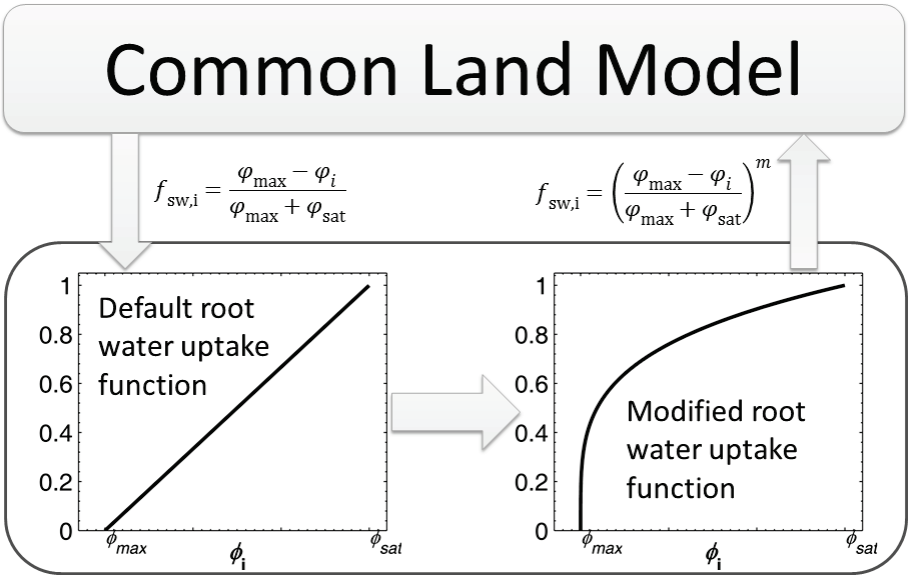

Figure 4-2. Flow diagram of the Common Land Model (CLM) with the default root water uptake function (left) and the modified non-linear one (right).

Table 4-2. Five configurations of the CLM model as used in the study. RWUF was referred to root water uptake function and SD was the total soil depth.

Simulation	Description
v1	Default CLM, with default RWUF and default SD (3.5 m)
v2	Modified CLM, with m=0.01 in the modified RWUF and default SD (3.5 m)
v3	Modified CLM, m=0.005 in the modified RWUF and default SD (3.5 m)
v4	Modified CLM, m=0.05 in the modified RWUF and default SD (3.5 m)
v5	Default CLM, with default RWUF and increased SD (7.0 m)

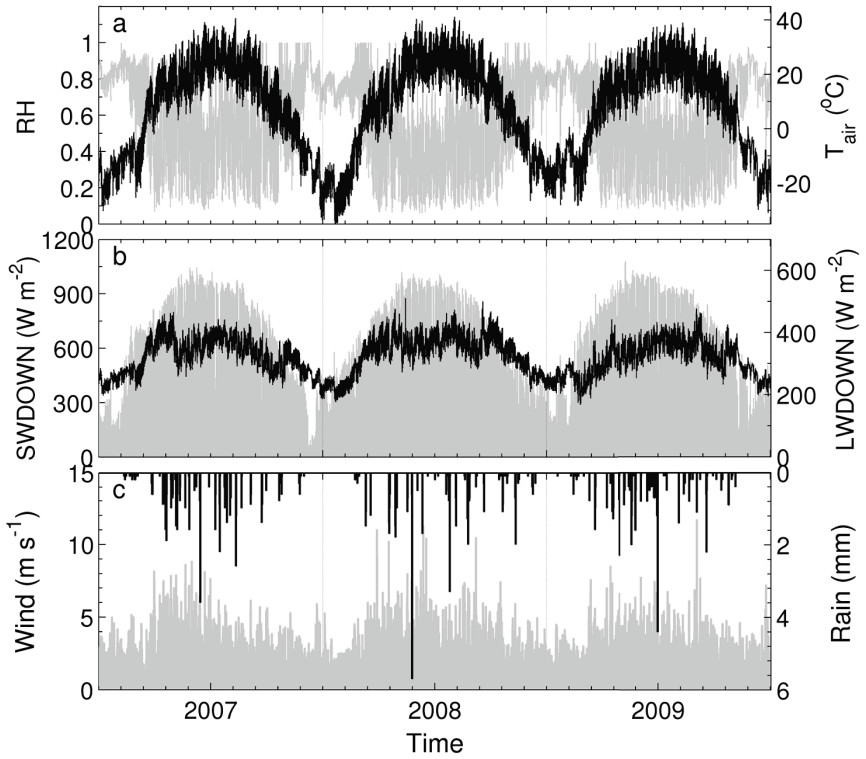

Figure 4-3. Half-hourly air temperature (Tair, black) and relative humidity (RH, grey) (a), short wave radiation (SWDOWN, black) and long wave radiation (LWDOWN, grey) (b), and wind speed (grey) and rain (black) (c) at FSDE site in Central Asia during 2007-2009.

4.3 Results

4.3.1 Meteorological conditions

Air temperature at FSDE ranges from a minimum of -35 °C in the winter to a maximum of 40 °C in the summer. Relative air humidity is 70-90% during winter season and 10-60% (mean value of 40%) during the growing season (April-September) (Figure 4-3a).

Solar radiation (downward short wave radiation, SWDOWN) exhibits obvious seasonal variations. The peak values of SWDOWN reaches 800-1000 W m^{-2} during growing season and 100-300 W m^{-2} during winter season. Downward long wave radiation (LWDOWN) shows seasonal variations as well, and ranges between 200 and 400 W m^{-2} (Figure 4-3b).

Maximum wind speed fluctuates between 3-10 m s^{-1} and wind speed in the summer was higher than in the winter. The precipitation at the study site was 185.9 mm, 116.3 mm, and 127.6 mm for 2007, 2008 and 2009, respectively; the average annual rainfall for these three years was 143.3 mm. The majority of daily precipitation amounts were less than 5 mm (Figure 4-3c).

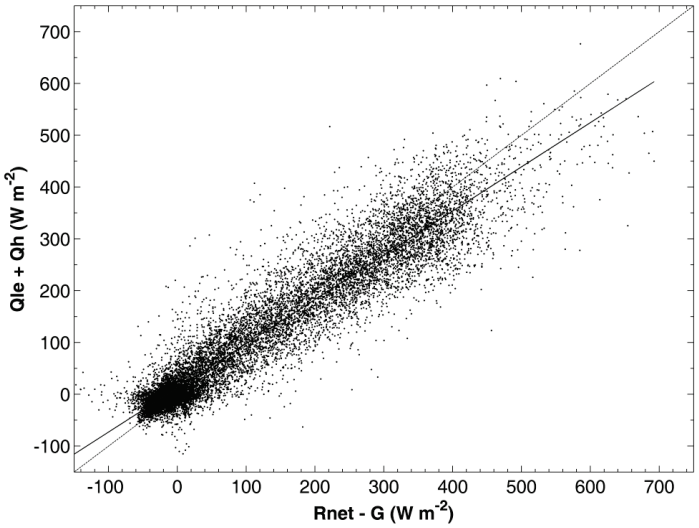

Figure 4-4. Energy balance closure at the FSDE eddy covariance site in Central Asia, with the 1:1 line (black) and a linear regression (blue).

4.3.2 Energy balance closure and footprint area

The slope of the linear regression between the observed Qle+Qh and Rnet-G was 0.85 at the FSDE site. The regression coefficient R of the observed Qle+Qh and Rnet-G was 0.94 (R^2=0.90) and the intercept was 12.47 W m^{-2} (Figure 4-4). These statistical indices in relation with energy balance closure at the studied desert ecosystem EC site are in similar to reported energy balance closure indicators at other sites of the FLUXNET network (Li et al., 2005; Wilson et al., 2012. The EBR at the FSDE site was 0.98, indicating that the bias is small when the annual ratio of total turbulent heat flux to available energy (Rnet-G) was used to evaluate the energy imbalance.

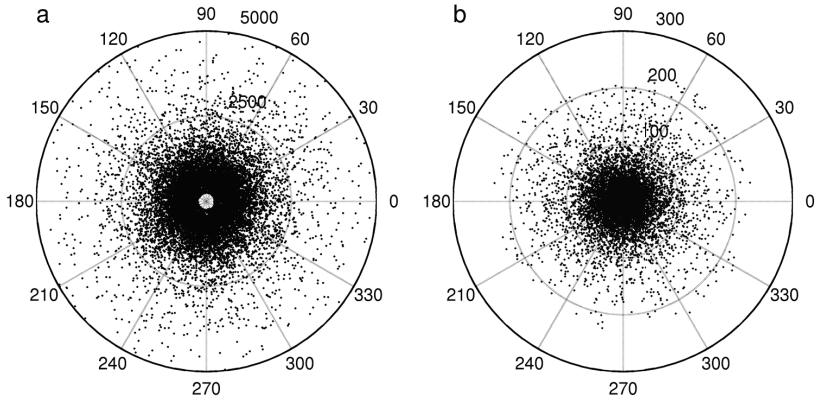

Figure 4-5. Footprint area (in meters) of the observed fluxes under stable (a) and unstable (b) conditions at FSDE in Central Asia.

A footprint analysis (Hsieh et al., 2000) indicates that the fetch length of the observed flux ranged 0-200 m under unstable conditions (Figure 4-5b). Under stable conditions, the fetch length ranges from 200 to 5000 m (Figure 4-5a). Overall, the source area of 2500 m contributes 95% of the observed fluxes. Figure 4-5 also shows that there was no dominant wind direction, with near uniform probability of different directions. Within the footprint area, heterogeneous mosaic patchiness were retrieved using Landsat TM imagery in 2006 based on the method of interactive interpretation and the area consisted of 75% of desert shrubs with some species of short life grasses and 25% of irrigated crops. This composition of mosaic land surface corresponded to the land cover types 9 and 4 as defined in the CLM model.

4.3.3 Performance of model simulations using default RWUF

Figure 4-6 shows the comparisons between the observed and the simulated diurnal values for four energy components. The default CLM model successfully reproduced Rnet using the default version of RWUF (Figure 4-6a). The values of R^2 and RMSE were 0.99 and 20.16 W m^{-2}, respectively (Table 4-3). Unfortunately, Qle, Qh and G are all inadequately simulated. For both Qle and Qh, the CLM simulated values were in agreement with the observed fluxes at nighttime, but the model severely underestimated daytime Qle and overestimated Qh (Figure 4-6b and 4-6c). As the residual of Rnet-(Qle+Qh), simulated ground heat flux (G) by the default and modified models were similar, and some discrepancy between the model and the measurements remain because the model assumes energy balance closure, while the measurements have a closure gap. The simulated mean diurnal values of G were smaller at

nighttime but greater than the observed at daytime, with the magnitude of 0-40 W m^{-2} (Figure 4-6d).

Table 4-3. Model performance indicated by correlation coefficient R, the slope (b_s), intercept (b_0) of linear regression between model and data, and root mean square error (RMSE). Unit of RMSE was ^oC for surface temperature (Ts) and W m^{-2} for all flux variables. v1 and v2 are referred to the description in Table 4-2.

Variables	Default CLM (v1)				Modified CLM (v2)			
	R	RMSE	b_s	b_0	*R*	RMSE	b_s	b_0
Diurnal Rnet	0.99	20.16	1.04	1.7	0.99	21.33	1.04	2. 6
Diurnal Qle	0.98	23.18	0.49	5.7	0.98	11.03	1.03	7.5
Diurnal Qh	0.99	36.39	1.39	3.5	0.99	18.52	1.14	-2.8
Diurnal G	0.99	9.89	1.15	-0.21	0.99	13.08	1.23	-5.26
Diurnal Qle on rainy days	0.99	12.28	0.88	10.7	0.99	16.43	1	13.2
Diurnal Qle on rainless days	0.98	23.7	0.47	5.6	0.98	10.94	1.04	7.3
Diurnal Qh on rainy days	0.95	30.1	1.28	-12.3	0.95	23.3	1.08	-12
Diurnal Qh on rainless days	0.99	36.7	1.4	4	0.98	18.44	1.14	-2.5
Half-hourly Qle	0.64	45.13	0.48	6.1	0.82	34.48	0.84	14.9
Half-hourly Qh	0.92	52.73	1.27	8.6	0.9	40.53	1.01	2.6
Half-hourly Ts	0.92	4.56	1	2.8	0.92	4.72	1.03	2.3

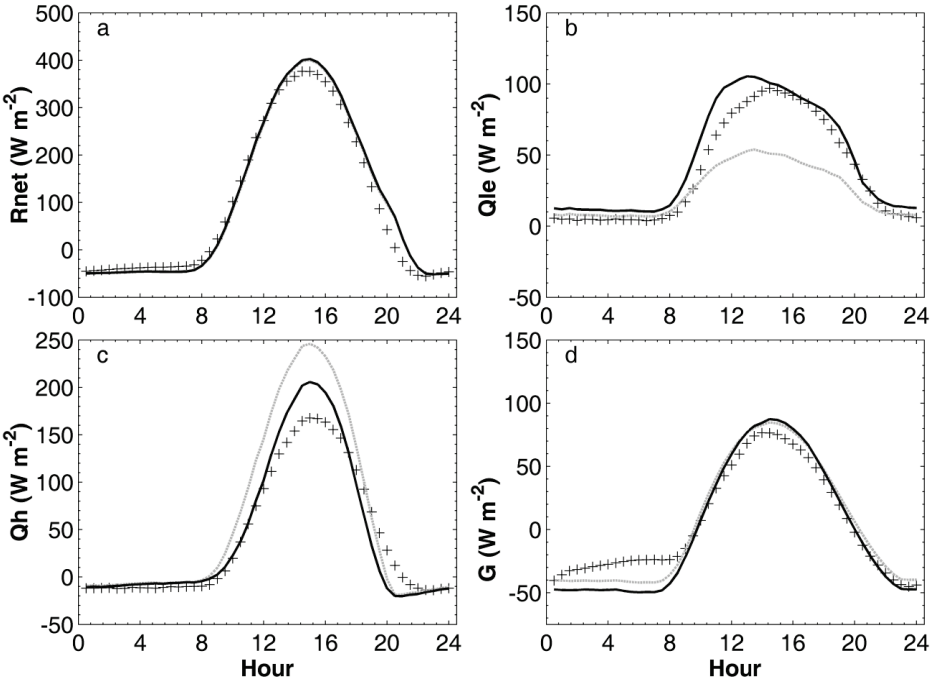

Figure 4-6. Diurnal courses of the observed and simulated energy components: net radiation (Rnet, a), latent heat flux (Qle, b), sensible heat flux (Qh, c), and ground heat flux (G, d). The diurnal values of the fluxes were obtained by averaging all available data into 24 hours in a day. The sign "+" was observation while the solid blue and dashed green lines represented the simulations with the modified and default CLM model.

The observed ground heat flux could be impacted by subsurface soil temperature (Ts). Evaluating the agreement between the simulation and the observation was helpful to identify the cause of the bias in simulated G. Figure 4-7a showed the comparison between the observed and the simulated Ts. The results showed that the values of b_s and R^2 were good at 1.0 and 0.84, respectively, but the RMSE was high of 4.56 ^oC. This result suggests that the bias in subsurface soil temperature may partially cause the error in G.

Focusing on Qle and Qh, the observed fluxes were categorized into two groups in terms of rainy and rainless days and averaged to the diurnal dynamics. The default CLM model reproduces the diurnal patterns of both Qle and Qh on rainy days (Figure 4-8a and 4-8c), but the CLM model with default RWUF (v1) severely underestimates Qle and overestimates Qh at daytime on rainless days. Especially around noon, the simulated Qle was less than half of the observed

values only and the simulated Qh was two third greater than the observations (Figure 4-8b and 4-8d).

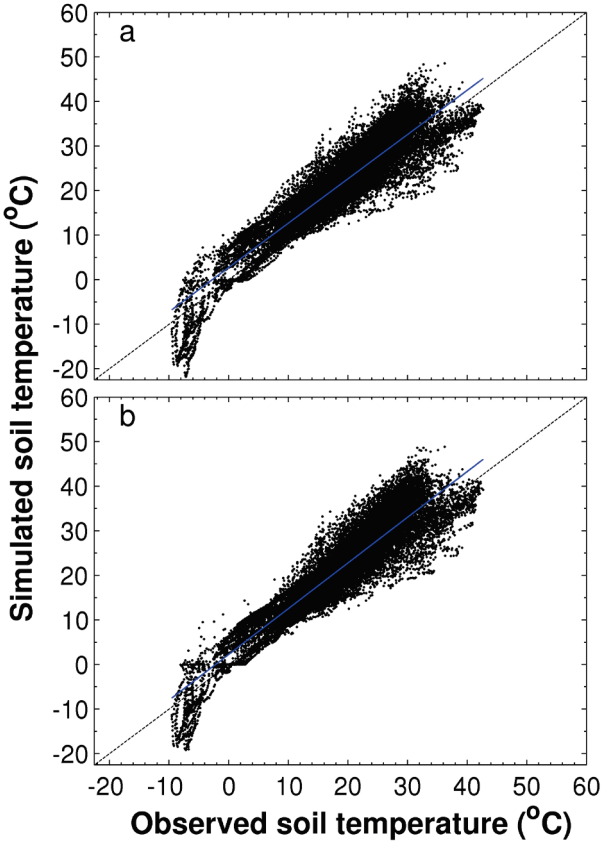

Figure 4-7. Comparison between the observed and the simulated sub-surface soil temperatures with the CLM model using the default (a) and modified (b) root water uptake function. The solid blue line represented the linear regression between the simulation and the observation, and the dashed was 1:1 line.

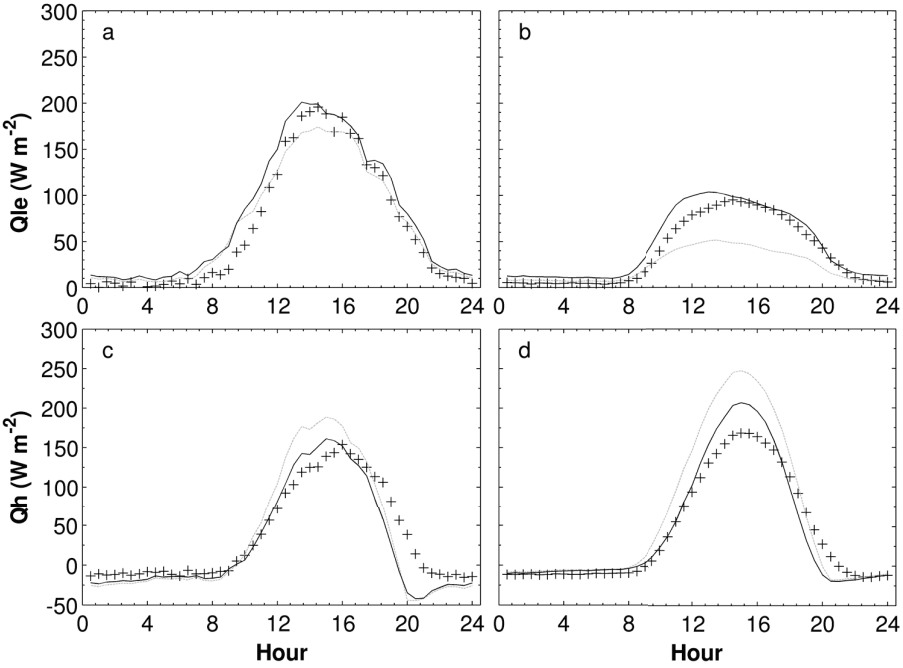

Figure 4-8. Comparison between the observed and the simulated latent (Qle) and sensible (Qh) heat fluxes on rainy (a and c) and rainless (b and d) days with the CLM model using the default and modified root water uptake function. The diurnal values of the fluxes were obtained by averaging all available data into 24 hours in a day. The sign "+" was observation while the solid blue and dashed green lines represented the simulations with the modified and default CLM model.

Figures 4-9a and 4-9c present scatter plots of observed half-hourly fluxes to the atmosphere (Qle and Qh) and simulated values with the CLM model using the default RWUF. The slopes of the linear regression between the simulated and the observed Qle and Qh with default CLM model were significantly different from 1 (0.48 for Qle and 1.27 for Qh, Table 4-3), indicating that the CLM with the default RWUF (Eq. 4-4) greatly underestimated Qle and overestimated Qh at FSDE site. Driven by high solar radiation, high temperature and small rain during the growing season (Li et al., 2011), atmospheric evaporative demand was substantially strong at the studied site. This implied that potential evapotranspiration simulated by the model was large. However, the CLM model severely underestimated Qle on rainless days.

The availability of soil water could constrain Qle by the effects on either plant stomatal conductance or the amount of water uptake by roots. Previous literature reported that the stomatal conductance of the desert shrub in the

studied area did not significantly respond to rainfall or subsurface soil water availability (Xu et al., 2007). Therefore, the model's insufficiency in Qle may result from the root water uptake process, similar to other versions of LSMs' weakness in application to forest ecosystems in dry period (Zheng & Wang, 2007). In the next section, we demonstrate the impact of a modified RWUF on the CLM's performance at the FSDE site.

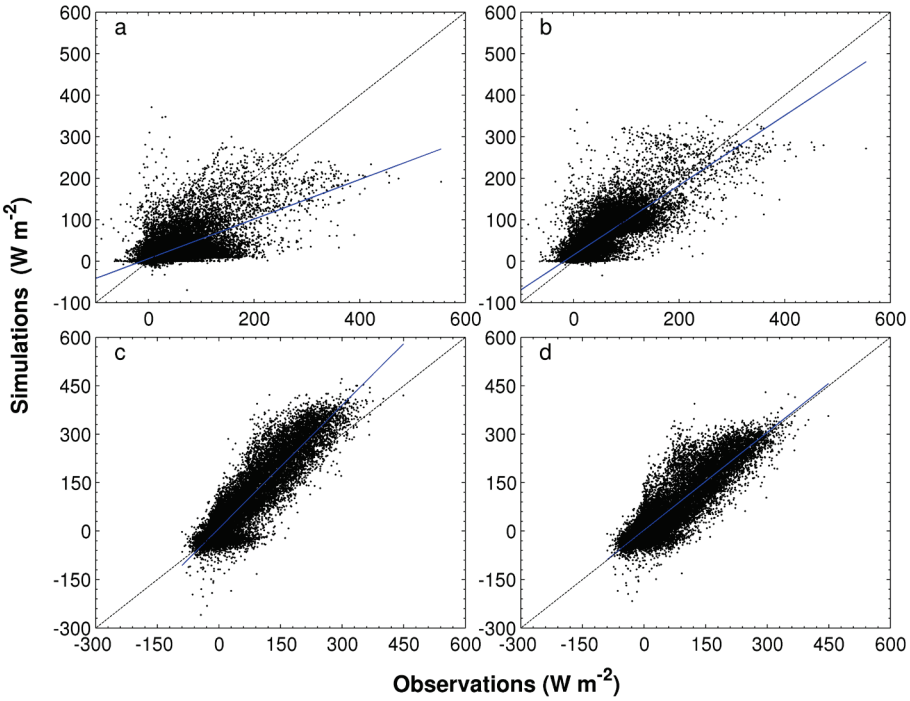

Figure 4-9. Comparison between the observed and the simulated half-hourly latent (a and b) and sensible heat (c and d) fluxes with the CLM model using the default (a and c) and modified (c and d) root water uptake function. The solid blue line represents the linear regression between the simulation and the observation, and the dashed is the 1:1 line.

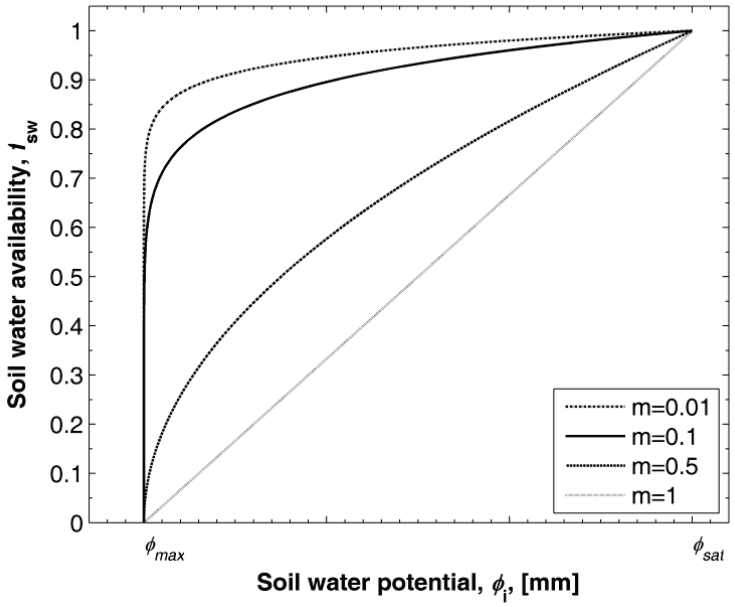

Figure 4-10. Comparison between the default and modified root water uptake functions. The linear line represented the default root water uptake function in CLM. The nonlinear curve cluster illustrated the modified root water uptake efficiency as a function of soil water potential () in dependence with the value of power m. Calculated root water uptake efficiency using the modified root water uptake function with m<1 always produced higher value than that using the default.

4.3.4 Impact of RWUF on the model's performance

With the newly proposed RWUF (Eq. 4-5), the CLM model produces similar results of Rnet and G like as produced by the default model (Figures 4-6a and 4-6d), but Qle and Qh are significantly improved. (Figures 4-6b and 4-6c). Consequently, the simulated Qle and Qh with the modified model agreed well with the diurnal courses of the observed fluxes, although the model still slightly overestimated Qle and Qh around noon.

Compared with Figure 4-7a, Figure 4-7b showed that the CLM with a modified RWUF did not affect predicted subsurface soil moisture. The resulting slope, R^2, and RMSE (Table 4-3) were similar to those of the default model.
The new RWUF improves the simulation of both Qle and Qh on rainless days (Figure 4-8b and 4-8d), while the simulation of Qle and Qh on rainy days is only slightly changed (Figure 4-8a and 4-8c).

The modification of RWUF also increases the agreement between the model and the observations for half-hourly Qle and Qh as indicated by the slope of linear regression, R^2 and RMSE. The slope for Qle increases from 0.48 to 0.84 and that for Qh decreases from 1.27 to 1.01 (Table 4-3). The slope values for Qle and Qh are closer to 1. The values of RMSE for both Qle and Qh decrease from 45.13 W m^{-2} to 34.48 W m^{-2} for Qle and from 52.73 W m^{-2} to 40.53 W m^{-2} for Qh. For Qle, the modified CLM model also improves the correlation coefficient R from 0.64 to 0.82 (Figure 4-9 and Table 4-3).

The improvement of the CLM's performance for Qle (and Qh) is due to the change of a linear into a non-linear root water uptake response to soil water potential (see Figure 4-10). The optimized value of m<1 indicates a more efficient root water uptake than the default. The larger f_{sw} in the modified model increases the simulated Qle, especially for dry soil was. Due to the energy balance, the increase in simulated Qle decreases simulated Qh. Thus the performance of CLM in application to CA desert shrub ecosystem is significantly improved with the modified root uptake function.

4.3.5 Sensitivity of CLM to the parameter m

The value the parameter m was empirically determined as 0.01 in v2 simulation. Simulated diurnal Qle and Qh fluxes by decreasing the value of m to 0.005 (v3) do not differ from v2 (Figure 4-11). In contrast, simulated diurnal Qle and Qh after increasing m to 0.05 (v4) are lower than those by v2. Increasing the rooting depth SD to 7.0 m (v5) does not improve the CLM model's performance for both Qle and Qh. Simulated diurnal fluxes of Qle and Qh are quite similar to the default CLM with SD of 3.5 m (Figure 4-11).

The performance indicators R and RMSE, with hour-hourly fluxes for simulations v1-v5 are shown in Figure 4-12. Decreasing m (v3) does not affect the model's performance, while increasing m to 0.05 (v4) decreases the model's performance compared to v2 (m=0.01), but the performance is still better than the default simulation (v1). Doubling the total soil depth only (v5) does not have a significant effect on the simulation of both Qle and Qh (Figure 4-12).

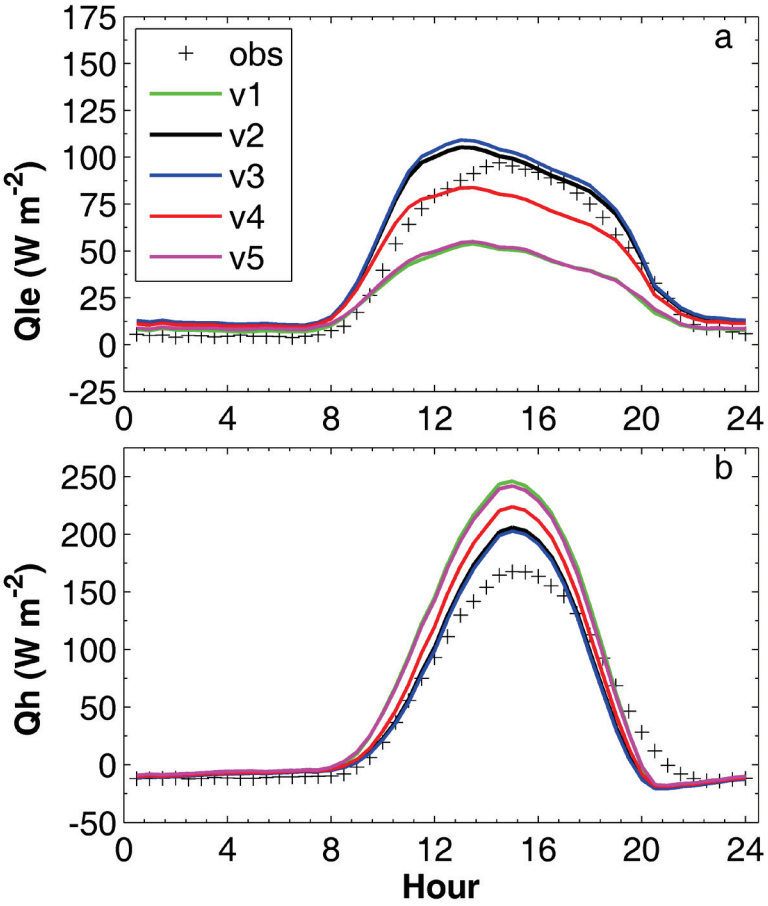

Figure 4-11. Sensitivity of the simulated mean diurnal patterns of latent (a) and sensible (b) heat fluxes to the parameter m in the modified root water uptake function and the total soil depth. Simulations v1-v5 are referred to the Table 2.

These sensitivity analyses indicate that increasing the total soil depth only does not to improve the simulation of Qle. In contrast, modifying the original RWUF with a linear function of soil water potential to one with exponential function (with power m) significantly improved the performances for both Qle and Qh fluxes, although the effect of the modified RWUF to the model's performance depended on the parameterization of the value m.

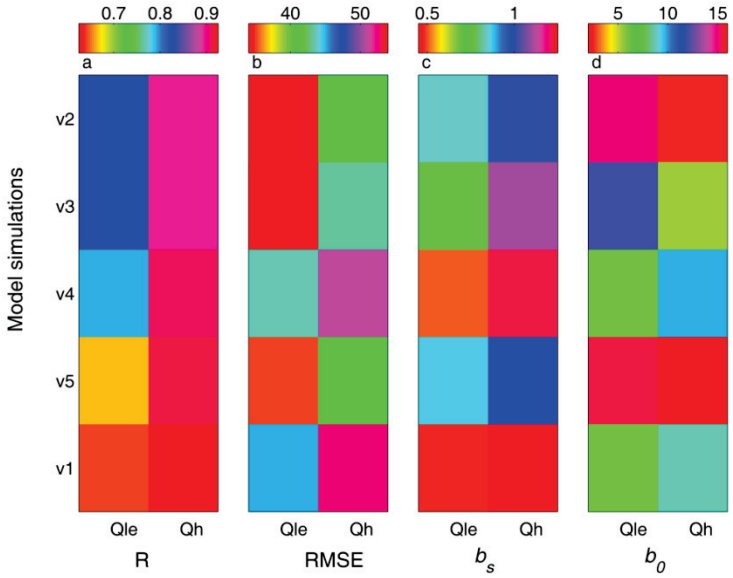

Figure 4-12. Sensitivities of the CLM simulated half-hourly latent (Qle) and sensible (Qh) heat fluxes to the parameter m and the total soil depth. Shown are R, RMSE, the slope (b_s) and interception (b_0) for all data combined. The units of RMSE are W m^{-2}. Simulations v1-v5 refer to the simulation options listed in Table 2.

4.4. Discussion

Arid and semiarid (or dryland) regions cover approximately 45% of the global terrestrial land surfaces (Asner et al., 2003; Lal, 2004). These areas are considered important in global environmental research (Bruemmer et al., 2008; Hastings et al., 2005). One unique feature of dryland ecosystems, including the Central Asia desert, is that sensible heat dominates the energy budget (Unland et al., 1996). At FSDE site, mean maximum daily latent heat was about 70 W m^{-2} lower than the maximum sensible heat flux. The energy balance closure observed in the studied site was in good agreement with that at other FLUXNET sites (Wilson et al., 2002), or other desert ecosystems, for example, Burkina Faso in West Africa (Bruemmer et al., 2008), or Baja California, Peninsula, Mexico (Hastings et al., 2005).

For global ecological modelling, desert ecosystems are important because of their vast spatial extent, but there are only few studies of energy, water and CO_2 in these ecosystems (Bruemmer et al., 2008; Hastings et al., 2005). In particular, the performance of LSMs at desert ecosystem sites has been largely unknown.

At FSDE in CA, the dominated role of sensible heat in energy budget was exaggerated in the CLM model, causing an underestimate of the latent heat flux. To overcome the weakness in the CLM model, likely also in other LSMs, a simply empirical RWUF was used instead of the default one in CLM and significantly corrected the bias in latent heat flux. The newly proposed function considered roots of desert shrubs were able to dynamically respond to varying soil wetness and more efficiently absorb water from soil layers, especially under low soil water conditions. This mechanism of desert plants in CA was associated with the long-term adaptation to extremely dry environment (Xu and Li, 2008; Xu et al., 2007), which enables desert plants being able to maximize the use of limited water from soil. The selected root function may affect the outcome of simulations of moisture recycling, the sustainability of plant physiological activities (transpiration and photosynthesis) and the regional climate (Lee et al., 2005). This research indicates that a suitable representation of root functioning in responding to soil wetness in the CLM model was necessary for the correct simulation of energy and water vapour fluxes in CA desert shrub ecosystems. Although the modified RWUF was essentially established on the empirical basis, it supported the previous hypothesis on desert plants' water use strategy and improved the performance of the CLM model significantly in desert environment.

Roots are the primary pathway for plants to uptake water and nutrients from soil. They connect the soil environment to the atmosphere through water, energy and mass exchanges between plant canopy and atmosphere (Feddes et al., 2001). Better understanding and generalising root water uptake function are important to improve the predictability of LSMs. Considerable studies have attempted to propose universal RWUFs which can be used for various water conditions and ecosystems, but none was found to be successful. Drought can occur in different patterns. For example, seasonal drought is a dominant type of drought in Amazon rainforest (Baker et al., 2008; Li et al., 2012). In contrast, Central Asia is characterized as chronic drought. Different ecosystem may show different strategy to adapt for different drought. In Amazon rainforest, hydraulic redistribution is an effective mechanism to maintain transpiration (Oliveira et al., 2005; Lee et al., 2005). In Central Asia, higher root water uptake efficiency may be a strategy for desert shrubs to adapt for environment (Xu et al. 2007). We have addressed this issue at a representative desert shrub site in Central Asia and introducing this mechanism into the RWUF in the CLM model demonstrated its significance for the estimation of evapotranspiration. The next

step is to investigate its effects on regional evapotranspiration estimation and hydrological budget.

4.5 Conclusion

To the best of our knowledge, this study provided the first evaluation of LSMs for energy and water vapour exchanges in application to desert ecosystem in Central Asia area. From this study, the following is concluded:

- The default CLM model was able to well reproduce net radiation, however, underestimated latent heat flux and overestimated sensible heat flux. The simulated latent heat flux was only around half of the observations while the simulated sensible heat flux was 27% higher than the observed values.
- A modified empirical RWUF, describing root water uptake efficiency as an exponential function of soil water potential matrix with a power m, was applied to the CLM model, significantly improved the model's performance for both latent and sensible heat fluxes. This implies that root water uptake process in CLM could be better improved by increasing the efficiency of water uptake by roots.

Chapter 5

Comparison of Root Water Uptake Functions to Simulate Surface Energy Fluxes within a Deep-rooted Desert Shrub Ecosystem*

* This chapter is based on:
Jing CQ, Li LH*, Chen X, Luo GP (2014) Comparison of root water uptake functions to simulate surface energy fluxes within a deep-rooted desert shrub ecosystem. Hydrological Processes 28(21): 5436-5449.

Abstract

Root water uptake (RWU) is a unique process whereby plants obtain water from soil, and it is essential for plant survival. The mechanisms of RWU are well understood, but their parameterization and simulation in current Land Surface Models (LSMs) fall short of the requirements of modern hydrological and climatic modelling research. Though various RWU functions have been proposed for potential use in LSMs, none was proven to be applicable for dryland ecosystems where drought was generally the limiting factor for ecosystem functioning. This study investigates the effect of root distribution on the simulated surface energy fluxes by incorporating the observed vertical root distribution. In addition, three different RWU functions were integrated into the Common Land Model (CLM) in place of the default RWU function. A comparison of the modified model's results with the measured surface energy fluxes measured by eddy covariance techniques in a Central Asian desert shrub ecosystem showed that both RWU function and vertical root distribution were able to significantly impact turbulent fluxes. Parameterizing the root distribution based on in-situ measurement and replacing the default RWU function with a revised version significantly improved the CLM's performance in simulating the latent and sensible heat fluxes. Sensitivity analysis showed that varying the parameter values of the revised RWU function did not significantly impact the CLM's performance, and therefore, this function is recommended for use in the CLM in Central Asian desert ecosystems and, possibly, other similar dryland ecosystems.

5.1 Introduction

Treatment of belowground processes such as the root water uptake (RWU) process is one of the most challenging tasks in land surface modelling (Feddes et al., 2001). Under well-watered conditions, plants do not suffer from water stress. However, around one-third of the world's area consists of arid or semi-arid ecosystems (Lal, 2004), where soil water availability is a significant limiting factor to ecosystem functions (i.e. carbon and water fluxes). Thus, results of land surface models (LSMs) applied to arid and semi-arid ecosystems are of limited confidence. Similarly, the ability of LSMs to predict carbon and water fluxes in response to drought is also highly challenged (Saleska et al., 2003). The underlying causes can be complicated but as plant root systems play a unique role in supplying water and nutrition to plants, inaccurate representation of RWU functions in the LSM may be one of the principal causes of error.

Improved understanding and accurate modelling of RWU processes were expected to improve the performance of LSMs in predicting water and carbon fluxes between terrestrial ecosystems and the atmosphere (Li et al., 2012). Numerous studies have attempted to describe the RWU process under various water conditions, and several types of RWU functions have been developed. These can be categorized into microscopic and macroscopic types (Li et al., 2006). Microscopic-type functions relate to root water movement based on individual roots (Zhao et al., 2004). This is a physical-based approach but requires geometric parameters of root systems that are difficult to obtain. Macroscopic RWU functions consider the root system as a whole object, and vertical root distribution throughout the soil profile is one of the important variables controlling the water uptake per unit of root fraction.

Actual evapotranspiration (ET) from a land surface is commonly simulated as the minimum of potential ET and the supply of water taken from the soil profile by plant root systems. In other words, actual ET is calculated as the reduction factor multiplied by potential ET. As such, the key to accurate description of the RWU function is the calculation of actual ET with dependence on potential ET, i.e. reduction factor. A reduction factor commonly consists of two items: a root fraction item and a soil water availability item. The soil water availability item is referred to as the root efficiency function by Lai and Katul (2000) and as the water stress function by Li et al. (2006). We prefer to use the term root efficiency as water stress function can be used in other processes such as soil

water effects on stomatal conductance. Since Feddes et al. (1978) first proposed a macroscopic type of RWU function describing the reduction factor as the product of vertical root fraction and a piecewise linear reduction function, a great number of variants have been proposed. Lai and Katul (2000) proposed a nonlinear "shut-down" function coupled with potential to actual transpiration to describe RWU efficiency. In contrast, Li et al. (2006) established a linear and dynamic RWU function based on a steady state of water flow from soil to root and leaf. Zheng and Wang (2007) used a linear relationship between RWU efficiency and soil water availability, but they proposed two threshold values to adjust root efficiency. The difference between Lai and Katul (2000) and Zheng and Wang (2007) RWU functions is the mathematical formula used.

In the original form of Feddes et al. (1978) RWU function, root efficiency, i.e. the ability per unit of root fraction at different depths and under conditions of different soil water content, is described as a piecewise linear function. The main disadvantage of this function is that it requires four critical values of soil characteristics. For convenience, the majority of LSMs, such as CLM (Dai et al., 2003), CABLE (Wang et al., 2010), and SiB (Sellers et al., 1986), simply use a single linear function to describe the soil water availability item in the reduction factor. However, this has been found to frequently underestimate ET, particularly during dry conditions (Saleska et al., 2003; Baker et al., 2008; Li et al., 2012). The main reason is that plant root systems can show a remarkable ability to adapt to soil depth and soil water availability, i.e. variation in the root distribution and root efficiency. Therefore, some different RWU functions have been incorporated into several LSMs, but adjusting the RWU function alone does not significantly improve the model's performance (Li et al., 2012). These findings demonstrate the high complexity of the RWU process in plants. Another neglected aspect of the RWU process is the effect of root distribution, a key item for computing the reduction factor from an estimate of ET. This has resulted from a lack of available observed root distribution data owing to the difficulty of measuring entire root distributions throughout the soil profile. As such, understanding of the possible effects of root distribution on ET estimates is still limited, although some modelling has been conducted (Zeng et al., 2001).

In dryland ecosystems, particularly deserts, plants have evolved special physiological and morphological traits to adapt to the extreme climate conditions (Martinez-Garcia et al., 2011). For example, desert plants in Central Asia have evolved to have well-developed and deep root systems and a high

root: shoot ratio (Xu et al., 2007). Such characteristics of the root system are used to classify functional types of desert shrubs, because its morphology or architecture is one of the most important determinants of the availability of soil water and thus is closely related with plant and water relations and photosynthesis (Sperry and Hacke, 2002). Arid and semi-arid halophyte desert ecosystems are reported to be quite heterogeneous with respect to root depth and vegetation structure (Xu and Li, 2009). This offers a good opportunity to investigate the effects of applying different RWU functions on LSM predictions of water and carbon exchanges between the dryland ecosystem and atmosphere.

The main objectives of this research are 1) to compare the performance of three different macroscopic RWU functions as alternatives to the default RWU function in the CLM model, and 2) to use observed root distribution within the root profile to drive the model to investigate the impact of root distribution on the ET estimates by validating the model results against the eddy covariance measured surface energy fluxes at a desert shrub ecosystem over Central Asia.

5.2 Materials and Methods

5.2.1 Experimental descriptions

Surface energy fluxes were monitored by a set of eddy covariance instruments at the Chinese Academy of Sciences Fukang Station of Desert Ecology (FSDE, 44º17´N, 87º56´E, 475 m a.s.l.). FSDE is representative of a typical continental arid desert ecosystem in Central Asia, with hot, dry summers and cold winters. The vegetation is dominated by the desert shrub Tamarix (75%), with a small component of irrigated cropland (25%). Tamarix has deep root systems. Soils are clay-loam textured with heavy salinity and alkalinity, consisting of 7% clay, 32% sand, and 61% silt. The subterranean water level fluctuates between 2.9-4.5 m. Mean annual precipitation is 163 mm and mean annual air temperature is 6.6ºC (Li et al., 2011).

We used half-hourly, gap-filled observations of meteorological variables from the FSDE to drive the model for the years 2007 to 2009. The meteorological variables consisted of short-wave solar radiation (SW), long-wave radiation (LW), precipitation (Prcp), air temperature (T_m), wind speed (Wind), atmospheric pressure (Press), and specific humidity (qm).

SW exhibited obvious seasonal variations. The peak values of SW reached 800-1000 W m^{-2} during growing seasons and were 100-300 W m^{-2} during winter seasons (Figure 5-1a). LW also showed seasonal variations, but mainly ranged between 200-400 W m^{-2} (Figure 5-1b). Observed annual precipitation during the study period was 185.9 mm (2007), 116.3 mm (2008), and 127.6 mm (2009) with mean annual precipitation of 143.3 mm (Figure 5-1c). Air temperature at FSDE ranged from minima of -35ºC in the winter to maximum values close to 40ºC in the summer (Figure 5-1d). Maximum wind speed fluctuated between ~3-10 m s^{-1}, and wind speed in the summer was greater than that in the winter (Figure 5-1e). The atmospheric pressure also showed seasonal variations. Missing values were defined as the annual mean value (Figure 5-1f). Specific humidity was less than 0.004 kg kg^{-1} during the winter and 0.004-0.014 kg kg^{-1} during growing seasons (April-September) (Figure 5-1g).

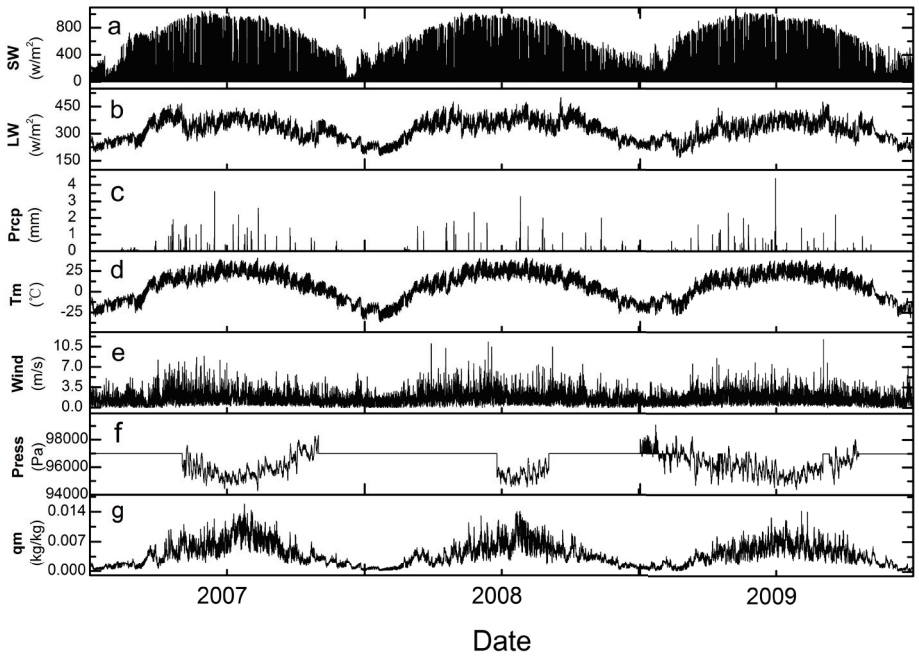

Figure 5-1. Half-hourly short wave radiation (SW, W m^{-2}) (a), long wave radiation (LW, W m^{-2}) (b), precipitation (Prcp, mm) (c), air temperature (Tm, ℃) (d), wind speed (Wind, m s^{-1}) (e), air pressure (Press, Pa) (f), and specific humidity (qm, kg kg^{-1}) (g) at the Fukang Station of Desert Ecology in Central Asia during 2007-2009. The missing values of air pressure were defined as the annual mean value.

The EC instrument consists of a three-dimensional ultrasonic anemometer thermometer (STA-5055, KAIJO Corporation, Tokyo, Japan) and an open-path

infrared gas (CO2/H2O) analyser (LI-7500, LI-COR, USA) for measuring latent (Qle) and sensible (Qh) heat fluxes. The former measures instantaneous fluctuations of the horizontal, vertical, and lateral wind speed and the virtual temperature; the latter measures instantaneous fluctuations in the concentration of CO_2 and water vapour. The average height of the dominate plant *Tamarix* in this site is approximately 1.75 m, and the equipment was placed at a height of 3 m. All data were collected at a frequency of 10 Hz. The mean, variance, and covariance of the variables were calculated and logged every 30 min by a CR23X data logger (Campbell Scientific, USA). Air temperature and humidity, soil temperature (Campbell Scientific, USA), and incoming and outgoing total radiation (CM21F, Kipp & Zonen, The Netherlands) were also logged by the CR23X. Two heat flux plates (HFP01SC, Hukseflux, The Netherlands) were installed at 5 and 7 cm below the soil surface to measure the ground heat flux. Ground heat flux at the soil surface (G, W m^{-2}) was calculated based on the approach used by Van der Tol (2012). The energy balance closure was 0.85 at the site (Li et al., 2013).

A whole-root-system excavation experiment for the desert shrub *Tamarix* was conducted at the end of the growing season in 2004. Five plants of approximately average height (1.75 m) and canopy size (1.55 m) were selected for excavation. Excavated depth was 3.5 m below the soil surface. The rooting depth of the main roots and the amount, length, diameter, and distribution scope of each order of lateral roots were recorded. Fine roots with diameters less than 1 mm could not be recorded, as they broke away as the soil was manually removed. Each absorption root can be approximately regarded as a cylinder, and the root surface area can be estimated using the diameters and lengths of lateral roots. The root fraction at different vertical depths can then be determined (Xu and Li, 2009).

5.2.2 Model Description

The CLM is a model that is useful to meteorologists for its ability to simulate the exchange of energy, mass, and momentum between the atmosphere and terrestrial biosphere, and it is useful to ecologists for its ability to do so in a process-based framework that allows for the simulation of explicit biophysical mechanisms, including the representation of thermodynamic, hydrologic, and physiological processes (Zheng and Wang, 2007). The basic version of the CLM (Dai et al., 2003) with a two-big-leaf model for canopy temperature, photosynthesis, and stomatal conductance scheme will be used in this research.

It considers one canopy layer, up to five snow layers, and ten soil layers summing up to 3.5 m (Dai et al., 2004). In the default CLM, all the biogeophysical processes and ecosystem dynamics are simulated at the plant functional type (PFT) level. RWU efficiency was assumed to be linearly proportional to soil water matric potential, which was found to underestimate ET under conditions of water stress (Zheng and Wang, 2007). It has been found that RWU was much more efficient in moist soil conditions than in dry conditions (Lai and Katul, 2000). A nonlinear response between RWU efficiency and soil water availability or an even higher RWU efficiency when the roots suffered from water stress were proven to be very useful in simulating RWU processes of plants (Lai and Katul, 2000; Li et al., 2006; Zheng and Wang, 2007). Based on these studies, three RWU functions were incorporated into the CLM to compare their effects on latent heat flux (Qle). The Lai and Katul (2000) RWU function is nonlinear. In contrast, Li et al. (2006) and Zheng and Wang (2007) RWU functions use a linear relationship between root efficiency and soil water availability, which are similar to the model default. The list of model parameters and variables used in this study are described in Table 5-1.

Table 5-1. List of model parameters and variables used in this paper.

Symbol	Description	Value	Unit
Qh	Sensible heat flux		W m^{-2}
Qle	Latent heat flux		W m^{-2}
Rnet	Net radiation		W m^{-2}
G	Ground heat flux		W m^{-2}
θj	Volumetric of soil water content		m^3 m^{-3}
θsat	Saturated soil water content		m^3 m^{-3}
ψ	Matric potential		mm
ψsat	Saturated soil water potential		mm
ψwilt	Wilting point potential	1.5E-5	mm
K	Hydraulic conductivity		mm s^{-1}
Ksat	Saturated hydraulic conductivity		mm s^{-1}
θwilt	Wilting point of soil moisture		m^3 m^{-3}
q	Soil moisture flux		mm s^{-1}
	The effective root fraction within layer j	0-1	--
W	The accumulates root resistance factor	0-1	--
αj	Soil water contribution to root resistance	0-1	--
froot,j	The root fraction within soil layer j	0-1	--
Sj	A sink term used in RWUF0		mm s^{-1}

Symbol	Description	Value	Unit
B	Empirical parameter based on Clapp and Hornberger		--
αj	Root-efficiency used in RWUF1	0-1	--
α1(θj)	Part of the root-efficiency used in RWUF1	0-1	--
α2(θj)	Part of the root-efficiency used in RWUF1	0-1	--
λ	An empirical constant used in RWUF1	0.01	--
h	Soil water pressure head		m
Tp	Potential transpiration		mm s^{-1}
Tm	Maximum transpiration		mm s^{-1}
hwilt	The pressure head at the wilting point		m
hsat,j	The pressure head when saturated		m
Hj	A variable used in RWUF2	0-1	--
Θj	A variable used in RWUF2	0-1	--
Wc	A threshold used in RWUF3	0.3	--
Wx	A threshold used in RWUF3	0.8	--
αmax	The water availability factor in the wettest layer	0-1	--
ωj	A variable used in RWUF3	0/1	--
m	A tunable parameter used in RWUF3	4	--
r(D)	The cumulative amount of roots above profile depth D	0-1	--
D	Soil profile depth	0-350	cm
Rmax	Total amount of roots	1	--
D50	The depth above which 50% of all roots were located	170	cm
D95	The depth above which 95% of all roots were located	240	cm
c	A dimensionless shape-parameter		--
j	Soil layer	1-10	--
z	Soil depth	0-3.5	m
t	Time		--

In the CLM, the latent heat flux from canopy height to the atmosphere is calculated by a two-big-leaf model, which includes the ET from leaves and evaporation heat flux from ground (Bonan et al., 2012). Land cover type, soil texture, and soil colour are used to define land surface characteristics (Dai et al., 2004). The soil thermal and hydraulic parameters are functions of the soil texture, which is determined by the percentages of the total masses of clay and silt and sand in the soil. The soil thermal and hydraulic properties are given in Bonan (1996). Root distribution follows Jackson et al. (2000) for shrubs, and every soil layer, even at depth, has a non-zero root fraction. Soil was divided into 10 layers in the CLM and the layer depths from top to down are 0.71, 2.79, 6.23, 11.89, 21.22, 36.61, 61.98, 103.80, 172.76, and 286.46 cm, respectively.

The soil water movement is defined as

$$\frac{\Delta Z_j}{\Delta t}\Delta\theta_j = -\Delta q - S_j \tag{5-1}$$

where θ_j is volumetric soil water content in soil layer *j*, *z* is the soil depth, *t* is time, and *q* is the water flow (from surface to bottom), as calculated by Darcy's law. The symbol Δ means the value of differences between the individual soil depths. The sink term S_j includes direct soil water loss due to evaporation from the top layer and the water contribution to transpiration from all soil layers, and it is calculated as

$$S_j = T_p * \varepsilon_j \tag{5-2}$$

where T_p is the plant transpiration, and it is calculated as

$$T_p = W * T_m \tag{5-3}$$

where T_m is the maximum transpiration, and plant photosynthesis and transpiration are scaled down by the accumulated root efficiency factor W. ε_j is the RWU factor within layer *j*. Root efficiency in the soil influences both T_p and ε_j.

5.2.3 Default RWU function in CLM – RWUF0

In the default CLM, the RWU, ε_j, in a given soil layer *j* can be calculated as

$$\varepsilon_j = \frac{f_{root,j}\,\alpha_j}{W} \tag{5-4}$$

$$W = \sum\left(f_{root,j}\,\alpha_j\right) \tag{5-5}$$

where $f_{\mathrm{root,j}}$ is the root fraction within soil layer *j*, and α_j represents the root efficiency determined by soil water availability. α_j in the CLM is a linear function of the soil matric potential:

$$\alpha_j = \frac{\Psi_{wilt} - \Psi_j}{\Psi_{wilt} - \Psi_{sat,j}} \tag{5-6}$$

where Ψ_{wilt} is the wilting point potential, i.e. the maximum negative potential value of leaves before desiccation, $\Psi_{sat,j}$ is the saturated soil water potential,

which is dependent on the soil texture. α_j ranges from 0 at the wilting point to 1 when soil is near saturation. ε_j in a given soil layer depends on the physical root distribution and the local root efficiency factor. This default RWU function of the model is defined as RWUF0 (Figure 5-2a).

5.2.4 Lai and Katul (2000) RWU function – RWUF1

In the Lai and Katul (2000) RWU function, a θ-based formula was used and RWU efficiency was defined by two terms: a maximum efficiency term ($\alpha_1(\theta_j)$) corresponding to times when soil water availability is not a restriction to RWU, and a nonlinear term ($\alpha_2(\theta_j)$) that describes the effects of soil water constraints on RWU:

$$\alpha_j = \alpha_1(\theta_j) \times \alpha_2(\theta_j) \tag{5-7}$$

$$\alpha_1(\theta_j) = Max\left(\frac{\theta_j}{\theta_{sat,j} - \theta_{wilt}}, \frac{\int_0^z \theta_z d_z}{\int_0^L \theta_z d_z}\right) \tag{5-8}$$

$$\alpha_2(\theta_j) = \left(\frac{\theta_j - \theta_{wilt}}{\theta_{sat,j}}\right)^{\lambda/(\theta_j - \theta_{wilt})} \tag{5-9}$$

where θ_{wilt} is the soil moisture of the wilting point, $\theta_{sat,j}$ is the saturated soil moisture content, and λ is an empirical constant. $\alpha_2(\theta_j)$ is defined between the wilting point and the saturation of the soil, and the value of it is close to 0 when soil moisture approaches the wilting point and gradually approaches unity when θ_j is approximately equal to $\theta_{sat,j}$. RWU ε_j is calculated using the CLM default. In this paper, the Lai and Katul (2000) RWU function is defined as RWUF1 (Figure 5-2a).

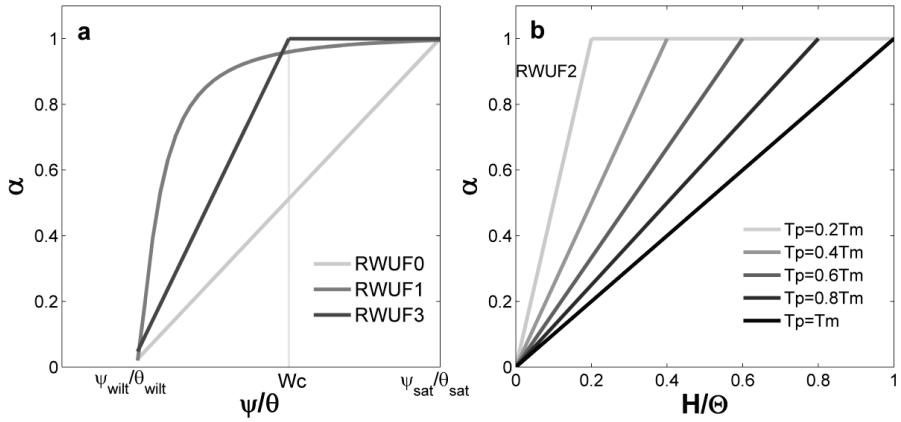

Figure 5-2. Comparison between the default and three other modified root water uptake functions (RWUF). Figure "a" represents RWUF0, RWUF1, and RWUF3 as functions of the soil matric potential or soil water content, ranging from 0 at the wilting point to 1 near saturation; Figure "b" represents RWUF2 versus geometric mean of the soil water pressure head H and soil water content Θ.

5.2.5 Li et al. (2006) RWU function – RWUF2

Li et al. (2006) proposed a dynamic and linear RWU function, defined herein as RWUF2. When soil moisture content is between the wilting point (θ_{wilt}) and saturated (θ_{sat}), RWU efficiency is defined as

$$\alpha_j = Min\left(\frac{(H_j \times \Theta_j)^{\frac{1}{2}}}{T_p/T_m} ,\ 1 \right) \tag{5-10}$$

where H_j and Θ_j are the dimensionless normalized soil water pressure head and soil

water content, both ranging from 0 at the wilting point to 1 when saturated. T_p/T_m is the relative potential transpiration rate. Equation (5-10) describes RWU efficiency as a cluster of linear relationships with the ratio of T_p/T_m. When the geometric mean of H_j and Θ_j $\left(H_j \times \Theta_j\right)^{\frac{1}{2}}$ is greater than T_p/T_m, α_j remains at 1; and when the geometric mean falls below T_p/T_m, α_j linearly decreases with the decrease in $\left(H_j \times \Theta_j\right)^{\frac{1}{2}}$; when the geometric mean approaches 0, α_j approaches 0. Intermediate variables H_j and Θ_j are calculated as

$$H_j = \frac{h - h_{wilt}}{h_{sat} - h_{wilt}} \tag{5-11}$$

$$\Theta_j = \frac{\theta(h) - \theta(h_{wilt})}{\theta(h_{sat}) - \theta(h_{wilt})} \tag{5-12}$$

where $\theta(h)$ is the soil water content at the soil water pressure head (h), and h_{wilt} and h_{sat} are the soil water pressure head at the soil water content θ_{wilt} and θ_{sat}, respectively. The allocation of water uptake ε_j is also calculated by the CLM default (Figure 5-2b).

5.2.6 Zheng and Wang (2007) RWU function – RWUF3

Zheng and Wang (2007) proposed a nonlinear empirical approach to represent a dynamic RWU efficiency by introducing two thresholds W_c and W_x. Their function is defined herein as RWUF3. Root efficiency α_j and the accumulated root efficiency factor W are calculated using the CLM default method, and then, the factor W is redefined as

$$W = \begin{cases} 1.0 & W \geq W_c \\ W/W_c & W < W_c \end{cases} \tag{5-13}$$

It is adjusted using a threshold value W_c to enable plant transpiration when part of the root system experiences water stress. The relevant water uptake variable ω_i is defined as

$$\omega_{\mathrm{j}} = \begin{cases} 0 & \alpha_j < \min(\alpha_{\max}, W_x) \\ 1 & \alpha_j \geq \min(\alpha_{\max}, W_x) \end{cases} \tag{5-14}$$

where α_{max} is the root efficiency in the wettest layer of the whole root zone, and the factor ε_j is redefined as

$$\varepsilon_j = \frac{f_{root,j}\,\alpha_j}{W} = \frac{f_{root,j}\,{\alpha_j}^m\,\omega_j}{\sum f_{root,j}\,{\alpha_j}^m\,\omega_j} \tag{5-15}$$

where the tuneable parameter m is defined as >1.0, reflecting the nonlinearity of water uptake in relation to water availability. Importantly, equation (5-15) suggests no water uptake is allowed from a layer where α_j is less than the threshold W_x, except for the wettest layer of the root zone (α_{max}). The tuneable parameter m can not only limit water uptake to layers of high water availability only but also increase the water uptake fraction from relatively wet layers (Figure 5-2a).

These four RWU functions represent the majority of developed RWU functions. As illustrated in Figure 5-2, they also represent a large domain in α-Ψ/θ space.

5.2.7 Root distribution function

A nonlinear root profile model used in this study was a logistic dose-response curve (Masek et al., 2011), which was fitted to cumulative root profiles:

$$r(D) = \frac{R_{max}}{1+\left(\frac{D}{D_{50}}\right)^{c}} \tag{5-16}$$

where r(D) is the cumulative amount of roots above the soil profile depth D, R_{max} is the total amount of roots (setting to 100%) in the profile, D50 is the depths above which 50% of all roots were located, and c is a dimensionless shape-parameter that is calculated as

$$c = \frac{-1.27875}{(log_{10}D_{95} - log_{10}D_{50})} \tag{5-17}$$

In this equation, D95 is the depths above which 95% of all roots were located. To demonstrate the impact of RWU processes on surface fluxes under different root profiles, the four RWU functions described above were incorporated in the CLM. For each RWU function, two different root profiles were examined: the vertical root distributions simulated by default Jackson model and by the data-fitted Jackson model (fitted with the observed data of D50 and D95).

5.2.8 Statistical analysis

A Taylor diagram (Taylor, 2001) was used to quantify the degree of similarity between the model simulations and the observations. Three statistical indicators - correlation coefficient R, standard error (STD), and root mean square error (RMSE) - are displayed on a Taylor diagram. The performance of the model simulation is specified by a single point, with the R value being the polar angle and STD, the polar axis. The "reference" field represents observed data, whereas the other fields all refer to the model results. The aim is to quantify how closely the simulated field resembles the reference field. The distances from the reference field to the points representing the consequence of the relationship indicate the RMSE. The linear regression coefficients, slope (b_s), and intercept (b_0) are also used to justify the model's performance.

5.2.9 Uncertainty and sensitivity analysis

The CLM, like other LSMs, predicted energy, water and carbon exchange between the land surface and atmosphere which directly impact weather and climate. Such predictions are subject to considerable uncertainties, and understanding these uncertainties are of great importance for ecosystem management and climate change projection. Uncertainties underlying the LSMs can be derived from model structure, model parameters and model forcing data. The CLM was considered as an implicated model which has synthesized majority physical and ecological processes (Dai et al., 2003). Model forcing data include meteorological variables, soil (soil type, colour, texture, and soil hydrological properties) and vegetation (vegetation type, fraction etc) information. Comparing with meteorological variables, soil properties and vegetation information have much larger spatial heterogeneities. However, turbulent fluxes simulated by the CLM were found less sensitive to soil colour, soil texture and vegetation type (Choi et al., 2010). In this paper, four RWUFs were compared for investigating the CLM's performance in simulating turbulent fluxes, so it is necessary to examine the uncertainties and sensitivities of the model to those newly-introduced model parameters. In detail, three parameters (W_c, W_x and m) of the RWUF3 were varied. Parameter values were varied by ±0.2 for W_c and W_x, and ±3 for m based on their default values 0.3, 0,8 and 4 for W_c, W_x and m, respectively. Therefore, six other simulations were made for uncertainty and sensitivity study. The six simulations are denoted M311 to M316 in Table 5-5.

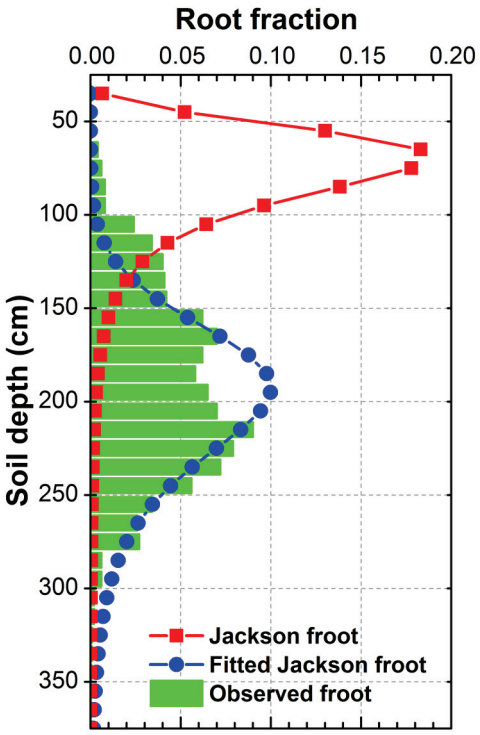

Figure 5-3. Vertical distribution of the feeder roots of *Tamarix* compared to observed root data. Simulations were conducted using both the default Jackson's root distribution model and the data-fitted Jackson root distribution model.

5.3 Results

5.3.1 Root distribution and its effects

Desert plants in Central Asia have deep root systems and a high root:shoot ratio. Root morphology and architecture are important determinants of the availability of soil water (Xu et al., 2007). Figure 5-3 shows the observed vertical root distribution for *Tamarix*. Within the depth of 0-50 cm below the soil surface, root distribution was low (1.2%), with a large proportion of roots distributed between 100-250 cm (89.4%). The root distribution model of Schenk and Jackson (2002) gives the fitted values of the parameter D50 and D95 of 170 cm and 240 cm, respectively. The fitted values of D50 and D95 were different from the default values used in the CLM (47 cm and 302 cm). Consequently, vertical root distributions simulated by the default Jackson model and the data-fitted Jackson model were significantly different. The default Jackson model predicted a high root distribution in the top 100 cm of the soil whereas the fitted

Jackson model predicted a high root distribution below 150 cm. The results indicated that *Tamarix* in the study area is deep-rooted. Such a deep root system may impact plant transpiration via the RWU process. Both the default Jackson root distribution model (as used in the CLM) and the fitted root distribution model will be used to drive the CLM for investigating the effect of root distribution on the CLM's performance.

Table 5-2. Model performance for simulating Rnet, Qle, Qh, and G, indicated by correlation coefficient R, slope (b_s), intercept (b_0), and root mean square error (RMSE, W m^{-2}) of linear regressions between model and observed data. One of the simulations is the default model with the default root distribution parameter setting (M00), and another is fitted observed root data (M01).

Variables	Default CLM (M00)				CLM with fitted root model (M01)			
	R	RMSE	bs	b0	R	RMSE	bs	b0
Rnet	0.98	35.24	1.03	5.56	0.98	33.7	1.02	4.03
Qle	0.65	45.45	0.49	8.02	0.69	43.39	0.54	7.41
Qh	0.93	54.19	1.32	4.38	0.93	49.3	1.25	4.71
G	0.65	49.56	1	10.89	0.69	51.26	1.14	9.46

Figure 5-4 presents the scatter plot between the observed energy components and the simulated fluxes (Rnet, Qle, Qh, and G) given by the CLM using the default root distribution. The default CLM model (M00) produced good estimates for Rnet (Figure 5-4a and Table 5-2) with R = 0.98, RMSE = 35.24W m^{-2}, and b_s = 1.03. However, M00 obviously underestimated Qle and overestimated Qh (Fig. 4b, Fig. 4c and Table 2). The slope values (b_s) of linear regressions between the model and the observations were 0.49 and 1.32 for Qle and Qh, respectively. When the fitted Jackson's root distribution function was used, the CLM's (M01) performance improved with regard to Qle and Qh (Figure 5-5 and Table 5-2). The values of b_s increased to 0.54 for Qle and decreased to 1.25 for Qh. Modifying the root distribution in the CLM did not have a significant impact on either Rnet or G (Figure 5-5 and Table 5-2).

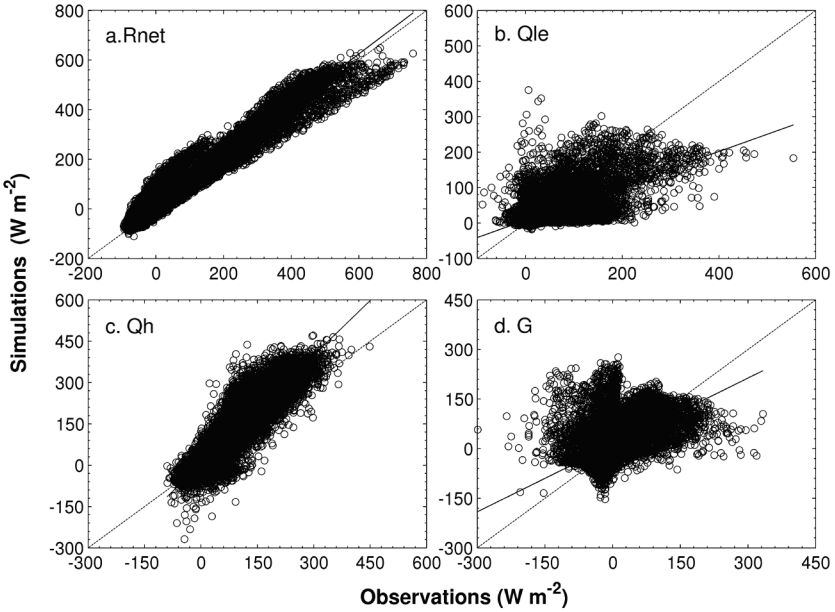

Figure 5-4. Comparison between the observed and the default Common Land Model-simulated (M00) half-hourly net radiation (Rnet, a), latent heat flux (Qle, b), sensible heat flux (Qh, c), and ground heat flux (G, d). The solid black line represents the linear regression between the simulation and the observed data, and the dashed line represents a 1:1 relationship between the datasets.

5.3.2 Effects of RWU functions on Qle and Qh

Application of the four RWU functions and two treatments of root distribution (default and fitted Jackson's root distribution) produced eight simulations in total (Table 5-3). A Taylor plot (Taylor, 2001) shows how the eight simulations (Table 4) agree with the observations (point "Obs" in Figure 5-6) based on R, RMSE and STD. With regard to Qle and Qh, the default CLM simulation using default RWU function and default root distribution (M00) performed the most poorly and the simulation with RWUF3 and the fitted root distribution, (M31) performed the best. R values for Qle given by the two simulations were 0.65 and 0.83, respectively. RMSE decreased from 45.45 in M00 to 33.31 W m^{-2} in M31. For Qh, the R values given by M00 and M31 were 0.92 and 0.93, and the RMSE for M00 was 54.19 W m^{-2}, as compared to 37.21 W m^{-2} for M31. The other six simulations produced results that fell in within the performance range of M00 and M31. The results indicate that incorporating the fitted root distribution into the CLM slightly improves the model's performance for both Qle and Qh (Figure 5-6).

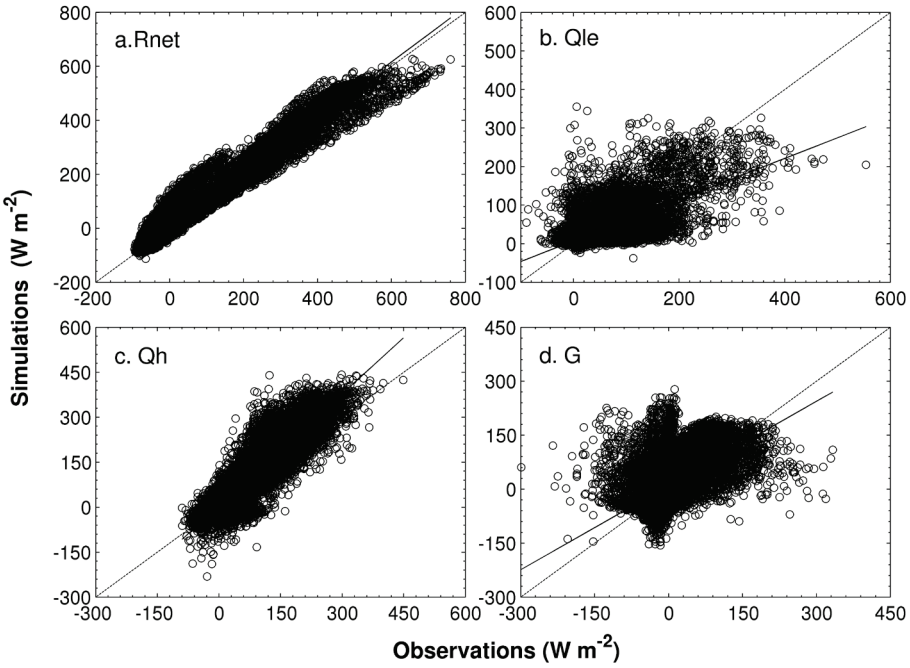

Figure 5-5. Comparison between the observed and the simulated (M01) half-hourly net radiation (Rnet, a), latent heat flux (Qle, b), sensible heat flux (Qh, c), and ground heat flux (G, d) with the model default root water uptake function and fitted with observed root data in Jackson's model. The solid black line represents the linear regression between the simulation and the observation, and the dashed line represents a 1:1 relationship between the datasets.

Table 5-3. Eight different configurations of the Common Land Model as used in this study. RWUF is the root water uptake function. "No" and "Yes" refer to two treatments of root distribution: default ("No") and the data-fitted Jackson root distribution model ("Yes").

Simulation	RWUF	Root distribution
M00	RWUF0	No
M01	RWUF0	Yes
M10	RWUF1	No
M11	RWUF1	Yes
M20	RWUF2	No
M21	RWUF2	Yes
M30	RWUF3	No
M31	RWUF3	Yes

Table 5-4. Model performance with regard to Qle and Qh, as indicated by the correlation coefficient R and root mean square error (RMSE), for four root water uptake functions using the default root distribution model and the data-fitted Jackson root distribution model.

Variables		M00	M01	M10	M11	M20	M21	M30	M31
Qle	R	0.65	0.69	0.72	0.77	0.67	0.71	0.82	0.83
	RMSE	45.45	43.39	40.82	37.38	44.32	41.75	34.98	33.31
Qh	R	0.93	0.93	0.93	0.93	0.93	0.93	0.92	0.92
	RMSE	54.19	49.3	50.11	42.22	50.39	46.11	39.62	37.21

Figure 5-6 presents the overall effects of RWU function and root distribution on the model's performance in simulating Qle and Qh. The results clearly indicated that RWUF had significant effects on both Qle and Qh. To further investigate these effects, we divided the data into two groups: wet and dry periods. Figure 5-7 shows the diurnal dynamics of the observed Qle compared to the simulated values using the four RWU functions and the two default root distribution models. The results show that all simulations (M00, M10 and M20) underestimated Qle, with b_s values of 0.53, 0.61, and 0.66, respectively. However, this underestimation was most pronounced during dry periods (except for simulation M30), with b_s values of 0.36, 0.47, and 0.41, whereas good estimates of Qle were produced during wet periods. When the fitted root distribution was implemented in the CLM, agreement between the observed and the simulated Qle was improved (with b_s values of 0.55, 0.69, and 0.66). RWUF3 was found to perform best among four RWUFs, and the b_s values for wet, dry and all periods were very close to 1. However, the simulation with the fitted root distribution and the RWUF3 (M31) was better than that only with the RWUF3 (M30). This indicated that RWUF had large effects on Qle than root distribution (Figure 5-7), especially for dry periods. As a consequence of the improved Qle, the simulation with the fitted root distribution and the RWUF3 (M31) produced best agreement for Qh between the simulation and the data.

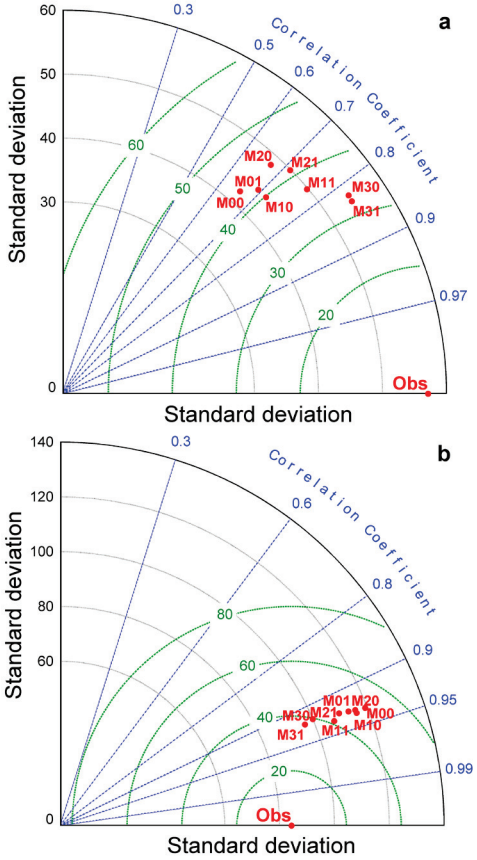

Figure 5-6. Taylor diagram plot of the simulated Qle (a) and Qh (b) computed from eight independent simulations (see Table 5-3) from the Common Land Model compared with the observed data. Standard deviation (STD, W m^{-2}) is calculated as the simulated variables divided by the observed data. "Obs" refers to observed data points. Root mean square error (RMSE, W m^{-2}) is represented by green lines. R is the correlation coefficient.

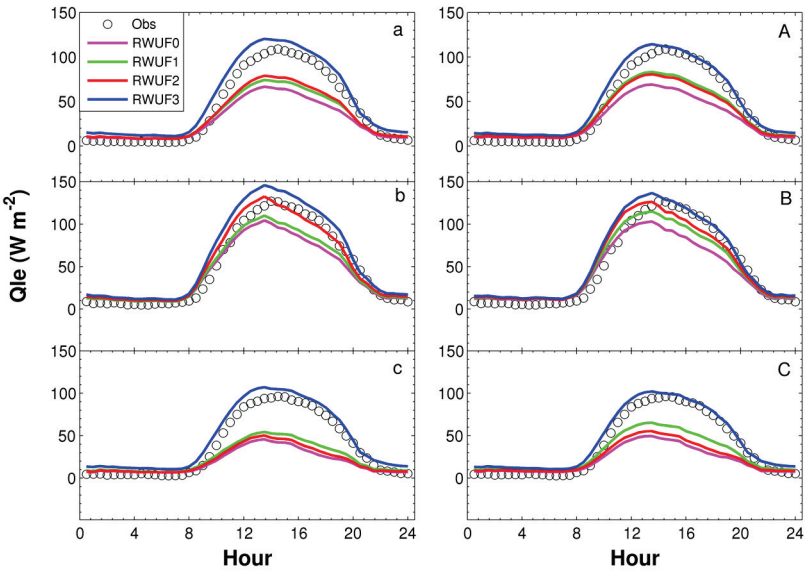

Figure 5-7. Comparison between the observed and the Common Land Model-simulated latent heat flux (Qle) on a diurnal course (a and A), rainy (b and B), and rainless (c and C) days using the default and the modified root water uptake functions to determine the effects of root distributions. The left side shows the simulations using the default root distribution, and the right side shows the simulations fitted with observed root data in Jackson's model. The diurnal flux values were calculated as the mean values of all data at same measurement time in a day for the entire time period (three years). The sign "o" indicates observed data; and the magenta line shows the simulation using RWUF0; the green line, RWUF1; the red line, RWUF2; and the blue line, RWUF3.

5.3.3 Uncertainty and Sensitivity of CLM to RWU parameters

We adjusted the values of the parameters in RWUF3 by a large range (Table 5-5) and performed the CLM to investigate the model sensitivity. There were three parameters (W_c, W_x, and m) in RWUF3. This generated six simulations (M311-M316 in Table 5-5) and the model's sensitivities to these parameters are shown in Figure 5-8. The CLM simulation with the default RWU function (RWUF0) was defined as the reference simulation (M00). As with the results shown in Fig. 5, incorporating the fitted root distribution data into the CLM (M01) improved the CLM performance as indicated by the R and RMSE values. b_s was also slightly improved for both Qle and Qh. Compared to RWUF0, the CLM with RWUF3 (M30) significantly improved the CLM's performance and combining the fitted root distribution into M30 (M31) slightly further improved the performance. Changing the values of the three parameters within a large range did not result in M31 performing better than M00 and M01 (M311–

M316). The results indicated that RWUF3 combined with the fitted Jackson's root distribution function was the best candidate for simulating the RWU process of deep-rooted desert shrubs in Central Asia. The sensitive analysis results demonstrated that varying the three parameters in the Zheng and Wang (2007) RWU function (RWUF3) in the CLM did not significantly affect the model performance, further justifying the applicability of the improved CLM in Central Asia.

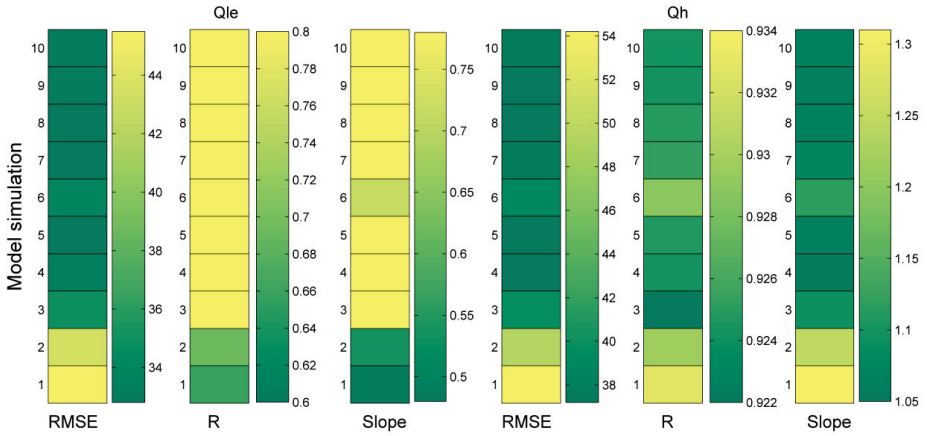

Figure 5-8. Sensitivities of the Common Land Model-simulated half-hourly latent (Qle) and sensible (Qh) heat fluxes to the empirical constants, and m in RWUF3. Root mean square error (RMSE W m^{-2}), the correlation coefficient R , and the slope (b_s) for the combined dataset are shown. Simulations ID number 1-10 are referred in Table 5-5.

Table 5-5. Ten different configurations of the Common Land Model, as used in this study for sensitivity testing. Two sets of the empirical constants , and m were used in RWUF3. RWUF is the root water uptake function. "No" and "Yes" refer to two treatments of root distribution: default ("No") and the data-fitted Jackson root distribution model ("Yes"). "NA" refers to simulations where no constant was applied.

ID	Simulation	Root distribution	RWUF	Wc (0.3)	Wx (0.8)	m (4)
1	M00	No	RWUF0	NA	NA	NA
2	M01	Yes	RWUF0	NA	NA	NA
3	M30	No	RWUF3	0.3	0.8	4
4	M31	Yes	RWUF3	0.3	0.8	4
5	M311	Yes	RWUF3	0.1	0.8	4
6	M312	Yes	RWUF3	0.5	0.8	4
7	M313	Yes	RWUF3	0.3	0.6	4
8	M314	Yes	RWUF3	0.3	1.0	4
9	M315	Yes	RWUF3	0.3	0.8	1
10	M316	Yes	RWUF3	0.3	0.8	7

5.4 Discussion

In dryland ecosystems, plant transpiration is generally controlled by the availability of soil water. Annual precipitation in dryland ecosystems is low, leading to a heterogeneous distribution of available water. Coupled with the nonlinearity of the relationship between local water uptake and local saturation, this produces a nonunique relationship when these quantities are scaled up (Guswa, 2005). Such complicated nonlinear processes still limit our understanding and modelling of RWU processes (Lai and Katul, 2000). Therefore, different RWU functions have been developed in the past few decades (Millan and Gonzalez-Posada, 2005), associated with the development of LSMs. Some of these RWU functions are high-order mechanisms and are generally difficult to incorporate into LSMs (Zhao et al., 2004). The majority of these RWU functions are empirical but easy to use in LSMs. The performance of different RWU functions can be significantly different, especially when applying models to dryland ecosystems, where drought is the most frequent stress factor for plants.

When compared to observations based on eddy covariance in a representative desert shrub ecosystem in Central Asia, the CLM with default root distribution and default RWU function was only able to explain 40% of the variance of the observed Qle. When the RWU function (RWUF3) of Zheng and Wang (2007) was used in the CLM, the model explained 69% of the variance of Qle. This demonstrated the importance of evaluating the performance of different RWUFs.

Root distribution function is also an important parameter in LSMs. Our results indicate that the effect of root distribution function on the model performance depends on the RWU function used, but more accurate root distribution functions always improve the model results.

Experimental studies have demonstrated that desert shrubs have a high capacity to adapt to dry environments, in that they can adjust their leaf evolution, root:shoot ratio, and improve water use strategies (Xu et al., 2007). These changes in morphological characteristics manifest in plant transpiration, photosynthesis, and photosynthate partitioning processes. This research attempts to incorporate these morphological adjustments into the CLM to improve the model's performance in simulating the energy fluxes in a Central Asian desert shrub ecosystem. The modelling results indicate that such efforts

can result in significant improvement of the CLM performance. Future development of LSMs should consider the adaptive ability of desert plants to dry environments to maximise model performance.

Dryland ecosystems account for more than one-third of the Earth's terrestrial surface (Lal, 2004). Improved predictions of energy fluxes over this vast area using LSMs will be helpful for hydrological, ecological, and climatic research. In the context of climate change, improving the understanding of the feedbacks between vegetation and climate and refining and improving the predictability of LSMs are very important. This research has emphasized the importance of root distribution and RWU function in LSMs in simulating the latent heat flux between ecosystem and atmosphere. A strongly associated issue is the plant carbon assimilation mechanisms (i.e. photosynthesis or gross primary production), and these will be assessed in future work.

Uncertainty is always present for any LSM simulation and prediction, which can significantly impact the predictability of future climate using climate and earth system models. The model uncertainties can originate from model structure (due to inappropriate mathematic form and/or incomplete processes), involved parameters, and input data. Root water uptake process, as a key component of LSMs, was evaluated with four different RWUFs and uncertainties from the associated parameters in RWUFs were investigated. Soil and land cover data were proven to have less effects on the turbulent fluxes in the CLM (Choi et al., 2010). Our results indicated that root distribution, another important input data for the CLM, had capacity to improve the model's predictability. The root water uptake process, a fundamental component of the CLM, was found to have significant effect on the model's performance in simulating turbulent fluxes. However, water and energy fluxes simulated by the CLM were less sensitive to those associated parameters of the "optimal" RWUF (i.e. RWUF3), justifying the applicability of the RWUF3 in dryland ecosystems in Central Asia.

Compared with canopy biophysical processes, understanding and modelling root water uptake process were more difficult in acquiring accurate and dynamic data for root distribution, root density and water transport from soil to root systems. During the past decade, root water uptake had received much attention (Feddes et al., 1974； Feddes et al., 2001; Jackson et al., 2000; Li et al., 2006) and a growing body of effort was beginning to incorporate different

RWUFs into LSMs (Li et al., 2006; Zheng & Wang, 2007). However, success in this endeavour is still elusive, mainly due to high complexity of root water uptake in diverse ecosystem and climatic conditions. This research comprehensively compared four commonly used RWUFs for the CLM and a best performed RWUF was determined. Uncertainty and sensitivity analysis were also conducted. These results improved our understanding on the root water uptake process in dryland ecosystems and also provided a practical guide on choosing a proper RWUF for applying LSMs into dryland ecosystems in Central Asia and other similar arid regions.

5.5 Conclusion

This study has investigated the significance of root distribution and RWU functions on the simulation of latent heat flux within a deep-rooted desert shrub ecosystem in Central Asia. Two root distributions and four RWU functions were incorporated into the CLM. Validation of model results against the observed energy flux using eddy covariance system resulted in the following conclusions:

The default CLM performed well in predicting net radiation, but significantly underestimated the latent heat flux and overestimated the sensible heat flux. Bias of the model mainly arose when simulating dry periods. Replacing the default RWU function with that of Zheng and Wang (2007) and considering the observed vertical root distribution in the CLM led to a significant improvement in the model's performance. Improved values for root distribution within the model always improved the model performance. This factor is dependent on the parameterisation of RWU in the CLM.

Sensitivity analysis whereby the key parameters involved in the selected RWU function (RWUF3) were adjusted indicated that the improvement of RWU functions in the CLM was not significantly impacted by the values of the model parameters influencing RWU. Therefore, RWUF3 is recommended for use in the CLM in Central Asian desert ecosystems and is possibly also applicable in other similar dryland ecosystems.

Chapter 6

Evaluating the Performance of the CLM in Simulating Water and Carbon Fluxes at two Central Asian Desert Ecosystems*

* This chapter is based on:
Li LH*, Van der Tol C, Su ZB. Evaluating the performance of the CLM in simulating water and carbon fluxes at two Central Asian Desert Ecosystems. (In preparation)

Abstract

Energy, water and carbon fluxes between the land surface and the atmosphere in dryland ecosystems have recently received considerable attention because they are viewed to have great impacts on the global carbon cycle and climate. However, limited by the available data for surface flux variables, the ability of land surface models for simulating water and carbon fluxes in Central Asian desert ecosystems remains unknown, despite work that has been done to compare the model with the measurements from the global FLUXNET in other geographic regions. The primary objective of this study is to investigate the performance of the Common Land Model (CLM) from half-hourly to monthly time scales at two desert ecosystems in Central Asia. In general, the CLM is able to satisfactorily reproduce the energy fluxes at both sites but net radiation during night-time was systematically overestimated. The performance of the CLM for simulating carbon flux is site-dependent and varies greatly with time scales and the simulated ecosystem respiration was poorly correlated to the observed. The CLM was proven to simulate energy fluxes better than carbon fluxes. We conclude that there is large potential to improve the land surface model when applied in Central Asian desert ecosystems. We suspect that providing accurate input information on vegetation fraction, composition, leaf area index and integrating advanced understanding on the morphological features into the current land surface models may greatly help to improve the model's performance in desert ecosystems.

6.1 Introduction

Numerous experiments have been carried out to evaluate land surface models (LSMs), which are aiming at improving the model's performance and quantifying the water and carbon fluxes between the land surface and the atmosphere. Until the late 20th century, most model evaluations were implemented under the Project for the Intercomparison of Land-Surface Processes (PILPS) (Henderson-Sellers et al., 1995; Pitman 1999) under the auspices of the Global Energy and Water Cycle Experiment (GEWEX). In the two decades, with the rapid development of eddy covariance (EC) techniques for monitoring energy, water and carbon fluxes between the land surface and the atmosphere, more and more work has focused on the comparison between simulation results and measurements from the global FLUXNET for various ecosystem types (Blyth et al., 2009; Li et al., 2011; Schwalm 2010; Williams et al., 2009) as the EC provides long-term, high-frequency (30 min) and continuous measurements for momentum, energy, water vapour and carbon fluxes, and ancillary meteorological variables and biological informatics.

The two main output variables of LSM that have been subject to validation studies are latent heat flux (Qle) and net ecosystem CO_2 exchange (NEE). The process of latent heat flux (in the form of evapotranspiration) is a major component of the global water cycle, and the NEE (as the net exchange of CO_2 between the land and the air) has large potential to alter global and regional climate in the long term. Both variables and corresponding eco-physical processes reflect the interactions between ecosystem and climate. Accurate estimation of water and carbon fluxes from the terrestrial ecosystems are therefore needed at the global scale for investigating the possible impacts of the global water cycle resulting from the change in climate and atmospheric CO_2 concentration. LSMs are designed for this purpose, mostly coupling with global climate models (Pitman, 2003). However, the performance of LSMs requires comprehensive evaluation against measurements across a wide range of ecosystem types and climate zones. For example, there is a large numbers of model-data comparisons in boreal and temperate forests in North Hemisphere and tropical rainforests in Amazonia regions, and grassland, cropland and savanna ecosystems worldwide (Li et al., 2011; Wang et al., 2012; Williams et al., 2009). However, spatial distribution of the global FLUXNET sites is largely uneven, and arid ecosystems are particularly poorly represented (Oliphant, 2012). For example, Central Asia occupies a total area of 5.67×10^6 km^2 and majority of the land surface is characterized as desert ecosystems, but only few

EC measurements are available. The availability of a growing season period of EC data from the Kazakhstan in 2012 (Li et al., 2014) allows us to make a first attempt on evaluating the performance of a global land surface model in predicting the energy, water and carbon fluxes from desert ecosystems.

Evaluating the performance of the land surface model at desert ecosystems was inspired and stimulated by the fact that a series of recent research based on both experiments and modeling indicated that arid and semi-arid ecosystems tend to greatly impact the global carbon budget and contribute to the interannual variations of global carbon cycle (Hastings et al., 2005; Poulter et al., 2014; Wohlfahrt et al., 2008). Another concern is that laboratory experiments reported that alkaline soil in Central Asia might absorb a considerable amount of carbon in an abiotic manner (Xie et al., 2009). The cause of such a strong sink for CO_2 in the desert ecosystems is still not clear but it was speculated to be related to abiotic carbon process (Stone, 2008), which may impact the performance of LSMs when applied in desert ecosystems. The main objective of this work is to comprehensively and rigorously evaluate the performance of Land Common Model (CLM) at two representative desert ecosystems in Central Asia.

6.2 Materials and Methods

6.2.1 Site description

Two sets of eddy covariance equipment were established in representative dryland ecosystem in Kazakhstan in 2012. One site is close to Aral Sea and the other is close to Balhash Lake.

The Aral Sea site (Ara, 61.08°E, 45.96°N) is located northeast of the Aral Sea, and at the edge of Aralkum Desert. Within radius of 5 km of the Ara site, the dominant plant species are weed-grass and reed vegetation in combination with xerophytic and halophytic desert semi-shrubs, shrubs. The average fraction of vegetation coverage was about 30% (Breckle et al., 2012). The dominant soil type was solonchak. Historical climatic records with long term observations showed that mean annual precipitation is 140 mm and mean annual air temperature is 8.3 °C.

The Balhash Lake site (Bal, 76.63°E, 44.57°N) is located between the Balhash Lake and the Kapshagay Reservoir, and between original deserts and oasis croplands. The dominant plant species are irrigated crops, grasses, and desert

shrubs. The average fraction of vegetation coverage was about 40%. The soil in the Bal site is saline solonchak (Starodubtsev & Trukavetskiy, 2011). Historical climatic records with long term observations showed that mean annual precipitation is 140 mm and mean annual air temperature is 5.7 °C.

More detailed information about the two sites is presented in Chapter 3.

6.2.2 Eddy covariance measurement and data processing

At each site, an eddy covariance system was used to measure energy, water vapour and CO_2 fluxes between the land surface and the atmosphere. The eddy covariance consists of an open path gas analyser (LI-7500, LICOR), and a three-dimensional sonic anemometer thermometer (Wind Master Pro, Gill Instruments, Lymington, UK). The EC also measures air temperature and humidity (HMP45C, Campbell), precipitation (TE525MM, Texas Electronics, Dallas, TX, USA), short-wave and long-wave radiation (CNR-1, Kipp & Zonen, Delft, the Netherlands), and soil heat flux (HFP01, Hukseflux, Delft, the Netherlands). All variables were recorded at 10 Hz. Available measurements covered from 30 April and 18 August 2012 at the Ara site and from 23 May to 6 September 2012 at the Bal site.

Before the analysis, originally raw data (10 Hz) was processed by the EddyPro software (version 4.0.0) and then stored at 30 min time step. EddyPro has already implemented tilt correction, turbulent fluctuation blocking, time lag compensation, spike detection and removal, and spectral corrections. 30 min blocks of flux data were processed to fill the data gaps through Self Organising Linear Output map (SOLO) Artificial Neural Network (ANN) (Hsu et al., 2002), and further processed with Hampel filter to remove and interpolate few outliers (Li et al., 2014). The last step of data processing is to partition the measured net ecosystem CO_2 exchange (NEE) into gross primary production (GPP) and ecosystem respiration (RES) using a online "Eddy covariance gap-filling and flux-partitioning tool" developed by the Max Planck Institute (http://www.bgc-jena.mpg.de/~MDIwork/eddyproc/faq.php).

6.2.3 Common Land Model (CLM)

The Common Land Model (CLM) is built on the Land Surface Model (Bonan, 1996), BATS (Dickinson et al., 1993) and IAP94 (Dai & Zeng, 1997). The design of the CLM was mainly for calculate the momentum, energy, water and carbon exchanges between the land surface and the atmosphere, and thus used

for climate research by coupling with global climate models. Since the release in 2003 (Dai et al., 2003), the CLM has been developed a lot and updated by the modelling community, its core modules remained unchanged. The basic version of CLM with a two-big leaf model for canopy temperature, photosynthesis, and stomatal conductance scheme (Dai et al., 2004) was used in this research.

The CLM calculates the total latent heat flux as the sum of the latent heat flux from canopy and ground. The detailed formulae for calculating latent heat flux (evapotranspiration) and soil water movement have been introduced in Chapter 4. A detailed description of CLM can be found in, for example (Dai et al., 2003) but in many other papers as well.

Generally, the CLM requires three clusters of input data: land surface characteristics, vegetation and soil properties, and meteorological variables. Meteorological variables were derived from the measurements by eddy covariance instrument. Vegetation properties include canopy roughness, zero-plane displacement, leaf dimension, rooting depth, and other optical and physiological properties that are mainly related to the functioning of vegetation photosynthesis and transpiration. Soil properties mainly include soil thermal and hydraulic parameters. For land surface characteristics, three indices are used, including land cover type, soil texture and soil colour. Land surface characteristics are derived from the global dataset for each element. In the CLM, each modelling grid can be subdivided into up to 25 tiles and each tile contains a single land cover type. Each land cover type corresponds to a prescribed fraction from a global dataset.

6.2.4 Model configuration

As described in the section “Site description”, fraction of vegetation is roughly known at each eddy covariance site, so it can be prescribed in the CLM. In addition, site-calibrated physiological parameters for desert shrub in the Chapter 2 (Li et al., 2011), the root water uptake function proposed in the Chapter 4 (Li et al., 2013) and the root distribution used in the Chapter 5 (Jing et al., 2014) have been implemented into the CLM for this study. All other parameters will be kept default.

6.2.5 Statistical analysis

Two common-used statistical indexes are used to quantify the model’s performance, including correlation coefficient R and root mean square error

(RMSE). In addition, slope (b_s) and intercept (b_0) of linear regression are used to justify the model's performance.

R is calculated as:

$$R = \frac{\sum_{i=1}^{n}(O_i-\bar{O})(P_i-\bar{P})}{\sqrt{\sum_{i=1}^{n}(O_i-\bar{O})^2 \sum_{i=1}^{n}(P_i-\bar{P})^2}} \quad (6\text{-}1)$$

where $\bar{O}$ and $\bar{P}$ are the mean values of the observed and modelled fluxes, O and P are the observed and modelled fluxes at time step i.

RMSE is calculated as:

$$\mathrm{RMSE} = \sqrt{\frac{\sum_{i=1}^{n}(P_i-O_i)^2}{n-1}} \quad (6\text{-}2)$$

6.3 Results

6.3.1 Performance of CLM in simulating half-hourly water vapour and carbon fluxes

Half-hourly net radiation simulated by the CLM (Rnet_mod) was generally in good agreement with the observation (Rnet_obs) at the two Central Asian desert sites. In detail, the values of the slope of linear regression between Rnet_mod and Rnet_obs are 0.87 and 0.99 at the Ara and the Bal sites, respectively. The corresponding correlation coefficient R values are 0.99 at the both sites (Figure 6-1 and Table 6-1).

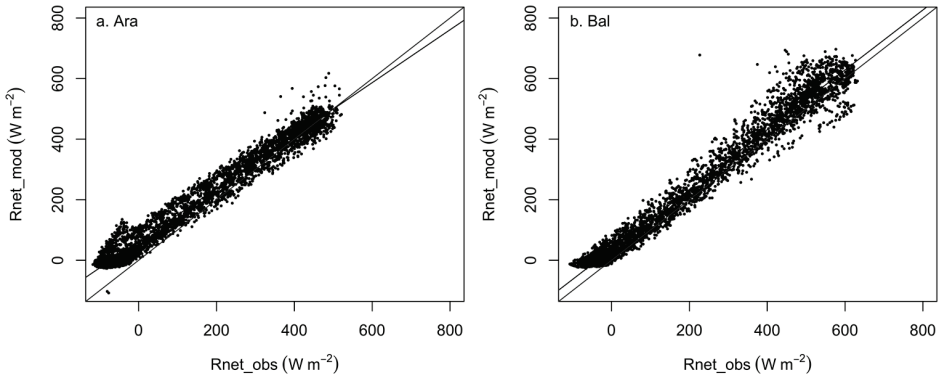

Figure 6-1. Comparison between observed (Rnet_obs) and simulated (Rnet_mod) net radiation at the Ara (a) and the Bal (b) sites. The blue line represents the 1:1 line and the black solid line represents the linear regression line between Rnet_obs and Rnet_mod.

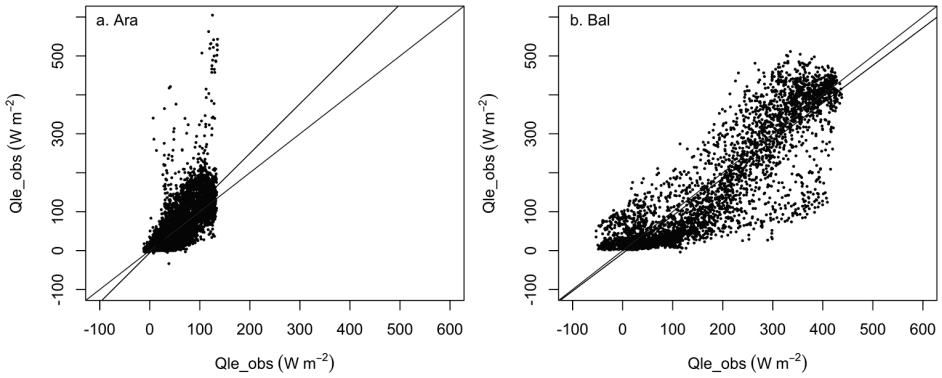

Figure 6-2. Comparison between observed (Qle_obs) and simulated (Qle_mod) latent heat fluxes at the Ara (a) and the Bal (b) sites. The blue line represents the 1:1 line and the black solid line represents the linear regression line between Qle_obs and Qle_mod.

Table 6-1. Model performance indicated by correlation coefficient R, the slope (b_s), intercept (b_0) of linear regression between model and data, and root mean square error (RMSE). Unit of RMSE was W m^{-2} for energy fluxes (Rnet: net solar radiation; Qle: latent heat flux) and μmol m^{-2} s^{-1} for carbon flux variables (NEE: net ecosystem CO_2 exchange; GPP: gross primary production; RES: ecosystem respiration).

Site	Variable	Time-scale	bs	b0	R	RMSE
Ara	Rnet	Half hour	0.87	62.3	0.99	61.62
Bal	Rnet	Half hour	0.99	35.67	0.99	48.99
Ara	Qle	Half hour	1.25	-4.98	0.73	48.25
Bal	Qle	Half hour	0.97	-7.23	0.91	64.03
Ara	NEE	Half hour	0.87	-0.06	0.7	2.14
Bal	NEE	Half hour	0.93	-1.43	0.71	6.28
Ara	GPP	Half hour	0.8	0.47	0.73	2.13
Bal	GPP	Half hour	0.96	1.2	0.82	5.96
Ara	RES	Half hour	-0.07	1.91	-0.06	1.02
Bal	RES	Half hour	0.49	2.46	0.52	3.22
Ara	Rnet	Diurnal	0.87	62.23	1	57.37
Bal	Rnet	Diurnal	0.99	35.37	1	35.94
Ara	Qle	Diurnal	1.36	-10.24	1	14.91
Bal	Qle	Diurnal	1.01	-13.55	0.99	24.12
Ara	NEE	Diurnal	1.04	0.06	0.99	0.33
Bal	NEE	Diurnal	1.29	-0.49	0.98	2.58
Ara	Rnet	Daily	0.9	60.01	0.79	51.28

Site	Variable	Time-scale	bs	b0	R	RMSE
Bal	Rnet	Daily	0.98	37.13	0.8	40.37
Ara	Qle	Daily	1.06	4.62	0.54	29.02
Bal	Qle	Daily	0.17	103.51	0.14	42.36
Ara	NEE	Daily	0.56	-0.29	0.33	1.02
Bal	NEE	Daily	-0.06	-3.97	-0.04	3.44

Received net radiation was mainly partitioned into three components, latent heat flux (Qle), sensible heat flux (Qh), and ground heat flux (G). Among the three energy components, the focus is on the latent heat flux, as Qle is closely related to plant transpiration and photosynthesis. For this reason only Qle has been analyzed in the present study. Figure 6-2 clearly shows that the CLM strongly over-estimates Qle at the Ara site. Qle simulated by the CLM (Qle_mod) for the Bal site shows an extreme mismatch with the observed Qle (Qle_obs). The resulting values of the slope of the linear regression between Qle_mod and Qle_obs were 1.28 and 0.97 at the Ara and the Bal sites, respectively. The R values were 0.73 and 0.91 at the Ara and the Bal sites, respectively. Root mean square root (RMSE) between Qle_mod and Qle_obs were 48.71 and 64.03 W m^{-2} at the Ara and the Bal sites, respectively.

Figure 6-3 shows a comparison between the CLM-simulated (NEE_mod) and the observed (NEE_obs) net ecosystem exchange (NEE) at the two desert sites. The values of the slope between NEE_mod and NEE_obs were 0.87 and 0.93 at the Ara and the Bal sites, respectively. And the values of r were 0.70 and 0.71 at the Ara and the Bal sites, respectively. The RMSE values at the two sites are 2.14 and 6.28 μmol m^{-2} s^{-1}, respectively.

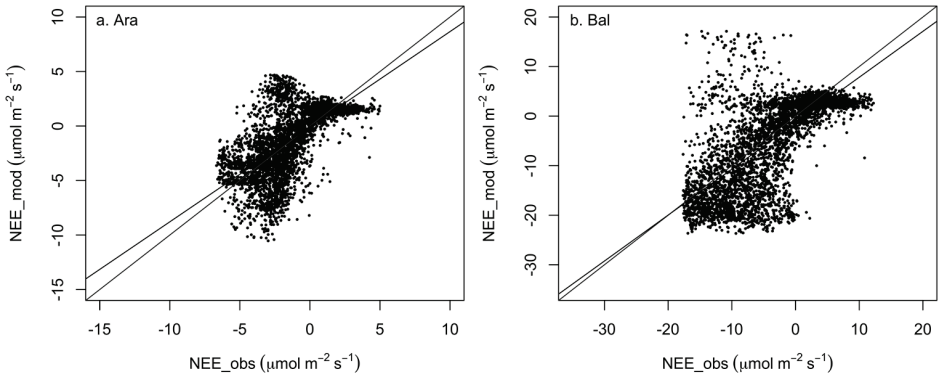

Figure 6-3. Comparison between observed (NEE_obs) and simulated (NEE_mod) net ecosystem exchanges (NEE) at the Ara (a) and the Bal (b) sites. The blue line represents the 1:1 line and the black solid line represents the linear regression line between Qle_obs and Qle_mod.

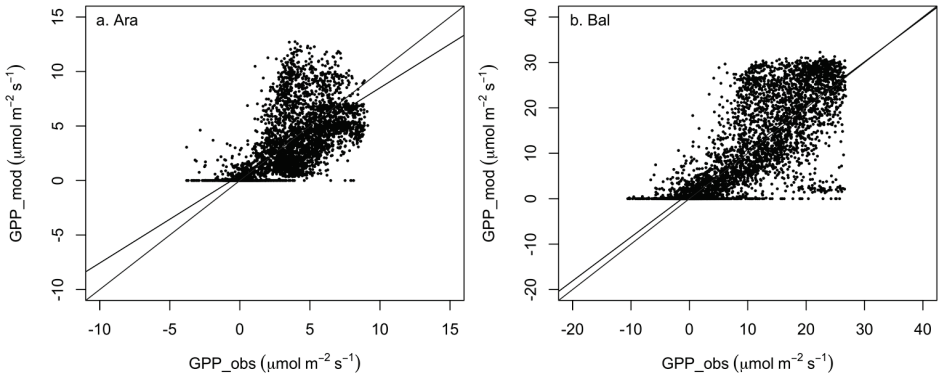

Figure 6-4. Comparison between observed (GPP_obs) and simulated (GPP_mod) gross primary production (GPP) at the Ara (a) and the Bal (b) sites. The blue line represents the 1:1 line and the black solid line represents the linear regression line between Qle_obs and Qle_mod.

Both gross primary production (GPP) and ecosystem respiration (RES) can be further compared between the model and the observation after partitioning of NEE. At the Ara site, the slope of linear regression between the simulated GPP (GPP_mod) and the observed GPP (GPP_obs) was 0.8, and the other two statistical indicators, R and RMSE were 0.73 and 2.13 μmol m^{-2} s^{-1} (Figure 4, Table 1). For Bal site, the slope value of the linear regression between GPP_mod and GPP_obs was 0.96, and the values of R and RMSE were 0.82 and 5.96 μmol m^{-2} s^{-1} (Figure 6-4, Table 6-1).

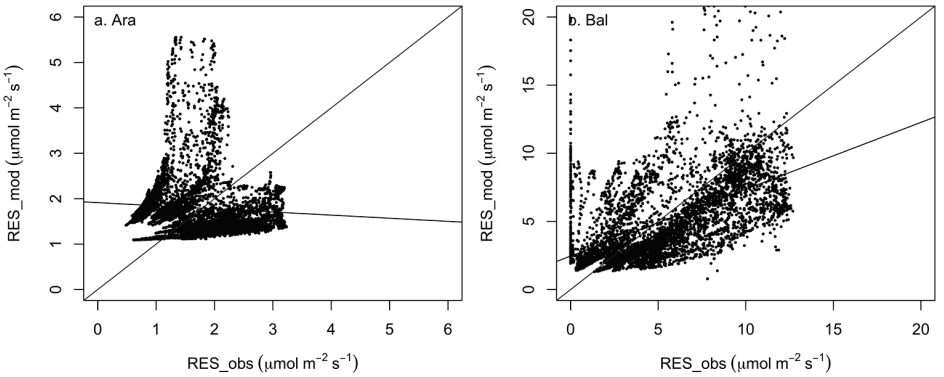

Figure 6-5. Comparison between observed (RES_obs) and simulated (RES_mod) ecosystem respiration (RES) at the Ara (a) and the Bal (b) sites. The blue line represents the 1:1 line and the black solid line represents the linear regression line between Qle_obs and Qle_mod.

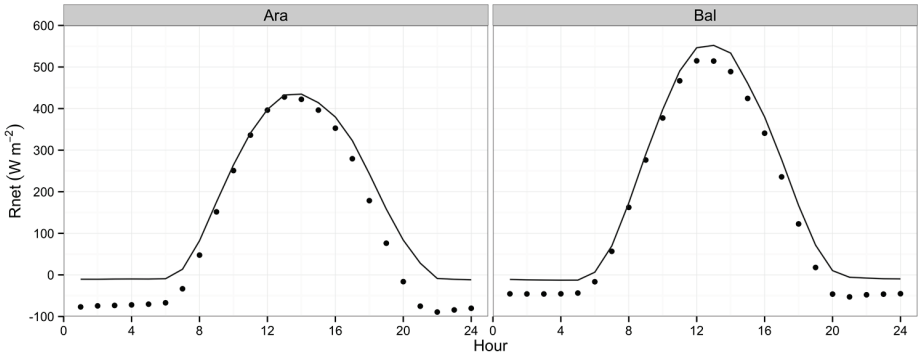

Figure 6-6. Comparison between the simulated diurnal net radiation (Rnet) (blue line) and the observed (black solid dot) at the Ara and Bal sites.

For ecosystem respiration (RES), the performance of the CLM was unsatisfactory (Figure 6-5). At the Ara site, the value of the slope between the simulated RES (RES_mod) and the observed RES (RES_obs) was even negative (-0.07), and the R value was as low as -0.06. RMSE value at the Ara site was 1.02 μmol m^{-2} s^{-1}. At the Bal site, the values of the slope (0.49) and R (0.52) were larger than those at the Ara site, but the RMSE was quite large as 3.22 μmol m^{-2} s^{-1}.

6.3.2 Performance of CLM in simulating diurnal water vapour and carbon fluxes

Figure 6-6 shows the diurnal variations of net radiation (Rnet) at the two sites. Overall, the CLM was able to capture the diurnal variations of Rnet at the two

sites well. This can be seen from the fact that the slope values were high, 0.87 and 0.99 at the Ara and Bal sites, respectively, and the R values were high as 1.0 at the two sites. However, we can see that the CLM generally over-estimated Rnet during nighttime at both sites. Therefore, the RMSE values for the two sites are still large as 57.37 and 35.94 W m^{-2} (Figure 6-6, Table 6-1). Over-estimates of Rnet during nighttime at the Ara site was more evident, which might be to the fact that the fraction of vegetation coverage at the Ara site was considerable lower than that at the Bal site. There is also a time lag in the afternoon. Both the nighttime overestimate of Rnet and the time lag indicate that ground heat flux G is not well predicted by the CLM, which has an effect on soil temperature, and this in turn affects the simulation of respiration (data not shown).

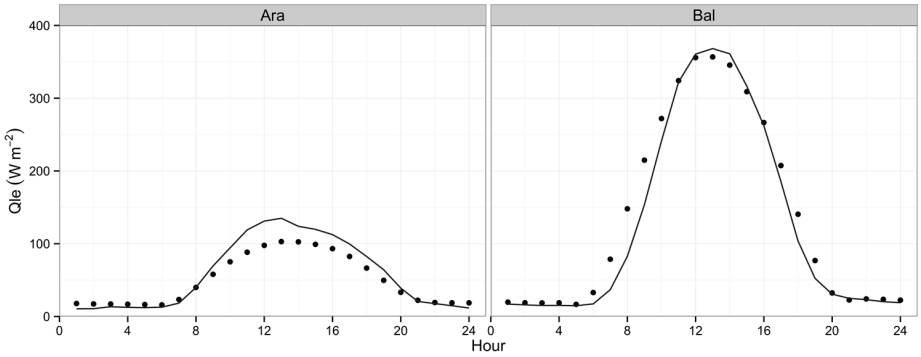

Figure 6-7. Comparison between the simulated diurnal latent heat flux (Qle) (blue line) and the observed (black solid dot) at the Ara and Bal sites.

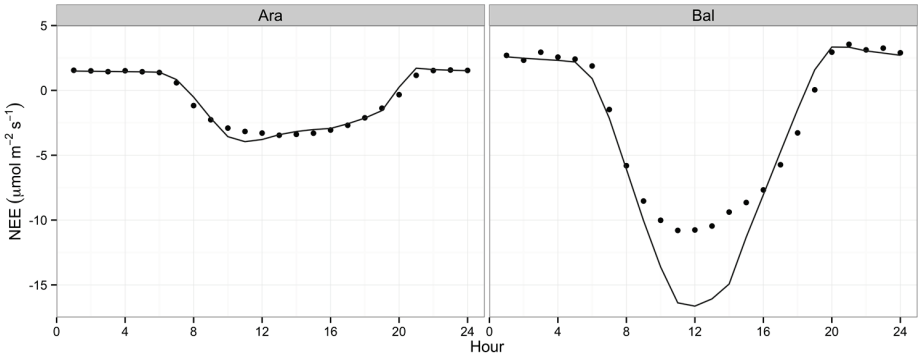

Figure 6-8. Comparison between the simulated diurnal net ecosystem exchange (NEE) (blue line) and the observed (black solid dot) at the Ara and Bal sites.

The diurnal variations of Qle were also well captured by the CLM, with the R values of 1.00 and 0.99 at the Ara and Bal sites, respectively. The slope values

were 1.38 and 1.01 at the two sites at the Ara and Bal sites, respectively (Figure 6-7, Table 6-1), indicating that the CLM over-estimated Qle at the Ara site, particularly around noon. Compared to the Ara site, the simulated Qle at the Bal site showed good agreements with the diurnal dynamics of the observed Qle.

The CLM was found to be able to well simulate the diurnal variations of NEE at the Ara site, with slope value of 1.04. At the Bal site, the CLM was found to negatively over-estimate NEE around noon. The observed mean noon peak NEE was -11 μmol m^{-2} s^{-1} but the model predicted peak NEE with -17 μmol m^{-2} s^{-1} (Figure 6-8), which is around 55% higher than the observed peak NEE at the Bal site.

6.3.3 Performance of CLM in simulating daily energy, water vapour and carbon fluxes

At the daily scale, Rnet simulated by the CLM were systematically larger than the observed values at the two sites (Figure 6-9). This can be indicated by the high values of the statistical index R (0.90 and 0.98 at the Ara and the Bal sites, respectively) but very large values of the interception (60.01 and 37.13 W m^{-2} at the Ara and Bal sites, respectively) of the linear regression between the model and the data and large RMSE value (51.28 and 40.37 W m^{-2} at the Ara and Bal sites, respectively) as well. Systematic overestimates of daily mean Rnet was mainly resulted from the overestimates of Rnet during nighttime as shown in Figure 6-6.

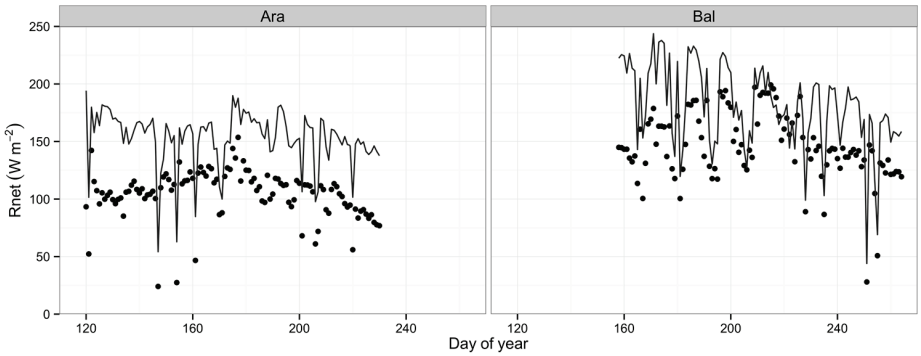

Figure 6-9. Mean daily net radiation (Rnet) simulated by the CLM (blue line) and observed by the eddy covariance (black solid dot) at the Ara and Bal sites.

A comparison between the simulated and the observed of mean daily Qle was shown in Figure 6-10. The mean daily Qle simulated by the CLM shows very

large fluctuations after rain-days at the Ara site. For example, the simulated mean daily Qle reached 250 and 200 W m^{-2} on the days of DOY 122 and 171, when there were two large rainfall events on the preceding day. However, the observed mean daily Qle were around 60 W m^{-2}. This result indicated that the CLM was strongly sensitive to the rainfall at the Ara site where the desert shrub was the dominant vegetation. The value of the slope for the mean daily Qle between the model the data was 1.07 and the R was 0.54, but with high RMSE of 29.33 W m^{-2} at the Ara site. At the Bal site, where desert grasses were the dominant vegetation species, the observed mean daily Qle was obviously larger than that at the Ara site (50.12 W m^{-2} vs. 139.42 W m^{-2}). The CLM-simulated mean daily Qle was significantly lower than the observed values, indicated by the low value of the slope of the linear regression (0.17). The correlation between the simulated mean daily Qle and the observed mean daily Qle was as low as 0.14 (Table 6-1).

Although the CLM predicted reasonable range of the observed mean daily NEE at the Ara site (-2.75~2.0 μmol m^{-2} s^{-1}) and the Bal site (-7.5~2.5 μmol m^{-2} s^{-1}), the performance of the CLM in simulating mean daily NEE at the two sites were poor. At the Ara site, the slope value of the linear regression between the simulated mean daily NEE and the observed mean daily NEE was 0.56 (R=0.33, RMSE=1.02 μmol m^{-2} s^{-1}). At the Bal site, the CLM showed worse performance. The slope of the linear regression between the model and the data was -0.06, with R of -0.04 and RMSE of 3.44 μmol m^{-2} s^{-1} (Figure 6-11, Table 6-1).

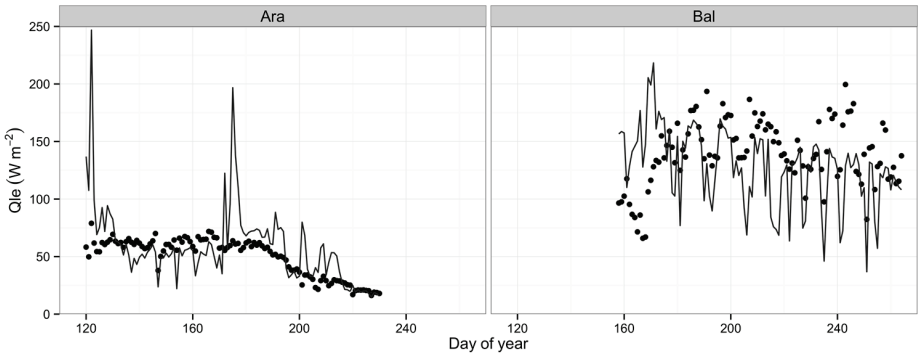

Figure 6-10. Mean daily latent heat flux (Qle) simulated by the CLM (blue line) and observed by the eddy covariance (black solid dot) at the Ara and Bal sites.

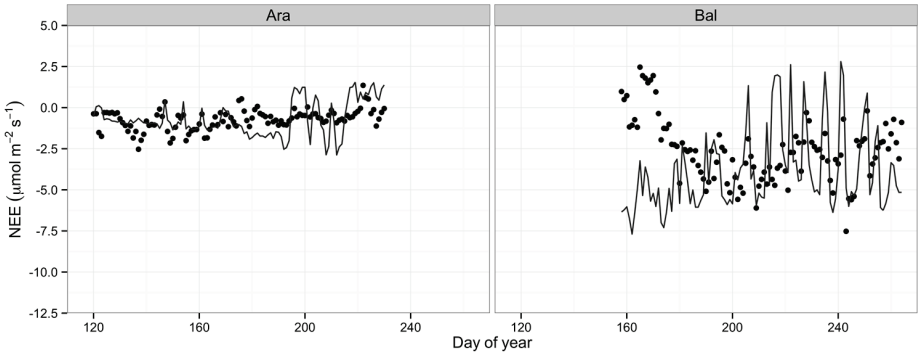

Figure 6-11. Mean daily net ecosystem exchange (NEE) simulated by the CLM (blue line) and observed by the eddy covariance (black solid dot) at the Ara and Bal sites.

6.3.4 Performance of CLM in simulating monthly water vapour and carbon fluxes

For water and carbon research, monthly or annual accumulated water and carbon fluxes were of more interests for the communities as they were ready for water and carbon budget calculations for a region. Limited by the data shortage in this study, we preferred to use unit of water and carbon fluxes at the scale of second, but monthly means were implemented to all available data at each site. Except on April, the CLM simulated comparable mean monthly Qle at the Ara site. Significant overestimate of April Qle was mainly resulted from that the CLM was too sensitive to the rainfall events and there is only one day measurement in April but with rainfall. At the Bal site, the CLM overestimated mean monthly Qle in May and June, but underestimated mean monthly Qle from July to September (Figure 6-12).

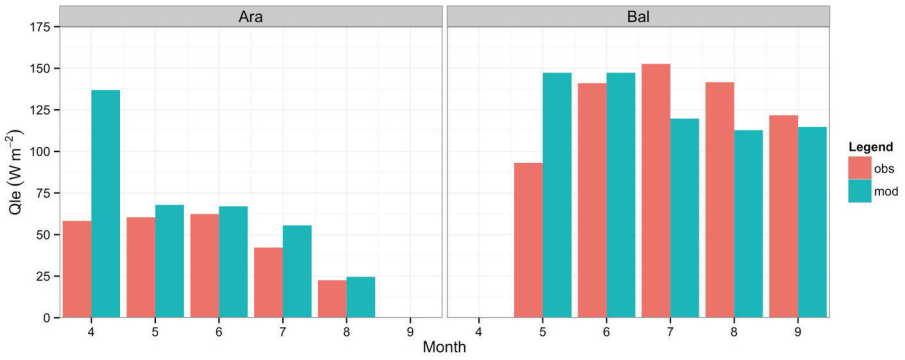

Figure 6-12. Mean monthly latent heat flux (Qle) simulated by the CLM and observed by the eddy covariance at the Ara and Bal sites.

The performance of the CLM in simulating mean monthly NEE was different from that in simulating mean monthly Qle. We can say that the ability of the CLM in simulating mean monthly NEE is not satisfactory at the Ara site, but the biases in all months were not too large. At the Bal site, excluding the two with incomplete months (May and September), the simulated mean monthly NEE showed very large differences from the measured mean monthly NEE (Figure 6-13). Overall, the performance of the CLM in simulating mean monthly NEE was worse than that in simulating mean monthly Qle. The performance of the CLM in simulating mean monthly NEE was quite similar with that in mean daily MEE (Figures 6-10 – 6-11).

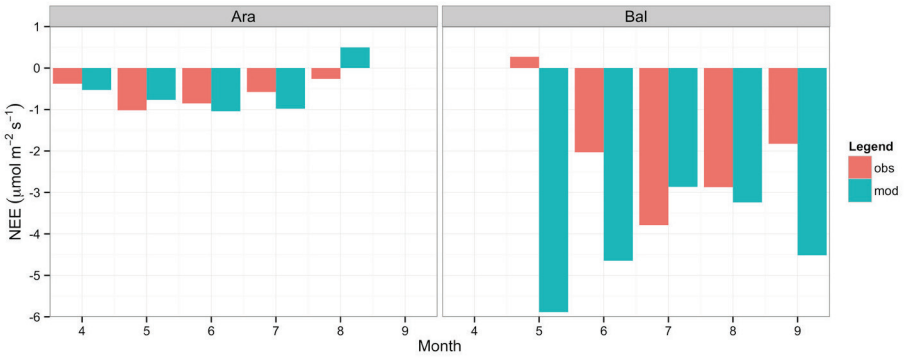

Figure 6-13. Mean monthly net ecosystem exchange (NEE) simulated by the CLM and observed by the eddy covariance at the Ara and Bal sites.

6.4 Discussion

6.4.1 Overall performance of the CLM in simulating energy, water and carbon fluxes at desert ecosystems

During the past decade, the water and carbon fluxes from the dryland ecosystems (including arid and semi-arid ecosystems) have received particular attention, based on measurements using eddy covariance technique (Hastings et al., 2005; Wohlfahrt et al., 2008). In a recent study, Poulter et al. (2014) found that semi-arid ecosystems have large potential to contribute to interannual variability of the global carbon cycles. Their conclusion was mainly based on an analysis of simulation results of global land surface models, but these were not validated against measurements in arid or semi-arid ecosystems. The present study implements previous work by evaluating the performance of a global land surface model in simulating the energy, water and carbon fluxes at two representative desert ecosystems in Central Asia. This evaluation allows us to

evaluate how a global land surface model performs in desert ecosystems, and to provide important information on model uncertainties and predictive accuracy.

Not contrary to our expectations the application of CLM is challenging in desert ecosystems where climate, vegetation composition and ecophysiological characteristics are largely different from other types of ecosystems. Although some aspects of the model structure (for example the root water uptake function proposed in Chapter 4) and parameters (for example initial quantum efficiency α and the maximum carboxylation rate V_{cmax} reported in Chapter 2 and root distribution reported in Chapter 5) have been adopted in the CLM, significant biases showed for some flux variables, particularly at daily and monthly scales. The performance of the CLM in simulating energy fluxes (Rnet and Qle) are better than that in simulating carbon fluxes (NEE, GPP, RES), which is quite similar to other LSMs (Li et al., 2011). The most likely reason is that energy is a more physical process but carbon is not only physical but also chemical one, and there are more other factors influencing the simulation of carbon fluxes. In addition, NEE is a net flux of GPP and RES, and each of GPP and RES is of its uncertainty as well.

Compared to previous model evaluations, the overall performance of the CLM in Central Asian desert ecosystems is poor, particularly for the simulation of carbon fluxes. For examples, in NACP (North American Carbon Project) site synthesis (Schwalm et al., 2010), 20 of 22 models performed relatively satisfactory for NEE with R-values ranging from 0.5 to 0.9. In this study, R-values of mean daily NEE for the CLM at the Ara and Bal sites are 0.33 and -0.04, respectively (Figure 6-11, Table 6-1). This weakness of the CLM in simulating carbon fluxes in desert ecosystems can be caused by many different sources.

6.4.2 Error sources of the CLM in application to desert ecosystems

Vegetation (biome) type was diagnosed as the most important variable to influence the performance of a LSM (Schwalm et al., 2010). In most parts of Central Asian desert ecosystems, the land surface is very heterogonous and the fraction of vegetation is low (Li et al., 2014). Thus, it is quite difficult to determine the fraction of vegetation and the proportion of each vegetation types accurately. The default scheme of the vegetation fraction and type compositions (Bonan, 1996; Dai et al., 2003; Lawrence et al., 2011) were used in the current simulation, which may be one of the main sources of the model error in desert

ecosystems. The fraction of vegetation is crucial as not only it is a direct coefficient to calculate transpiration and photosynthesis but also it impacts the average surface albedo and thus alters the energy partition and plant productivity. Sparse vegetation can be the most important cause of the mismatch of nighttime net radiation (Figure 6-6) between the simulations and the observations. This may be mainly because that surface temperature is not well simulated by the CLM.

Global model sensitivity analysis found that leaf area index (LAI) is also a crucial parameter to impact the model's performance (Lu et al., 2013). LAI is simulated using an imperial function in the CLM (Dai et al., 2003), however, its accuracy in desert ecosystem is unknown yet. Available LAI measurements in the two EC sites are absent, and no validation to LAI was done before. As one of important variables, errors in LAI may cause significant effects on the simulated carbon and water fluxes. For example, in the early stage of the study period at the Bal site, the simulated mean daily NEE showed very large departures from the observations, which may be mainly resulted from the mismatch of LAI between the CLM-simulated and the real values.

Besides the vegetation fraction, component and LAI, the model structure is also important to the performance of land surface models. Desert shrubs were one of key species in desert ecosystems. A number of studies has demonstrated that desert shrubs has some significant characteristics in water use strategy differing from the vegetation in humid regions, including their evolutionary adaptations to extreme dry climate, special leaf shape (actually no "real" leaf more for desert shrubs), very deep rooting depth and distinctly vertical root distribution in the soil profile (Xu & Li, 2008; Xu et al., 2007). Among these important features of desert shrubs, only root distribution was incorporated into the CLM, and it has been proven to significantly improve the model performance (Jing et al., 2014). However, it is still not clear how other "special" features of desert shrubs and grass can be incorporated into the current land surface model and how their impacts are. We assume that the mechanisms and processes of these morphological adjustments to environment for desert vegetation could exert substantial impacts on the model's performance once they can be well integrated into the models. Obviously, much more studies on this issue should be addressed in the future. A clear example from the present study is that the simulated Qle showed very large sensitivity to rainfall (as shown in Figure 6-10) at the Ara site, but the observations do not. The underlying reason is that the

adaption of desert shrubs to very dry climate also makes them not too sensitive to the rainfall as well.

For the poor performance of the CLM in simulating carbon components, another issue is that the information about ecosystem carbon pools (vegetation carbon pool and soil carbon pool) is unknown at the two study sites and set as default values in our simulations. Carbon pool sizes are able to greatly impact the simulated ecosystem respiration and alter the simulations for NEE and GPP. Simulation of RES is closely related to the simulated soil moisture and temperature by the land surface model. Limited by the data availabilities of soil temperature and moisture in the study sites, it is difficult to track the impacts of the simulated soil temperature and moisture on the performance of the CLM in simulating carbon components, particularly for RES. Finally, but not last, abiotic carbon process in desert ecosystems with alkaline soils is still in debate worldwide, although one initial research claimed that biotic processes dominated the carbon processes, and the contribution of abiotic carbon process to net ecosystem CO_2 exchange may be trivial in alkaline soil desert ecosystems over Central Asia (Li et al., 2014). This also can be one of the main sources of model errors for the CLM when applied in desert ecosystems.

6.5 Conclusions

Key attempt of this evaluation study is to obtain the first-impression on the performance of the common land model in simulating the energy, water and carbon fluxes at desert ecosystems. By comparing the CLM-simulated energy, water and carbon fluxes at diurnal, daily and monthly scales, we found that the CLM is able to well simulate net radiation at the half-hourly scale for both desert sites in Kazakhstan. The performance of the CLM in simulating half-hourly latent heat flux and carbon fluxes (net ecosystem CO_2 exchange, gross primary production and ecosystem respiration) were relatively poor. Diurnal comparison between the CLM-simulated and the observed found that the CLM can well capture the diurnal variations of all flux variables but significantly over-estimated net radiation at night-time for both sites, and negatively over-estimated peak NEE around noon at the Bal site. At the daily scale, the CLM systematically over-estimated Rnet, and the agreement between the simulated mean daily Qle and NEE and the observed was unsatisfactory for both sites. The CLM was proven to be too sensitive to rainfall. While, the performance of the CLM in simulating mean monthly Qle and NEE was largely different among months and between sites. We conclude that there is large potential to

improve the land surface model when applied in desert ecosystems. Providing accurate input information on vegetation fraction, composition, leaf area index and integrating advanced understanding on the morphological features into the current land surface models may greatly help to improve the model's performance in desert ecosystems.

Chapter 7

Concluding Remarks

7.1 Results

Energy, water and carbon fluxes between the land surface and the atmosphere in arid and semi-arid regions have received considerable attentions because their significance to global carbon cycle and climate. Land surface models serve for this functioning and are widely used in ecological, hydrological and climatic research. Central Asia has 5.67×10^6 km^2 land areas and the majorities are in extremely dry conditions and are of good representativeness of desert ecosystems in the world. Limited by the available surface flux measurements in CA, the performance of the LSMs in CA desert ecosystems remains far unknown. Inspired by this general question, this thesis uses the joint approaches of field experiments, eddy covariance (EC) technique and land surface modelling to address the energy, water and carbon flux issues. The main results from this thesis are as follows.

- By calibrating a coupled model of stomatal conductance, photosynthesis and transpiration against measurements from field experiments of transpiration and photosynthesis of desert shrubs at leaf scale, this thesis determined two important parameters, the initial quantum efficiency (α) and the maximum carboxylation rate (V_{cmax}), required in the current widely used modelling strategies. The values of α are 0.0235 and 0.0164, and the values of V_{cmax} are 15 μmol m^{-2} s^{-1} and 10~25 μmol m^{-2} s^{-1} for *Tamarix ramosissima* and *Haloxylon ammodendron*, respectively. The derived V_{cmax} values for desert shrubs are smaller than the default values used in the most LSMs (40~60 μmol m^{-2} s^{-1}).
- Through analysing long-term, continuous and high-frequency EC data at two representative desert sites with alkaline soils in Kazakhstan, we found that the diurnal course of mean monthly NEE followed a clear sinusoidal pattern during growing season at both sites. Both sites showed significant net carbon uptake during daytime on sunny days with high photosynthetically active radiation (PAR) but net carbon loss at nighttime and on cloudy and rainy days. NEE has strong dependency on PAR and the response of NEE to precipitation resulted in an initial and significant carbon release to the atmosphere, largely similar to other ecosystems. These findings indicate that biotic processes dominated the carbon processes and the contribution of abiotic carbon process to net ecosystem CO_2 exchange may be trivial in alkaline soil desert ecosystems over Central Asia.

- Representation of root water uptake efficiency is extremely difficult to determine, and is considered insufficient in current generation of LSMs but correct representation of root water uptake process is essential for a correct simulation of energy, water and carbon fluxes in dry climate. This thesis (Chapter 4) evaluates the performance of the Common Land Model (CLM) in simulating energy and water vapour fluxes measured with an eddy covariance system in a Central Asian desert ecosystem. The default CLM appears to be able to reproduce observed net radiation, soil subsurface temperature, and wet period latent (Qle) and sensible heat (Qh) fluxes, but significantly underestimate Qle and overestimate Qh during dry period. Underestimation of Qle is attributed to the inappropriate representation of root water uptake process in the CLM model. Modifying the original root water uptake function (RWUF) with a linear function of soil water potential to one with an exponential function significantly improves the performances for both Qle and Qh. The net radiation and ground heat flux simulations did not change noticeably with the new RWUF. We concluded that an exponential RWUF is a valuable improvement of the CLM model and likely for other similar LSMs that use a linear RWUF for Central Asian desert ecosystems.
- This thesis investigated the effect of root distribution on the simulated surface energy fluxes by incorporating the observed vertical root distribution. In addition, three different RWU functions were integrated into the Common Land Model (CLM) in place of the default RWU function. A comparison of the modified model's results with the measured surface energy fluxes by eddy covariance techniques in a Central Asian desert shrub ecosystem showed that both RWU function and vertical root distribution were able to significantly impact turbulent fluxes. Parameterizing the root distribution based on in-situ measurement and replacing the default RWU function with a revised version significantly improved the CLM's performance in simulating the latent and sensible heat fluxes. Sensitivity analysis showed that varying the parameter values of the revised RWU function did not significantly impact the CLM's performance, and therefore, this function is recommended for use in the CLM in Central Asian desert ecosystems and, possibly, other similar dryland ecosystems.
- This thesis evaluated the performance of the Common Land Model (CLM) from half-hourly to monthly time scales at two desert ecosystems in Central Asia. In general, the CLM is able to satisfactorily reproduce

the energy fluxes at both site but net radiation during night-time was systematically overestimated. The performance of the CLM for simulating carbon flux was site-dependent and varied greatly with time scales but the simulated ecosystem respiration was poorly correlated to the observed. The CLM was proven to simulate energy fluxes better than carbon fluxes. We concluded that there is large potential to improve the land surface model when applied in Central Asian desert ecosystems. We suspect that providing accurate input information on vegetation fraction, composition, leaf area index and integrating advanced understanding on the morphological features into the current land surface models may greatly help to improve the model's performance in desert ecosystems.

7.2 Discussion and Future Work

The key contribution of this thesis is that the performance of a global land surface model, the Common Land Model, is comprehensively and rigorously evaluated at three desert sites where long-term, continuous and high-frequency of surface flux variables (energy, water and carbon fluxes) were measured based on the eddy covariance technique. Particularly, measured surface flux variables at the two sites in Kazakhstan are first-hand and newly obtained, which is crucially important for modellers to assess how a land surface model performs in desert ecosystems.

In general, the default version of the Common Land Model performed poorly in Central Asian desert ecosystems. The site-calibrated ecophysiological parameters (the initial quantum efficiency and maximum carboxylation rate), root distribution, and a nonlinear root water uptake function were integrated into the CLM, and the performance of the CLM in simulating the energy and water vapour fluxes was significantly improved. However, the ability of the CLM for predicting carbon fluxes remains quite limited. Sources of the model errors can be searched from several aspects.

The first cluster of the important error sources is lack of available measurements of surface flux variables, which makes it impossible to evaluate land surface models. State-of-the-art land surface models have a large number of parameters, mostly a few hundred (Dai et al., 2003). It is easy to understand that most ecophysiological parameters in the land surface models are site-specific (vegetation-, soil- or climate-varying), and model parameters should be known possibly before applying land surface models into a new region. This

thesis has determined two important vegetation parameters (α and V_{cmax}). Parameter optimizing strategies such as Markov Chain Monte Carlo (MCMC) or Bayes inference may help this under the constraints of available measurements (Wang et al., 2007; Wang et al., 2011). Future work should also focus on the model's sensitivities to parameters in desert ecosystems, similar to some research in other ecosystems (Lu et al., 2013), which is helpful to diagnose model errors and improve the model's performance (Wang et al., 2011). For the deficiency of the Common Land Model in simulating the carbon fluxes, inaccurate parameterization of carbon pool is also an important source error for estimating ecosystem respiration.

The second source of model errors can be the issue of inaccurate information of land surface characteristics, which are actually used to drive land surface models. Currently, land surface characteristics properties are generally produced by satellite images with relative coarse resolution and insufficient accuracy. The problem of the inaccuracy of land surface characteristics from remote sensing data is particularly significant in vegetation-sparse regions, such as Central Asia desert ecosystems. Another problem associated with the inaccuracy of land surface characteristics is that grid information from the remote sensing data can't represent the real conditions where the measurements were made. The real surface characteristics can be highly heterogeneous that remotely sensed information cannot adequately represent. Particularly, the fractions of land cover types in a grid are full of high uncertainties, but this variable is crucial for calculating the surface fluxes. During the recent years, with the development of high-resolution satellite, it is possible to obtain accurate land surface characteristics information as the input for land surface models, and therefore to improve the model's performance.

The model structure is another important source of model errors. The model structure refers to the representations of the ecological or hydrological processes in the land surface models. Compared to aboveground ecophysiological processes controlling the energy and mass exchange between the land surface and the atmosphere that have been well represented in sufficient detail in the current land surface models, belowground processes are poorly described (Feddes et al., 2001). The key problem of belowground processes mainly involve the root water uptake, which can be representation of root water uptake function in the land surface models or integration of new root functioning process such as hydraulic redistribution (Baker et al., 2008; Li et

al., 2012). Either representation of root water uptake function or integration of hydraulic redistribution directly impacts the calculation of surface energy flux through describing how stomatal conductance of vegetation responds to water stress (Lai & Katul, 2000). This thesis has proposed a new exponential root water uptake function in replace of the original linear one, which improved the performance of the Common Land Model significantly (Li et al., 2013). By comparing four root water uptake functions in land surface models, we found that representation of root water uptake function has important effect on the simulation of surface energy and water fluxes at desert site (Jing et al., 2014). In addition, biases in the simulation of soil moisture and temperature by the Common Land Model may influence the simulation of energy, water and carbon fluxes, but the comparisons of the soil temperature and soil moisture between the model and the measurement are not well complemented in this thesis. Obviously this should be exploited in future work. Finally, the process of abiotic carbon absorption in desert ecosystems is not represented in the state-of-the-art land surface models. Given the contribution of abiotic carbon absorption was significant; this process should be included in modeling desert ecosystems in Central Asia.

This thesis is the first study to evaluate the performance of a land surface model in Central Asian desert ecosystems. The Common Land Model was selected an example in this study of a land surface model. It had some problems in representing desert ecosystems. The deficiency of the CLM at the studied desert sites was consistent with the performance of Noah model for semi-arid sites in Mexico (Hogue et al., 2005). Future work should focus on model parameter optimization using MCMC, Bayes inference or similar schemes (Hupet et al., 2003; Wang et al., 2007) and model process improvement by incorporating morphological adjustment and adaption of desert vegetation to desert environments (Xu & Li, 2008; Xu et al., 2007) into LSMs. Another potential way to improve the performance of LSMs in simulating surface energy, water and carbon fluxes would be to assimilate field measured or remotely sensed state variables of the ecosystem into the model (Verbeeck et al., 2011; Zhou et al., 2012).

Bibliography

Agam N, Kustas W.P., Anderson M.C., Norman J.M., Colaizzi P.D., Howell T.A., Prueger J.H., Meyers T.P., Wilson T.B. (2010) Application of the Priestley-Taylor approach in a two-source surface energy balance model. J. Hydrometeorol. 11, 185-198.

Allen R.G., Pereira L.S., Raes D., Smith M. (1998) Crop evapotranspiration. Guidelines for computing crop water requirements. FAO Irrigation and Drainage Paper No. 56, FAO, Rome. pp 300.

Anthoni P.M., Knohl A., Rebmann C. et al. (2004) Forest and agricultural land-use-dependent CO2 exchange in Thuringia, Germany. Global Change Biology, 10, 2005-2019.

Asner G.P., Archer S., Hughes R.F., Ansley R.J., Wessman C.A. (2003) Net changes in regional woody vegetation cover and carbon storage in Texas Drylands, 1937-1999. Global Change Biology, 9, 316-335.

Bai J., Chen X., Li J., Yang L., Fang H. (2011) Changes in the area of inland lakes in arid regions of central Asia during the past 30 years. Environmental Monitoring and Assessment, 178, 247-256.

Baker I.T., Prihodko L., Denning A.S., Goulden M., Miller S., Da Rocha H.R. (2008) Seasonal drought stress in the Amazon: Reconciling models and observations. Journal of Geophysical Research-Biogeosciences, 113.

Baldocchi D. (1994) A comparative study of mass and energy exchange over a close C3 (wheat) and an open C4 (corn) canopy: I. The partitioning of available energy into latent and sensible heat exchange. Agricultural and Forest Meteorology 67, 191-220.

Baldocchi D. (1997) Measuring and modelling carbon dioxide and water vapor exchange over a temperate broad-leaved forest during the 1995 summer drought. Plant, Cell and Environment 20, 1108-1122.

Baldocchi D. (2008) TURNER REVIEW No. 15.'Breathing' of the terrestrial biosphere: lessons learned from a global network of carbon dioxide flux measurement systems. Australian Journal of Botany, 56, 1-26.

Baldocchi D., Falge E., Gu L. et al. (2001) FLUXNET: A New Tool to Study the Temporal and Spatial Variability of Ecosystem–Scale Carbon Dioxide, Water Vapor, and Energy Flux Densities. Bulletin of the American Meteorological Society, 82, 2415-2434.

Baldocchi D., Meyers T. (1998) On using eco-physiological, micrometeorological and biogeochemical theory to evaluate carbon dioxide, water vapor and trace gas fluxes over vegetation: a perspective. Agricultural and Forest Meteorology, 90, 1-25.

Baldocchi D., Wilson K. (2001) Modeling CO2 and water vapor exchange of a temperate broadleaved forest across hourly to decadal time scales. Ecological Modelling 142, 155-184.

Ball J.T., Woodrow I.E., Berry J.A. (1987) A model predicting stomatal conductance and its contribution to the control of photosynthesis under different environmental conditions. In Progress in Photosynthesis Research (Ed. I. Biggens), Martinus-Nijhoff Publishers, Dordrecht, the Netherlands. pp. 221-224.

Bastiaanssen W.G.M., Harshdeep N.R. (2005) Managing scarce water resources in Asia: The nature of the problem and can remote sensing help? Irrigation and Drainage System 19, 269-284.

Batra N., Islam S., Venturini V., Bisht G., Jiang L. (2006) Estimation and comparison of evapotranspiration from MODIS and AVHRR sensors for clear sky days over the Southern Great Plains. Remote Sensing of Environment 103, 1–15.

Beljaars A.C.M., Viterbo P., Miller M.J., Betts A.K. (1996) The Anomalous Rainfall over the United States during July 1993: Sensitivity to Land Surface Parameterization and Soil Moisture Anomalies. Monthly Weather Review, 124, 362-383.

Bell T.W., Menzer O., Troyo-Diequez E., Oechel W.C. (2012) Carbon dioxide exchange over multiple temporal scales in an arid shrub ecosystem near La Paz, Baja California Sur, Mexico. Global Change Biology, 18, 2570-2582.

Bernacchi C.J., Portis A.R., Nakano H., von Caemmerer S., Long S.P. (2002) Temperature response of mesophyll conductance. Implication for the determination of Rubisco enzyme kinetics and for limitations to photosynthesis in vivo, Plant Physiology 130, 1992-1998.

Best M.J., Pryor M., Clark D.B. et al. (2011) The Joint UK Land Environment Simulator (JULES), model description – Part 1: Energy and water fluxes. Geosci. Model Dev., 4, 677-699.

Black T.A., Den Hartog G., Neumann H.H. et al. (1996) Annual cycles of water vapour and carbon dioxide fluxes in and above a boreal aspen forest. Global Change Biology, 2, 219-229.

Blyth E., Gash J., Lloyd A., Pryor M., Weedon G.P., Shuttleworth J. (2009) Evaluating the JULES Land Surface Model Energy Fluxes Using FLUXNET Data. Journal of Hydrometeorology, 11, 509-519.

Blyth E., Gash J., Lloyd A., Pryor M., Weedon G.P., Shuttleworth J. (2009) Evaluating the JULES Land Surface Model Energy Fluxes Using FLUXNET Data. Journal of Hydrometeorology, 11, 509-519.

Bonan G. (1996) A land surface Model (LSM version 1.0) for ecological, hydrological, and atmospheric studies: Technical description and user's guide. NCAR Tech. Note NCAR/TN-417+STR, 150pp.

Bonan G.B., Lawrence P.J., Oleson K.W. et al. (2011) Improving canopy processes in the Community Land Model version 4 (CLM4) using global flux fields empirically inferred from FLUXNET data. Journal of Geophysical Research: Biogeosciences, 116, G02014.

Bonan G.B., Oleson K.W., Fisher R.A., Lasslop G. and Reichstein M., 2012. Reconciling leaf physiological traits and canopy flux data: use of the try and fluxnet databases in the Community Land Model version 4. Journal of Geophysical Research, 117: G02026.

Bondeau A., Smith P.C., Zaehle S. et al. (2007) Modelling the role of agriculture for the 20th century global terrestrial carbon balance. Global Change Biology, 13, 679-706.

Branson F.A., Gifford G.F., Owen R.J. (1972) Rangeland Hydrology, Range Sci. Ser. Soc. For Range Manage: Denver, CO, 84.

Breckle S.W., Wucherer W., Dimeyeva L.A. (2012) Vegetation of the Aralkum. Aralkum - a Man-Made Desert, 127-159.

Brisson N., Itier B., L'Hotel J.C., Lorendeau J.Y. (1998) Parameterisation of the Shuttleworth–Wallace model to estimate daily maximum transpiration for use in crop models. Ecological Modelling 107, 159–169.

Bruemmer C., Falk U., Papen H., Szarzynski J., Wassmann R., Brueggemann N. (2008) Diurnal, seasonal, and interannual variation in carbon dioxide and energy exchange in shrub savanna in Burkina Faso (West Africa). Journal of Geophysical Research-Biogeosciences, 113.

Canal N., Calvet J.C., Decharme B., Carrer D., Lafont S., Pigeon G. (2014) Evaluation of root water uptake in the ISBA-A-gs land surface model using agricultural yield statistics over France. Hydrol. Earth Syst. Sci. Discuss., 11, 5421-5461.

Chen H., Xu X.L., Song M.H., Ouyang H. (2008) Photosynthetic pathway of dominant plant species in the Qaidam Basin: evidence form foliar stable carbon isotope measurement. Photosynthetic 46, 303-306.

Choi, M., S.O. Lee and H. Kwon, 2010. Understanding of the Common Land Model performance for water and energy fluxes in a farmland during the growing season in Korea. Hydrological Processes, 24:1063-1071.

Ciais P., Reichstein M., Viovy N. et al. (2005) Europe-wide reduction in primary productivity caused by the heat and drought in 2003. Nature, 437, 529-533.

Clapp R.B. and Hornberger G.M., 1978. Empirical equations for some soil hydraulic properties. Water Resources Research, 14:601-604.

Clark D.B., Mercado L.M., Sitch S. et al. (2011) The Joint UK Land Environment Simulator (JULES), model description – Part 2: Carbon fluxes and vegetation dynamics. Geosci. Model Dev., 4, 701-722.

Cleverly J.R., Smith S.D., Sala A., Devitt D.A. (1997) Invasive capacity of Tamarix ramosissima in a Mojave Desert floodplain: the role of drought. Oecologia 111, 12-18.

Collatz G.J., Ball J.T., Grivet C., Berry J.A. (1991) Physiological and environmental regulation of stomatal conductance, photosynthesis and transpiration: A model that includes a laminar boundary layer. Agricultural and Forest Meteorology 54, 107-136.

Collatz G.J., Ribas-Carbo M., Berry J.A. (1992) Coupled photosynthesis-stomatal conductance model for leaves of C4 plants. Australia Journal of Plant Physiology 19, 519-538.

Cox P.M., Betts R.A., Bunton C.B., Essery R.L.H., Rowntree P.R., Smith J. (1999) The impact of new land surface physics on the GCM simulation of climate and climate sensitivity. Climate Dynamics, 15, 183-203.

Cui B.S., Yang Q.C., Zhang K.J., Zhao X.S., You Z.Y. (2010) Responses of saltcedar (Tamarix chinensis) to water table depth and soil salinity in the Yellow River Delta, China. Plant Ecology doi:10.1007/sl1258-010-9273-z.

Dai Y., Zeng X., Dickinson R.E. et al. (2003) The Common Land Model. Bulletin of the American Meteorological Society, 84, 1013-1023.

Dai Y.J., Dickinson R.E., Wang Y.P. (2004) A two-big-leaf model for canopy temperature, photosynthesis, and stomatal conductance. Journal of Climate, 17, 2281-2299.

Dai Y.J., Zeng Q.C. (1997) A land surface model (IAP94) for climate studies, Part I: Formulation and validation in off-line experiments. Adv. Atmos. Sci, 14, 433-460.

Dai Y.J., Zeng X.B., Dickinson R.E., Baker I., Bonan G.B., Bosilovich M.G., Denning A.S., Dirmeyer P.A., Houser P.R., Niu G.Y., Oleson K.W., Schlosser C.A. and Yang Z.L. (2003) The Common Land Model. Bulletin of the American Meteorological Society, 84:1013-1023.

Davidson E., Lefebvre P.A., Brando P.M. et al. (2011) Carbon Inputs and Water Uptake in Deep Soils of an Eastern Amazon Forest. Forest Science, 57, 51-58.

Deardorff J.W. (1978) Efficient prediction of ground surface temperature and moisture, with inclusion of a layer of vegetation. Journal of Geophysical Research: Oceans, 83, 1889-1903.

Dickinson R.E. (1983) Land surface processes and climate surface: albedos and energy balance. Advances in Geophysics, 25, 305-353.

Dickinson R.E., Henderson-Sellers A., Kennedy P.J. (1993) Biosphere-atmosphere Transfer Scheme (BATS) Version 1e as Coupled to the NCAR Community Climate Model. NCAR Technical Note NCAR/TN-387+STR.

Dickinson R.E., Henderson-Sellers A., Kennedy P.J., Wilson M.F. (1986) Biosphere-atmosphere Transfer Scheme (BATS) for the NCAR Community Climate Model. NCAR Technical Note NCAR/TN-275-+STR.

Dickinson R.E., Henderson-Sellers A., Kennedy P.J., Wilson M.F. (1993) Biosphere–Atmosphere Transfer Scheme (BATS) version 1e as coupled to Community Climate Model. NCAR Tech. Note NCAR/TN-387+STR, 72.

Dregne H. (1983) Desertifcation of arid lands. In: Advances in desert and arid lands. Harwood Academic, New York. 202pp.

Dubois J.B., Fiscus E.L., Booker F.L., Flowers M.D., Reid C.D. (2007) Optimizing the statistical estimation of the parameters of the Farquhar-von Caemmerer-Berry model of photosynthesis. Plant, Cell and Environment 176, 402-414.

Dunne T., Zhang W., Aubry B. (1991) Effects of rainfall, vegetation, and microtopography on infiltration and runoff. Water Resources Research 27, 2271–2285.

Falge E., Baldocchi D., Olson R.J., Anthoni P., Aubinet M., Bernhofer C., Burba G., Ceulemans R., Clement R., Dolman H., Granier A., Gross P., Grünwald T., Hollinger D., Jensen N.O., Katul G., Keronen P., Kowalski A., Ta Lai C., Law B.E., Meyers, T. Moncrieff J., Moors E., Munger J.W., Pilegaard K., Rannik Ü., Rebmann C., Suyker A., Tenhunen J., Tu K., Verma S., Vesala T., Wilson K., Wofsy S. (2001a) Gap filling strategies for defensible annual sums of net ecosystem exchange. Agricultural Forest Meteorology 107, 43-69.

Falge E., Baldocchi D., Olson R.J., Anthoni P., Aubinet M., Bernhofer C., Burba G., Ceulemans R., Clement R., Dolman H., Granier A., Gross P., Grünwald T., Hollinger D., Jensen N.O., Katul G., Keronen P., Kowalski A., Ta Lai C., Law B.E., Meyers T., Moncrieff J., Moors E., Munger J.W., Pilegaard K., Rannik Ü., Rebmann C., Suyker A., Tenhunen J., Tu K., Verma S., Vesala T., Wilson K., Wofsy S. (2001b) Gap filling strategies for longterm energy flux data sets. Agricultural Forest Meteorology 107, 71-77.

Falge E., Tenhunen J., Baldocchi D. et al. (2002) Phase and amplitude of ecosystem carbon release and uptake potentials as derived from FLUXNET measurements. Agricultural and Forest Meteorology, 113, 75-95.

Farquhar G.D., von Caemmerer S., Berry J.A. (1980) A biochemical model of photosynthetic CO2 assimilation in leaves of C3 species. Planta 149, 78-90.

Feddes R.A., Bresler E., Neuman S.P. (1974) Field-Test of a Modified Numerical-Model for Water Uptake by Root Systems. Water Resources Research, 10:1199-1206.

Feddes R.A., Hoff H., Bruen M. et al. (2001) Modeling root water uptake in hydrological and climate models. Bulletin of the American Meteorological Society, 82, 2797-2809.

Feddes, R.A., Kowalik, P.J. and Zaradny, H. (1978) Simulation of field water use and crop yield. Pudoc, Wageningen. Simulation Monographs.

Fisher J.B., DeBiase T.A., Qi Y., Xu M., Goldstein A.H. (2005) Evapotranspiration models compared on a Sirra Nevada forest ecosystem. Environmental Modelling & Software 20, 783-796.

Flint A.L., Childs S.W. (1991) Use of the Priestley–Taylor evaporation equation for soil water limited conditions in a small forest clearcut. Agric. For. Meteorol. 56, 247–260.

Gao Q., Yu M., Zhang X.S., Xu H.M., Huang Y.M. (2005) Modelling seasonal and diurnal dynamics of stomatal conductance of plants in a semiarid environment. Functional Plant Biology 32, 583-598.

Gao Y.H., Li X.R., Liu L.C., Jia R.L., Yang H.T., Li G., Wei Y.P. (2012) Seasonal variation of carbon exchange from a revegetation area in a Chinese desert. Agricultural and Forest Meteorology, 156, 134-142.

Gay L.W., Fritschen L.J. (1979) An energy budget analysis of water use by saltcedar. Water Resources Research 15, 1589-1592.

Gay L.W., Sammis T.W. (1977) Estimating phreatophyte transpiration. Hydrology and Water Resources in Arizona and the Southwest 7, 133-139.

Gay L.W., Sammis T.W., Ben-Asher J. (1976) An energy budget analysis of evapotranspiration from saltcedar. Hydrology and Water Resources in Arizona and the Southwest 6, 181-187.

Gilmanov T., Johnson D.A., Saliendra N.Z., Akshalov K., Wylie B.K. (2004) Gross promary productivity of the true steppe in Central Asia in relation to NDVI: scaling up CO2 fluxes. Environmental Management, 33, S492-S508.

Grace J., Malhi Y., Lloyd J.O.N., Mcintyre J., Miranda A.C., Meir P., Miranda H.S. (1996) The use of eddy covariance to infer the net carbon dioxide uptake of Brazilian rain forest. Global Change Biology, 2, 209-217.

Gries D., Zeng F., Foetzki A., Arndt S.K., Burelheide H., Thomas F.M., Zhang X., Runge M. (2003) Growth and water relations of Tamarix ramosissima and Populus euphratica on Taklamakan desert dunes in relation to depth to a permanent water table. Plant, Cell and Environment 26, 726-736.

Gu J.J., Smith E.A., Merritt J.D. (1999) Testing energy balance closure with GOES-retrieved net radiation and in situ measured eddy correlation fluxes in BOREAS. Journal of Geophysical Research-Atmospheres, 104, 27881-27893.

Guswa A.J., 2005. Soil-moisture limits on plant uptake: an upscaled relationship for water-limited ecosystems. Advances in Water Resources, 28:543-552.

Hanan N.P., Berry J.A., Verma S.B., Walter-Shea E.A., Suyker A.E., Burba G.G., Denning A.S. (2005) Testing a model of CO2, water and energy exchange in Great Plains tallgrass prairie and wheat ecosystems. Agricultural and Forest Meteorology, 131, 162-179.

Hastings S.J., Oechel W.C., Muhlia-Melo A. (2005) Diurnal, seasonal and annual variation in the net ecosystem CO2 exchange of a desert shrub community (Sarcocaulescent) in Baja California, Mexico. Global Change Biology, 11, 927-939.

Hayes W.E., Walker L.R., Powell E.A. (2009) Competitive abilities of Tamarix aphylla in southern Nevada. Plant Ecology 202, 159-167.

Heavens N.G., Ward D.S., Natalie M.M. (2013) Studying and projecting climate change with Earth System Models. Nature Education Knowledge, 4.

Henderson-Sellers A., Pitman A.J., Love P.K., Irannejad P., Chen T.H. (1995) The Project for Intercomparison of Land Surface Parameterization Schemes (PILPS): Phases 2 and 3. Bulletin of the American Meteorological Society, 76, 489-503.

Hess T.M. (1998) Trends in reference evapotranspiration in the North East Arid Zone of Nigeria, 1961–91. Journal of Arid Environments 38, 99–115.

Hogue T.S., Bastidas L., Gupta H., Sorooshian S., Mitchell K., Emmerich W. (2005) Evaluation and Transferability of the Noah Land Surface Model in Semiarid Environments. Journal of Hydrometeorology, 6, 68-84.

Horton J.L., Clark J.L. (2001) Water table decline alters growth and survival of Salix gooddingii and Tamarix chinesnsis seedlings. Forest Ecology and Management 140, 239-247.

Hsieh C.I., Katul G., Chi T. (2000) An approximate analytical model for footprint estimation of scaler fluxes in thermally stratified atmospheric flows. Advances in Water Resources, 23, 765-772.

Hsu K.L., Gupta H.V., Gao X.G., Sorooshian S, Imam B (2002) Self-organizing linear output map (SOLO): An artificial neural network suitable for hydrologic modeling and analysis. Water Resources Research, 38.

Hu Z.M., Yu G.R., Zhou Y.L., Sun X.M., Li Y.N., Shi P.L., Wang Y.F., Song X., Zheng Z.M., Zhang L., Li S.G. (2009) Partitioning of evapotranspiration and it's controls in four grassland ecosystems: Application of a two-source model. Agricultural and Forest Meteorology 149, 1410-1420.

Huang Y.Q., Mo L., Zhao P., Zhang Z.F., He C.X. (2009) Comparison of gas exchanges between in situ and abscised leaves of high arbor trees: a case study of Cylobalanopsis glauca under three habitats, Frontiers of Forestry in China. 4, 464-471. doi: 10.1007/s11461-009-0065-8.

Hupet F., Lambot S., Feddes R.A., Van Dam J.C., Vanclooster M. (2003) Estimation of root water uptake parameters by inverse modeling with soil water content data. Water Resources Research, 39, 1312.

Idso S.B. (1981) A dry of equations for full spectrum thermal-radiation from cloudless skies. Water Resources Research, 17, 295-304.

Iritz Z., Lindroth A., Heikinheimo M., Grelle A., Kellner E. (1999) Test of a modified Shuttleworth-Wallace estimate of boreal forest evaporation. Agricultural and Forest Meteorology 98-99, 615-619.

Jackson R.B., Sperry J.S., Dawson T.E. (2000) Root water uptake and transport: using physiological processes in global predictions. Trends in Plant Science, 5, 482-488.

Jarvis P.G. (1976) The Interpretation of the Variations in Leaf Water Potential and Stomatal Conductance Found in Canopies in the Field. Philosophical Transactions of the Royal Society of London. B, Biological Sciences, 273, 593-610.

Jasoni R.L., Smith S.D., Arnone J.A. (2005) Net ecosystem CO2 exchange in Mojave Desert shrublands during the eighth year of exposure to elevated CO2. Global Change Biology, 11, 749-756.

Jing C-Q., Li L., Chen X., Luo G-P. (2014) Comparison of root water uptake functions to simulate surface energy fluxes within a deep-rooted desert shrub ecosystem. Hydrological Processes, 28, 5436-5449.

Katerji N., Perrier A. (1983) Modélization de l'évapotranspiration réelle ETR d'une parcelled de luzerne: rôle d'un coefficient cultural. Agronomie 3(6), 513-521. (in French)

Kenzo T., Ichie T., Watanabe W., Yoneda R., Ninomiya I., Koike T. (2006) Changes in photosynthesis and leaf characteristics with tree height in five dipterocarp species in a tropical rain forest. Tree Physiology 26, 865-873.

Kowalczyk E.A., Wang Y.P., Law R.M., Davies H.L., McGregor J.L., Abramowitz G. (2006) The CSIRO Atmosphere Biosphere Land Exchange (CABLE) model for use in climate models and as an offline model, CSIRO Marine and Atmospheric Research Paper 013, 37 pp.

Krinner G., Viovy N., De Noblet-Ducoudre N., Ogée J., Polcher J., Friedlingstein P., Ciais P., Sitch S., Prentice E.C. (2005) A dynamic global vegetation model for studies of the coupled atmosphere-biosphere system. Global Biogeochemical Cycles 19, GB1015. doi:10.1029/2003GB002199.

Kustas W.P., Humes K.S., Norman J.M., Moran M.S. (1996) Single- and dual-source modeling of surface energy fluxes with radiometric surface temperature. Journal of Applied Meteorology, 35, 110-121.

Lai C.T., Katul G., Oren R., Ellsworth D., Schafer K. (2000) Modeling CO2 and water vapor turbulent flux distributions within a forest canopy. Journal of Geophysical Research 105, 333-351.

Lal R. (2004) Carbon sequestration in dryland ecosystems. Environmental Management 33, 528-544.

Lawrence D.M., Oleson K.W., Flanner M.G. et al. (2011) Parameterization improvements and functional and structural advances in Version 4 of the Community Land Model. Journal of Advances in Modeling Earth Systems, 3, M03001.

Lee J-E., Oliveira R.S., Dawson T.E., Fung I. (2005) Root functioning modifies seasonal climate. Proc Natl Acad Sci U S A, 102, 17576-17581.

Leuning R. (1990) Modelling Stomatal Behaviour and and Photosynthesis of *Eucalyptus grandis*. Functional Plant Biology, 17, 159-175.

Leuning R. (1995) A critical appraisal of a combined stomatal-photosynthesis model for C3 plants. Plant Cell Environ, 18, 339-355.

Li K.Y., De Jong R., Coe M.T., Ramankutty N. (2006) Root-water-uptake based upon a new water stress reduction and an asymptotic root distribution function. Earth Interactions, 10.

Li L., Chen X., Tol C., Luo G., Su Z. (2014) Growing season net ecosystem CO2 exchange of two desert ecosystems with alkaline soils in Kazakhstan. Ecology and Evolution, 4, 14-26.

Li L., Luo G., Chen X., Li Y., Xu G., Xu H., Bai J. (2011a) Modelling evapotranspiration in a Central Asian desert ecosystem. Ecological Modelling, 222, 3680-3691.

Li L., Van Der Tol C., Chen X., Jing C., Su B., Luo G., Tian X. (2013) Representing the root water uptake process in the Common Land Model for better simulating the energy and water vapour fluxes in a Central Asian desert ecosystem. Journal of Hydrology.

Li L., Vuichard N., Viovy N. et al. (2011) Importance of crop varieties and management practices: evaluation of a process-based model for simulating CO2 and H2O fluxes at five European maize (Zea mays L.) sites. Biogeosciences, 8, 1721-1736.

Li L., Wang Y.P., Yu Q. et al. (2012) Improving the responses of the Australian community land surface model (CABLE) to seasonal drought. Journal of Geophysical Research-Biogeosciences, doi:10.1029/2012JG002038.

Li L., Yu Q., Su Z., van der Tol C. (2009) A simple method using climatic variables to estimate canopy temperature, sensible and latent heat fluxes in a winter wheat field on the North China Plain. Hydrological Processes 23, 665-674.

Li L.H., Yu Q. (2007) Quantifying the effects of advection on canopy energy budgets and water use efficiency in an irrigated wheat field in the North China Plain. Agric. Water Manage. 89, 116-122.

Li L.H., Yu Q., Zheng Y.F., Wang J., Fang Q.X. (2006) Simulating the response of photosynthate partitioning during vegetative growth in winter wheat to environmental factors. Field Crops Research 96, 133-141.

Li Y., Xu H., Cohen S. (2005) Long-term hydraulic acclimation to soil texture and radiation load in cotton. Plant Cell Environ. 28, 492-499.

Li Z.Q., Yu G.R., Wen X.F., Zhang L.M., Ren C.Y., Fu Y.L. (2005) Energy balance closure at ChinaFLUX sites. Science in China Series D-Earth Sciences, 48, 51-62.

Lin J.D., Sun S.F. (1983) Moisture and heat flow in soil and theirs effects on bare soil evaporation. Trans. Water Conservancy 7, 1–7. (in Chinese)

Liu R., Li Y., Wang Q.X. (2012a) Variations in water and CO2 fluxes over a saline desert in western China. Hydrological Processes, 26, 513-522.

Liu R., Pan L-P., Jenerette G.D., Wang Q-X., Cieraad E., Li Y. (2012b) High efficiency in water use and carbon gain in a wet year for a desert halophyte community. Agricultural and Forest Meteorology, 162–163, 127-135.

Long S.P. (1991) Modification of the response of photosynthetic productivity to rising temperature by atmospheric CO2 concentrations: Has its importance been underestimated? Plant Cell Environ. 14, 729-739.

Lu X., Wang Y-P., Ziehn T., Dai Y. (2013) An efficient method for global parameter sensitivity analysis and its applications to the Australian community land surface model (CABLE). Agricultural and Forest Meteorology, 182–183, 292-303.

Ma J., Zheng X-J., Li Y. (2012) The response of CO2 flux to rain pulses at a saline desert. Hydrological Processes. 26(26), 4029-4037.

Mahrt L. (1998) Flux sampling errors for aircraft and towers. Journal of Atmospheric and Oceanic Technology, 15, 416-429.

Manabe S. (1969) Climate and the ocean circulation: the atmospheric circulation and the hydrology of the Earth's sufrace. Monthly Weather Review, 97, 36.

Martinez-Garcia L.B., Armas C., Miranda J.D., Padilla F.M. and Pugnaire F.I. (2011) Shrubs influence arbuscular mycorrhizal fungi communities in a semi-arid environment. Soil Biology & Biochemistry, 43:682-689.

Masek J.G., Cohen W.B., Leckie D., Wulder M.A., Vargas R., de Jong B., Healey S., Law B., Birdsey R., Houghton R.A., Mildrexler D., Goward S. and Smith W.B., 2011. Recent rates of forest harvest and conversion in north america. Journal of Geophysical Research, 116: G00K03.

Mauder M., Foken T. (2006) Impact of post-field data processing on eddy covariance flux estimates and energy balance closure. Meteorologische Zeitschrift, 15, 597-609.

Maxwell R.M., Miller N.L. (2005) Development of a coupled land surface and groundwater model. Journal of Hydrometeorology, 6, 233-247.

Mcelrone A.J., Pockman W.T., Martinez-Vilalta J., Jackson R.B. (2004) Variation in xylem structure and function in stems and roots of trees to 20 m depth. New Phytologist, 163, 507-517.

Medlyn B.E., Dreyer E., Ellsworth D., Forstreuter M., Harley P.C., Kirschbaum M.U.F., Le Roux X., Montpied P., Strassemeyer J., Walcroft A., Wang K., Loustau D. (2002) Temperature reposne of parameters of a biochemically based model of photosynthesis. II. A review of experimental data. Plant, Cell and Environment 25, 1167-1179.

Millan H. and Gonzalez-Posada M. (2005) Modelling soil water retention scaling. Comparison of a classical fractal model with a piecewise approach. Geoderma, 125:25-38.

Mitchell J.F.B., Karoly D.J., Hegerl G.C., Zwiers F.W., Allen M.R., Marengo J. (2001) Detection of climate change and attribution of causes. In: Climate Change 2001: The Scientific Basis [Houghton, J.T., Y. Ding, D.J. Griggs, M. Noguer, P.J. van der Linden, X. Dai, K. Maskell, and C.A. Johnson (eds.)]. Cambridge University Press, Cambridge, United Kingdom, pp., 695-738.

Mo X.G., Chen J.M., Ju W.M., Black T.A. (2008) Optimization of ecosystem model parameters through assimilating eddy covariance flux data with an ensemble Kalman filter. Ecological Modelling 217, 157-173.

Moffat A.M., Papale D., Reichstein M. et al. (2007) Comprehensive comparison of gap-filling techniques for eddy covariance net carbon fluxes. Agricultural and Forest Meteorology, 147, 209-232.

Moffat A.M., Papale D., Reichstein M., Hollinger D.Y., Richardson A.D., Barr A.G., Beckstein C., Braswell B.H., Churkina G., Desai A.R., Falge E., Gove J.H., Heimann M., Hui D., Jarvis A.J., Kattge J., Noormets A., and Stauch V.J. (2007) Comprehensive comparison of gap-filling techniques for eddy covariance net carbon fluxes. Agric. For. Meteorol. 147, 209-232.

Monin A.S., Obukhov A.M. (1954) Osnovnye zakonomemosti turbulentnogo peremeshivanija v prizemnom sloe atmosfery (Basic laws of turbulent mixing in the atmosphere near the ground). Trudy geofiz. inst., 24, 163-187.

Monteith J.L. (1965) Evaporation and environment. pp. 205-234. In G.E. Fogg (ed.) Symposium of the Society for Experimental Biology. The State and Movement of Water in Living Organisms. 19, Academic Press, Inc, NY.

Moore C.J. (1986) Frequency response corrections for eddy correlation systems. Boundary-Layer Meteorology, 37, 17-35.

Nichols J., Eichinger W., Cooper D.I., Prueger J.H., Hipps L.E., Neale C.M.U., Bawazir A.S. (2004) Comparison of evaporation estimation methods for a riparian area. Final report. UHR Technical Report No. 436. College of Engineering. University of Iowa, USA.

Noy-Meir E. (1973) Desert ecosystems: environment and producers. Annual Review of Ecology and Systematics 4, 23–51.

Obukhov A.M. (1946) Turbulentnost'v temperatumoj - neodnorodnoj atmosfere (Turbulence in an atmosphere with non-uniform temperature). Trudy Inst. Theor. Geofiz, 1, 95-115.

Oleson K.W., Niu G.Y., Yang Z.L. et al. (2008) Improvements to the Community Land Model and their impact on the hydrological cycle. Journal of Geophysical Research-Biogeosciences, 113.

Oliphant A.J. (2012) Terrestrial Ecosystem-Atmosphere Exchange of CO2, Water and Energy from FLUXNET; Review and Meta-Analysis of a Global in-situ Observatory. Geography Compass, 6, 689-705.

Papale D., Reichstein M., Aubinet M. et al. (2006) Towards a standardized processing of Net Ecosystem Exchange measured with eddy covariance technique: algorithms and uncertainty estimation. Biogeosciences, 3, 571-583.

Penman H.L. (1948) Natural evaporation from open water, bare soil, and grass. Proc. Roy. Soc. London. A193, 120-146.

Pereira A.R., Green S.R., Nova N.A.V. (2007) Sap flow, leaf area, net radiation and the Priestley–Taylor formula for irrigated orchards and isolated trees. Agricultural Water Management 92, 48-52.

Pereira A.R., Nova N.A.V., (1992) Analysis of the Priestley–Taylor parameter. Agric. For. Meteorol. 61, 1–9.

Philip J.R. (1975) Evaporation and moisture and heat fields in the soil. J. Meteorol, 14, 354-366.

Piao S., Friedlingstein P., Ciais P., De Noblet-Ducoudré N., Labat D., Zaehle S. (2007) Changes in climate and land use have a larger direct impact than rising CO2 on global river runoff trends. Proceedings of the National Academy of Sciences, 104, 15242-15247.

Pitman A.J. (2003) The evolution of, and revolution in, land surface schemes designed for climate models. International Journal of Climatology, 23, 479-510.

Pitman A.J., Henderson-Sellers A., Desborough C.E. et al. (1999) Key results and implications from phase 1(c) of the Project for Intercomparison of Land-surface Parametrization Schemes. Climate Dynamics, 15, 673-684.

Poulter B., Frank D., Ciais P. et al. (2014) Contribution of semi-arid ecosystems to interannual variability of the global carbon cycle. Nature, 509, 600-603.

Priestley C.H.B., Taylor R.J. (1972) On the assessment of surface heat flux and evaporation using large scale parameters. Monthly Weather Review 100, 81-92.

Reichstein M., Falge E., Baldocchi D. et al. (2005) On the separation of net ecosystem exchange into assimilation and ecosystem respiration: review and improved algorithm. Global Change Biology, 11, 1424-1439.

Reynolds J.F., Kemp P.R., Ogle K., Fernandez R.J. (2004) Modifying the 'pulse-reserve' paradigm for deserts of North America: precipitation pulses, soil water and plant responses. Oecologia 141: 194–210, doi: 10D1007/s00442-004-1524-4.

Reynolds O. (1895) On the dynamical theory of incompressible viscous fluids and the determination of the criterion. Philosphical Transaction of the Royal Society of London, 186, 123-164.

Ridler M.E., Sandholt I., Butts M. et al. (2012) Calibrating a soil–vegetation–atmosphere transfer model with remote sensing estimates of surface temperature and soil surface moisture in a semi arid environment. Journal of Hydrology, 436–437, 1-12.

Rihani J.F., Maxwell R.M., Chow F.K. (2010) Coupling groundwater and land surface processes: Idealized simulations to identify effects of terrain and subsurface heterogeneity on land surface energy fluxes. Water Resources Research, 46.

Robinson T.W. (1970) Evapotranspiration by woody phreatophytes in the Humboldt River Valley near Winnemucca, Nevada. United States Geological Survey Professional Paper. pp. 491-D.41.

Romo J.T., Haferkamp M.R. (1989) Water relations of Artemisia tridentata spp. Wyomingensis and Sarcobatus vermiculatus in the steppe of southeastern Oregon. American Midland Naturalist 121, 155-164.

Rotenberg E., Yakir D. (2010) Contribution of semi-arid forests to the climate system. Science 327, 451-454.

Sala A., Smith S.D., Devitt D.A. (1996) Water use by Tamarix ramosissima and associated phreatophytes in a Mojave Desert floodplain. Ecological Application 6, 888-898.

Saleska S.R., Didan K., Huete A.R., Da Rocha H.R. (2007) Amazon Forests Green-Up During 2005 Drought. Science, 318, 612.

Saleska S.R., Miller S.D., Matross D.M. et al. (2003) Carbon in amazon forests: Unexpected seasonal fluxes and disturbance-induced losses. Science, 302, 1554-1557.

Savabi M.R., Stockle C.O. (2001) Modeling the possible impact of increased CO2 and temperature on soil water balance, crop yield and soil erosion. Environmental Modelling & Software 16 (7), 631-640.

Schenk H.J. and Jackson R.B. (2002) The global biogeography of roots. Ecological Monographs, 72:311-328.

Schlesinger W.H., Belnap J., Marion G. (2009) On carbon sequestration in desert ecosystems. Global Change Biology, 15, 1488-1490.

Schwalm C.R., Williams C.A., Schaefer K. et al. (2010) A model-data intercomparison of CO_2 exchange across North America: Results from the North American Carbon Program site synthesis. Journal of Geophysical Research: Biogeosciences, 115, G00H05.

Sellers P.J., Dickinson R.E., Betts A.K., Hall F.G., Berry J.A., Collatz G.J., Denning A.S., Mooney H.A., Nobre C.A., Sato N., Field C.B., Henderson-Sellers A. (1997) Modeling the exchanges of energy, water, and carbon between continents and the atmosphere. Science 275, 502-509.

Sellers P.J., Mintz Y., Sud Y.C., Dalcher A. (1986) A Simple Biosphere Model (Sib) for Use within General-Circulation Models. Journal of the Atmospheric Sciences, 43, 505-531.

Sellers P.J., Randall D.A., Collatz G.J., Berry J.A., Field C.B., Dazlich D.A., Zhang C., Collelo G.D., Bounoua L. (1996) A revised land surface parameterization (SiB2) for atmospheric GCMs. part I: model formulation. Journal of Climate 9, 676-705.

Sellers P.J., Tucker C.J., Collatz G.J., Los S.O., Justice C.O., Dazlich D.A., Randall D.A. (1994) A global 1° by 1° NDVI data set for climate studies. Part 2: The generation of global fields of terrestrial biophysical parameters from the NDVI. International Journal of Remote Sensing, 15, 3519-3545.

Serrano-Ortiz P., Roland M., Sanchez-Moral S., Janssens I.A., Domingo F., Godderis Y., Kowalski A.S. (2010) Hidden, abiotic CO2 flows and gaseous reservoirs in the terrestrial carbon cycle: Review and perspectives. Agricultural and Forest Meteorology, 150, 321-329.

Shao C., Chen J., Li L. (2013) Grazing alters the biophysical regulation of carbon fluxes in a desert steppe. Environmental Research Letters, 8, 025012.

Shuttleworth W.L., Wallace J.S. (1985) Evaporation from sparse crops - an energy combination theory. Quanterly Journal of the Royal Meteorological Society 111, 839-855.

Sitch S., Smith B., Prentice I.C. et al. (2003) Evaluation of ecosystem dynamics, plant geography and terrestrial carbon cycling in the LPJ dynamic global vegetation model. Global Change Biology, 9, 161-185.

Smith S., Devitt D., Sala A., Cleverly J., Busch D. (1998) Water relations of riparian plants from warm desert regions. Wetlands 18, 687-696.

Smithwick E.A.H., Lucash M.S., McCormack M.L., Sivandran G. (2014) Improving the representation of roots in terrestrial models. Ecological Modelling, 291, 193-204.

Sperry J.S. and Hacke U.G., 2002. Desert shrub water relations with respect to soil characteristics and plant functional type. Functional Ecology, 16:367-378.

Stannard D.I. (1993) Comparison .of Penman-Monteith, Shuttleworth-Wallace, and modified Priestly-Taylor evapotranspiration models for wildland vegetation in semiarid rangelands. Water Resources Research 29, 1379-1392.

Starodubtsev V.M., Truskavetskiy S.R. (2011) Desertification processes in the Ili River delta under anthropogenic pressure. Water Resources, 38, 253-256.

Steiner A.L., Pal J.S., Giorgi F., Dickinson R.E., Chameides W.L. (2005) The coupling of the Common Land Model (CLM0) to a regional climate model (RegCM). Theoretical and Applied Climatology, 82, 225-243.

Stockli R., Lawrence D.M., Niu G.Y. et al. (2008) Use of FLUXNET in the community land model development. Journal of Geophysical Research-Biogeosciences, 113.

Stone R. (2008) Ecosystems - Have desert researchers discovered a hidden loop in the carbon cycle? Science, 320, 1409-1410.

Stoy P.C., Dietze M.C., Richardson A.D. et al. (2013) Evaluating the agreement between measurements and models of net ecosystem exchange at different times and timescales using wavelet coherence: an example using data from the North American Carbon Program Site-Level Interim Synthesis. Biogeosciences, 10, 6893-6909.

Stromberg J., Chew M. (2002) Foreign visitors in riparian corridors of the American Southwest: is xenophobia justified? In: Tellman, B. (Ed.), Invasive Exotic Species in the Sonoran Region. University of Arizona Press, Tucson, AZ, pp. 195-219.

Sumner, D.M, Jacobs, J.M, 2005. Utility of Penman–Monteith, Priestley–Taylor, reference evapotranspiration, and pan evaporation methods to estimate pasture evapotranspiration. J. Hydrol. 308, 81-104.

Susiluoto S., Berninger F. (2007) Interactions between morphological and physiological drought responses in Eucalyptus microtheca. Silva Fennica, 41, 221-233.

Tanaka K., Kosugi Y., Nakamura A. (2002) Impact of leaf physiological characteristics on seasonal variation in CO2, latent and sensible heat exchanges over a tree plantation. Agricultural and Forest Meteorology 114, 103-122.

Taylor K.E., 2001. Summarizing multiple aspects of model performance in a single diagram. Journal of Geophysical Research, 106:7183-7192.

Thornton P.E., Running S.W., Hunt E.R. (2005) Biome-BGC: terrestiral ecosystem process model, Version 4.1.1. Model product. Available on-lin [http://www.daac.ornl.ogv] from Oak Ridge National Laboratory Distributed Active Archive Center. Oak Ridge, Tennessee. U.S.A.

Trenberth K.E., Fasullo J.T., Kiehl J. (2009) Earth's Global Energy Budget. Bulletin of the American Meteorological Society, 90, 311-323.

Tuzet A., Perrier A., Leuning R. (2003) A coupled model of stomatal conductance, photosynthesis and transpiration. Plant, Cell and Environment 26(7), 1097-1116.

Unland H.E., Houser P.R., Shuttleworth W.J., Yang Z.L. (1996) Surface flux measurement and modeling at a semi-arid Sonoran Desert site. Agricultural and Forest Meteorology, 82, 119-153.

Valentini R., De Angelis P., Matteucci G., Monaco R., Dore S., Mucnozza G.E.S. (1996) Seasonal net carbon dioxide exchange of a beech forest with the atmosphere. Global Change Biology, 2, 199-207.

Van der Tol C., 2012. Validation of remote sensing of bare soil ground heat flux. Remote Sensing of Environment, 121:275-286.

van Hylckama T.E.A. (1974) Water use by saltcedar as measured by the water budget method. United States Geological Survey Professional Paper 491-E. United States Government Printing Office, Washington, D.C, USA.

Verbeeck H., Peylin P., Bacour C., Bonal D., Steppe K., Ciais P. (2011) Seasonal patterns of CO_2 fluxes in Amazon forests: Fusion of eddy covariance data and the ORCHIDEE model. Journal of Geophysical Research: Biogeosciences, 116, G02018.

Vickers D., Mahrt L. (1997) Quality control and flux sampling problems for tower and aircraft data. Journal of Atmospheric and Oceanic Technology, 14, 512-526.

Viterbo P., Beljaars A., Mahfouf J-F., Teixeira J. (1999) The representation of soil moisture freezing and its impact on the stable boundary layer. Quarterly Journal of the Royal Meteorological Society, 125, 2401-2426.

Wang T., Brender P., Ciais P. et al. (2012) State-dependent errors in a land surface model across biomes inferred from eddy covariance observations on multiple timescales. Ecological Modelling, 246, 11-25.

Wang Y.G., Xiao D.N., Li Y., Li X.Y. (2008) Soil salinity evolution and its relationship with dynamics of groundwater in the oasis of inland river basins: case study from the Fubei region of Xinjiang Province, China. Environmental Monitor and Assessment 140, 291-302.

Wang Y.P., Baldocchi D., Leuning R., Falge E., Vesala T. (2006) Estimating parameters in a land-surface model by applying nonlinear inversion to eddy covariance flux measurements from eight FLUXNET sites. Global Change Biology 12, 1-19. Doi:10.1111/j.1365-2486.2006.01225.x.

Wang Y.P., Baldocchi D., Leuning R.A.Y., Falge E.V.A., Vesala T. (2007) Estimating parameters in a land-surface model by applying nonlinear inversion to eddy covariance flux measurements from eight FLUXNET sites. Global Change Biology, 13, 652-670.

Wang Y.P., Kowalczyk E., Leuning R. et al. (2011) Diagnosing errors in a land surface model (CABLE) in the time and frequency domains. Journal of Geophysical Research, 116.

Wang Y.P., Law R.M., Pak B. (2010) A global model of carbon, nitrogen and phosphorus cycles for the terrestrial biosphere. Biogeosciences, 7, 2261-2282.

Wang Y.P., Lu X.J., Wright I.J., Dai Y.J., Rayner P.J., Reich P.B. (2012) Correlations among leaf traits provide a significant constraint on the estimate of global gross primary production. Geophysical Research Letters, 39, L19405.

Webb E.K., Pearman G.I., Leuning R. (1980) Correction of Flux Measurements for Density Effects Due to Heat and Water-Vapor Transfer. Quarterly Journal of the Royal Meteorological Society, 106, 85-100.

Whitford W.G. (2002) Ecology of Desert Systems. Academic Press: San Diego, CA.

Williams M., Richardson A.D., Reichstein M. et al. (2009) Improving land surface models with FLUXNET data. Biogeosciences, 6, 1341-1359.

Wilson K., Goldstein A., Falge E. et al. (2002) Energy balance closure at FLUXNET sites. Agricultural and Forest Meteorology, 113, 223-243.

Wofsy S.C., Goulden M.L., Munger J.W. et al. (1993) Net Exchange of CO2 in a Mid-Latitude Forest. Science, 260, 1314-1317.

Wohlfahrt G., Fenstermaker L.F., Arnone J.A. (2008) Large annual net ecosystem CO2 uptake of a Mojave Desert ecosystem. Global Change Biology, 14, 1475-1487.

Wolf A., Akshalov K., Saliendra N., Johnson D.A., Laca E.A. (2006) Inverse estimation of Vcmax, leaf area index, and the Ball-Berry parameter from carbon and energy fluxes. Journal of Geophysical Research 111, D08S08. doi:10.1029/2005JD005927.

Xie J.X., Li Y., Zhai C.X., Li C.H., Lan Z.D. (2009) CO2 absorption by alkaline soils and its implication to the global carbon cycle. Environmental Geology, 56, 953-961.

Xu G.Q. and Li Y., 2009. Root distribution of three desert shrubs and their reponse to precipitation. Sciences in Cold and Arid Regions, 1:120-127.

Xu G.Q., Li Y. (2008) Rooting depth and leaf hydraulic conductance in the xeric tree Haloxyolon ammodendron growing at sites of contrasting soil texture. Funtional Plant Biology 35, 1234-1242.

Xu H., Li Y. (2006) Water-use strategy of three central Asian desert shrubs and their responses to rain pulse events. Plant Soil 285, 5-17.

Xu H., Li Y., Xie J.X., Cheng L., Zhao Y., Liu R. (2010) Influence of solar radiation and groundwater table on carbon balance of phreatophytic desert shrub Tamarix. Chinese Journal of Plant Ecology. 34, 375-386. (in Chinese)

Xu H., Li Y., Xu G., Zou T. (2007) Ecophysiological response and morphological adjustment of two Central Asian desert shrubs towards variation in summer precipitation. Plant Cell and Environment, 30, 399-409.

Xu L., Baldocchi D.D. (2004) Seasonal variation in carbon dioxide exchange over a Mediterranean annual grassland in California. Agricultural and Forest Meteorology, 123, 79-96.

Yan H.L., Liang S.M., Zhang X.M., Wang W.H., Ma J.B., Zhu J.T. (2008) Photosynthesis responses of endemic shrubs of Taklimakan Desert to adverse temperature, humidity and radiation. Chinese Science Bulletin 53, 84-92.

Yang F.L. and Zhou G.S. (2011) Characteristics and modeling of evapotranspiration over a temperate desert steppe in Inner Mongolia, China. Journal of Hydrology 396, 139-147.

Yang F.L., Zhou G.S., Hunt J.E., Zhang F. (2011) Biophysical regulation of net ecosystem carbon dioxide exchange over a temperate desert steppe in Inner Mongolia, China. Agriculture Ecosystems & Environment, 142, 318-328.

Yin X., Struik P.C. (2009) C3 and C4 photosynthesis models: An overview from the perspective of crop modelling. NJAS - Wageningen Journal of Life Sciences 57(1), 27-38.

Yu Q., Goudriaan J., Wang T.D. (2001) Modelling diurnal courses of photosynthesis and transpiration of leaves on the basis of stomatal and non-stomatal responses, including photoinhibition. Photosynthetica 39, 43-51.

Yu Q., Liu Y.F., Liu J.D., Wang T.D. (2002) Simulation of leaf photosynthesis of winter wheat on Tibetan Plateau and in North China Plain. Ecological Modelling 155, 205-216.

Zampieri M., Serpetzoglou E., Anagnostou E.N., Nikolopoulos E.I., Papadopoulos A. (2012) Improving the representation of river–groundwater interactions in land surface modeling at the regional scale: Observational evidence and parameterization applied in the Community Land Model. Journal of Hydrology, 420–421, 72-86.

Zeng X.B., Dai Y.J., Shaikh M., Dickinson R.E. and Myneni R., 2001. Common Land Model (CLM) and its coupling with the NCAR CCM3. 12th Symposium on Global Change and Climate Variations, 1:19-20.

Zeng X.B., Shaikh M., Dai Y.J., Dickinson R.E., Myneni R. (2002) Coupling of the common land model to the NCAR community climate model. Journal of Climate, 15, 1832-1854.

Zhang B.Z., Kang S.Z., Li F.S., Zhang L. (2008) Comparison of evapotranspiration models to Bowen ratio-energy balance method for vineyard in an arid desert region of northwest China. Agricultural and Forest Meteorology 148, 1629-1640.

Zhang H., Pak B., Wang Y.P., Zhou X., Zhang Y., Zhang L. (2013) Evaluating Surface Water Cycle Simulated by the Australian Community Land Surface Model (CABLE) across Different Spatial and Temporal Domains. Journal of Hydrometeorology, 14, 1119-1138.

Zhao C.X., Deng X.P., Zhang S.Q., Ye Q., Steudle E. and Shan L. (2004) Advances in the studies on water uptake by plant roots. Acta Botanica Sinica, 46:505-514.

Zheng Z. and Wang G. (2007). Modeling the dynamic root water uptake and its hydrological impact at the reserva jaru site in amazonia. Journal of Geophysical Research, 112: G04012.

Zhou M.C., Ishidaira H., Hapuarachchi H.P., Magome J., Kiem A.S., Takeuchi K. (2006) Estimating potential evapotranspiration using Shuttleworth-Wallace model and NOAA-AVHRR NDVI data to feed a distributed hydrological model over the Mekong River basin. Journal of Hydrology 327, 151-173.

Zhou X., Zhang Y., Wang Y. et al. (2012) Benchmarking global land surface models against the observed mean annual runoff from 150 large basins. Journal of Hydrology, 470-471, 269-279.

Zou T., Li Y., Xu H., Xu G.Q. (2010) Responses to precipitation treatment for Haloxylon ammodendron growing on contrasting textured soils. Ecol. Resear. 25, 185-194.

Summary

Quantifying the exchanges of energy, water and CO_2 between the land surface and the atmosphere is the principal objective of Land Surface Models. Despite considerable advances in LSMs during the past few decades, predictive ability of the LSMs in dry environments remains low and unsatisfactory, and hindered our ability to understand the interactions of climate and vegetation. Therefore, this thesis is aiming at evaluating the performance of the Common Land Model (CLM) in simulating energy, water and CO_2 at desert sites in Central Asia. By comparing the results from CLM against the eddy covariance measured surface flux variables, we found that, in general, the CLM is able to satisfactorily reproduce the energy fluxes at three desert sites in Central Asia but net radiation during night-time was systematically overestimated. We confirmed that more realistic representation of vertical distribution of root in soil profile and the root water uptake function has significant improvements on the simulation of water and carbon fluxes at desert sites. However, the performance of the CLM for simulating carbon flux was site-dependent and varied greatly with time scales and the simulated ecosystem respiration was poorly correlated to the observed one. Overall, the CLM was proven to simulate energy fluxes better than carbon fluxes. We concluded that there is large potential to improve the land surface model when applied in Central Asian desert ecosystems. Generating accurate input information on vegetation coverage, compositions, and improving the ability in estimating leaf area index and integrating our latest understanding on the morphological functions into the current land surface models may greatly help advancing LSMs in desert ecosystems.

Samenvatting

Het doel van landoppervlakmodellen ('Land Surface Models' LSM) is om de uitwisseling van energie, water en CO_2 tussen land en atmosfeer te kwantificeren. Ondanks alle vooruitgang op het gebied van LSM gedurende de afgelopen decennia, blijven voorspellingen met LSMs in aride gebieden onnauwkeurig. Dit is onbevredigend, omdat het ons de toegang tot een beter begrip van de wisselwerking tussen klimaat en vegetatie in die gebieden belemmert. Dit proefschrift heeft tot doel de prestaties van het Common Land Model (CLM) te beoordelen voor de woestijn van centraal Azië. Door modeluitkomsten te vergelijken met Eddy Correlatiedata (EC) werd duidelijk dat CLM de energieuitwisseling redelijk goed reproduceert voor drie locaties in de woestijn in centraal Azië, maar dat de netto straling gedurende de nacht systematisch wordt overschat. Een meer realistische modellering van de verticale verdeling van wortels in het bodemprofiel, en het introduceren van een wateropname functie bracht significante verbetering in de gesimuleerde flux van water en koolstof in de woestijn. De prestatie van CLM voor de flux van koolstof was afhankelijk van de locatie, en varieerde enorm met de tijdsschaal. De gesimuleerde respiratie was slecht gecorreleerd met de gemeten respiratie. Over de hele linie simuleert CLM de fluxen van energie beter dan die van koolstof. De conclusie is dat er potentieel is om LSMs te verbeteren voor de Centraal Aziatische woestijn. Dit kan door nauwkeurige informatie te verzamelen over bedekkingsgraad en samenstelling van de vegetatie, door het verbeteren van schattingen van de horizontale projectie van het bladoppervlak (LAI) en door ons begrip van morfologische functies in te bouwen in LSMs.

ITC Dissertation List

http://www.itc.nl/research/phd/phd_graduates.aspx